Estimation of Spatio-Temporal Variations in Water Balance Components and Nutrient Transport for Indian River Basins Using Statistical Analysis and Hydrological Modeling

---

A Dissertation

presented to

The Faculty of the School of Engineering and Applied Sciences

University of Virginia

In partial fulfillment

of the requirements for the Degree

Doctor of Philosophy (Civil Engineering)

by

Prakrut Kansara

May 2022

Abstract

The Indian subcontinent suffers from a decline in water resources per capita and water quality deterioration in the course of recent decades due to exponential population growth. With the impact of climate change being intensified by the increasing anthropogenic interventions, there is a significant risk to the water resources. This dissertation focuses on analysis and modeling of water quantity and quality resources for improving water management in the Indian river basins. In the first study, nine major river basins in India were analyzed utilizing publicly-available satellite and modelled dataset information for the time period from 2002 to 2019. Water balance components - Precipitation (P), Runoff (R), Evapotranspiration (ET), and Total Water Storage Anomaly (TWSA) - were examined for each of these river basins. Time-series of the water balance components demonstrated that all the river basins exhibit strong seasonality with peaks during the Monsoon season (June – September). The seasonal analysis demonstrated that Southern and North-Eastern parts of India experience water deficit due to decreasing monsoonal precipitation combined with increasing ET and decrease in TWSA. I found that 74% of the monotonic trends were associated with 'Agricultural' land whereas 19% were associated with 'Urban' land. In the second and third studies, a semi-distributed, physically-based hydrological model (SWAT) was built to characterize the catchment hydrology and nutrient transport for the Narmada and Ganga River Basins respectively. Using the flow calibrated hydrological model, I compared simulated and observed Nitrogen (N) at 17 locations inside the Narmada River Basin. Through the calibration of flow parameters at five calibration sites, I obtained a mean R^2 of 0.77 during the calibration phase (2001-2010) and mean R^2 of 0.76 during the validation phase (2011-2019). The trend analysis revealed that subbasins near the watershed boundaries showed increasing trend for N concentration over the study period. In the third study, using streamflow, N flux and N concentration calibrated SWAT models, I compared simulated and observed N flux and concentration at 92 locations inside the Ganga River Basin. Through multi-site calibration of flow parameters at 3 sites, I obtained a mean R^2 of 0.76 during the calibration phase (2001-2010) and a mean R^2 of 0.73 during the validation phase (2011-2017) for streamflow. Model results showed that 35 of 650 SWAT simulated subbasins have increasing nitrogen concentration trends with most of the trends in the downstream eastern part of the watershed. For both of these studies, nitrogen contamination can be attributed to anthropogenic activities - specifically farming - as these activities use large amounts of N based fertilizers, excess of which is drained into the river through runoff. For Ganga, point source pollution through industries and urban sewage were significant contributors of nitrogen pollution, but they were not captured due to the data limitations.

To Mita, Haresh, Nisarg, Swati and Atharva

Acknowledgements

I would first like to thank my advisor, Dr. Venkataraman Lakshmi, without whom this dissertation would not have been possible. From the time I met you as a summer intern to starting my journey as a PhD student to finishing my PhD, you have been a constant source of motivation, inspiration and support. You have provided me countless opportunities to learn and grow as a student, researcher, and TA. Thank you, Venkat, for all your guidance, not just for research but towards my overall professional growth.

My dissertation committee deserves a special thank you for their time and guidance. Thanks to Dr. Jonathan Goodall for agreeing to chair the committee and for mentoring me as a student and as a TA for your Water Resources Engineering class. Thank you, Dr. Julianne Quinn, for your insightful questions and suggestions in improving my research. Thank you, Dr. Jim Smith, for your discussions on groundwater and nutrient transport. Thank you, Dr. Todd Scanlon, for your thought provoking questions on my research. Thank you, Dr. Harihar Rajaram, for your time and effort in serving as an external committee member and providing me with the right resources to further my research.

A big thank you to Dr. Vimal Mishra for always believing in me. I cannot thank you enough for your support.

My colleagues from UVA including Hung Manh Le, Hyunglok Kim, Bin Fang, Reyadh Al Barakat, Benjamin Goffin, Robin Kim, Runze Zhang, Chelsea Dandridge, Gigi Pavur, Jessica Besnier who contributed and supported in different ways. Thank you, Hyunglok Kim, for always being a good friend and fellow researcher. Thank you, Hung, for your constant help throughout my PhD. Starting my PhD along with you guys made it so much easier and I cannot imagine what I would have done without you. Thank you, Ben, for making my fourth year of PhD much more enjoyable.

In addition, I would like to thank my parents – Mita and Haresh, my brother – Nisarg, and my sister-in-law – Swati, for their constant support and effort in making me capable of doing a PhD. From making sure that I don't stress too much about work and staying healthy, your love has been an important pillar in my PhD journey. I also want to thank Bhavesh Parmar, Jolly Parmar, Apurva Kansara and Kanika Kansara for being my support system in the United States where I am so far away from my family.

I would also like to thank my friends outside of my research group including Saikat Kumar, Pooja Dubey, Prathamesh Badve, Viraj Jagani, Paras Patel, Samarth Singh, Preksha Jain, Sukriti Singh, Ajeeta Khatri, and Paris Karakasis for making my PhD journey much more memorable. Thank you all for being there with me through the ups and downs.

Contents

List of Tables

List of Figures

Chapter 1: Introduction

The Indian population of roughly 1.4 billion individuals relies upon agriculture for food and livelihood as cultivable land is the principal source of financial security (https://www.indiawaterportal.org/topics/agriculture). Several global studies point to India being a global hotspot of exponentially depleting water quantity and quality resources. Rodell et al., (2018) shows North-Western and Eastern India as regions with one of the highest declines in Gravity Recovery And Climate Experiment (GRACE) derived Total Water Storage Anomaly (TWSA) (**Figure 1.1**).

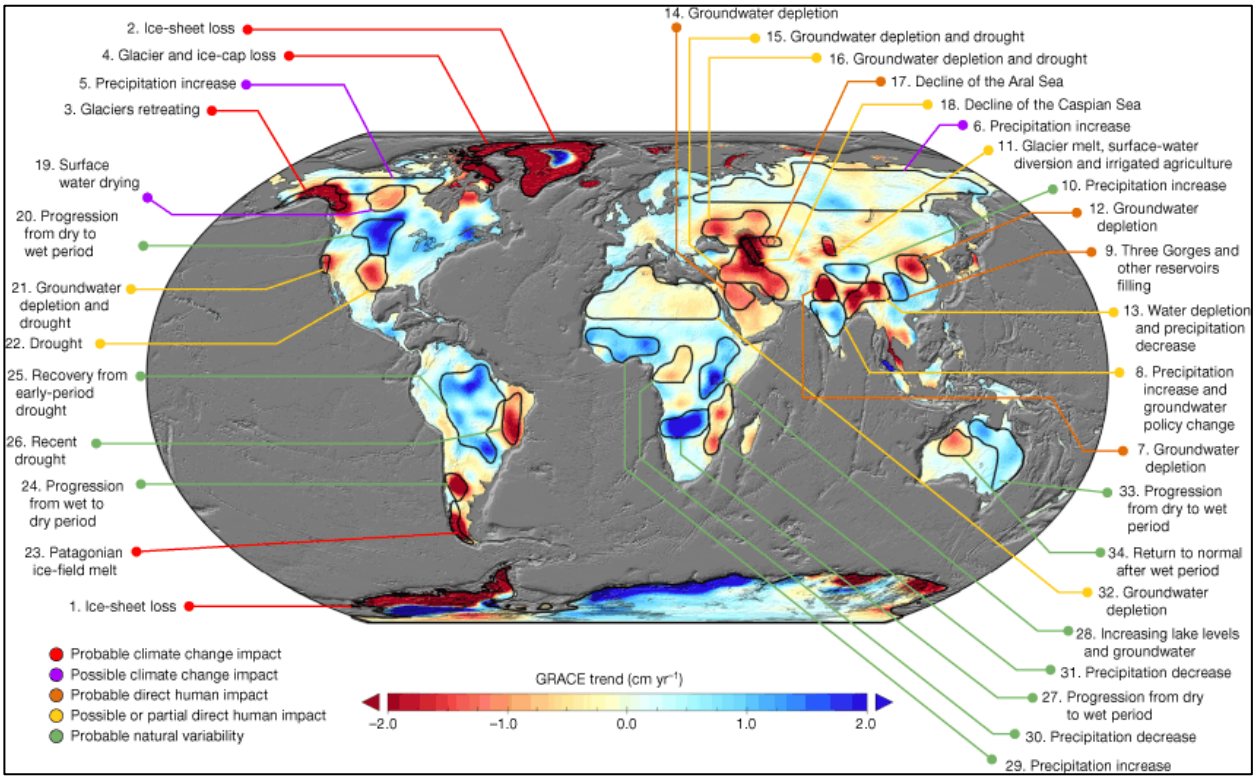

Figure 1.1: Global map of GRACE TWSA trends. (Source: Rodell et al., 2018)

Additionally, under different socio-economic and climate change scenarios, He et al., (2021) identifies India as the country facing the highest water scarcity in 2016 and in 2050 for urban population (**Figure 1.2**). The study concludes that the global urban population facing water scarcity will increase from 933 million in 2016 to 1.693-2.373 billion people in 2050. The study also predicts that out of total global urban population facing water scarcity in 2050, one fourth of it will belong to India.

The per capita water accessibility has fallen by 400% in the past 60 years (The World Bank, 2019; World Bank, 2010). Owing to these issues, it is critical to consider the changes in accessible water (i.e., surface water and groundwater) for all the major river basins in India, which are lifelines of India's economy (Asoka et al., 2018, 2017; Misra, 2014; Wada

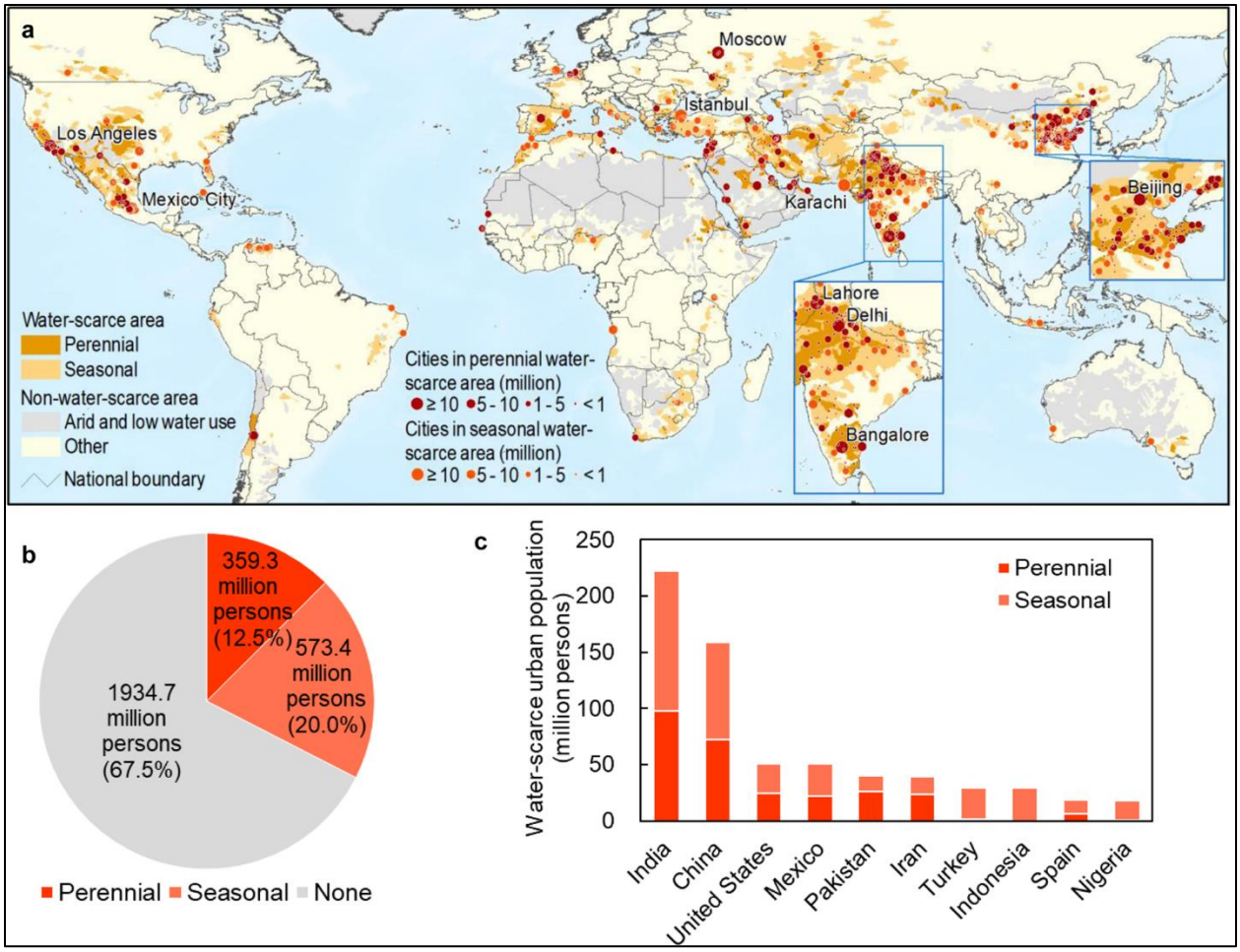

Figure 1.2: Global urban population water scarcity map. (Source: He et al., 2021)

et al., 2010). Agribusiness, a fundamental segment of the economy, represents 14% of India's Gross Domestic Product (GDP). A study by Bhanja and Mukherjee (2019) shows that despite the increasing precipitation, some regions display high rates of groundwater losses attributed due to excessive pumping. The anthropogenic impact on water utilization has triggered the impractical utilization of accessible water resources (Ashraf et al., 2017; Taylor et al., 2013b; Vörösmarty et al., 2000). While the studies in literature have focused on estimating trends in water balance components for a particular watershed or administrative boundary, the linkage of these trends based on land-cover distribution has not been explored in the Indian subcontinent (Mishra and Lilhare, 2016a; Soni and Syed, 2015; Syed et al., 2008).

Rodell et al., (2018) and He et al., (2021) only considers water quantity in their analysis and discussions of depleting water resources. But water quality also plays an equally important role in creating water scarcity. Even with the availability of water, if the water is not fit for domestic use and maintaining healthy watershed ecosystems, the water scarcity is going to be much more exacerbated. Vliet et al., (2021) performed a global

study analyzing the impact of including water quality parameters into water scarcity evaluations. The study found that majority of India faces extremely high-water stress and the impact intensifies by more than 20% if water quality is considered as well (**Figure 1.3**). Water quantity and quality were identified as equally important drivers of water scarcity for India.

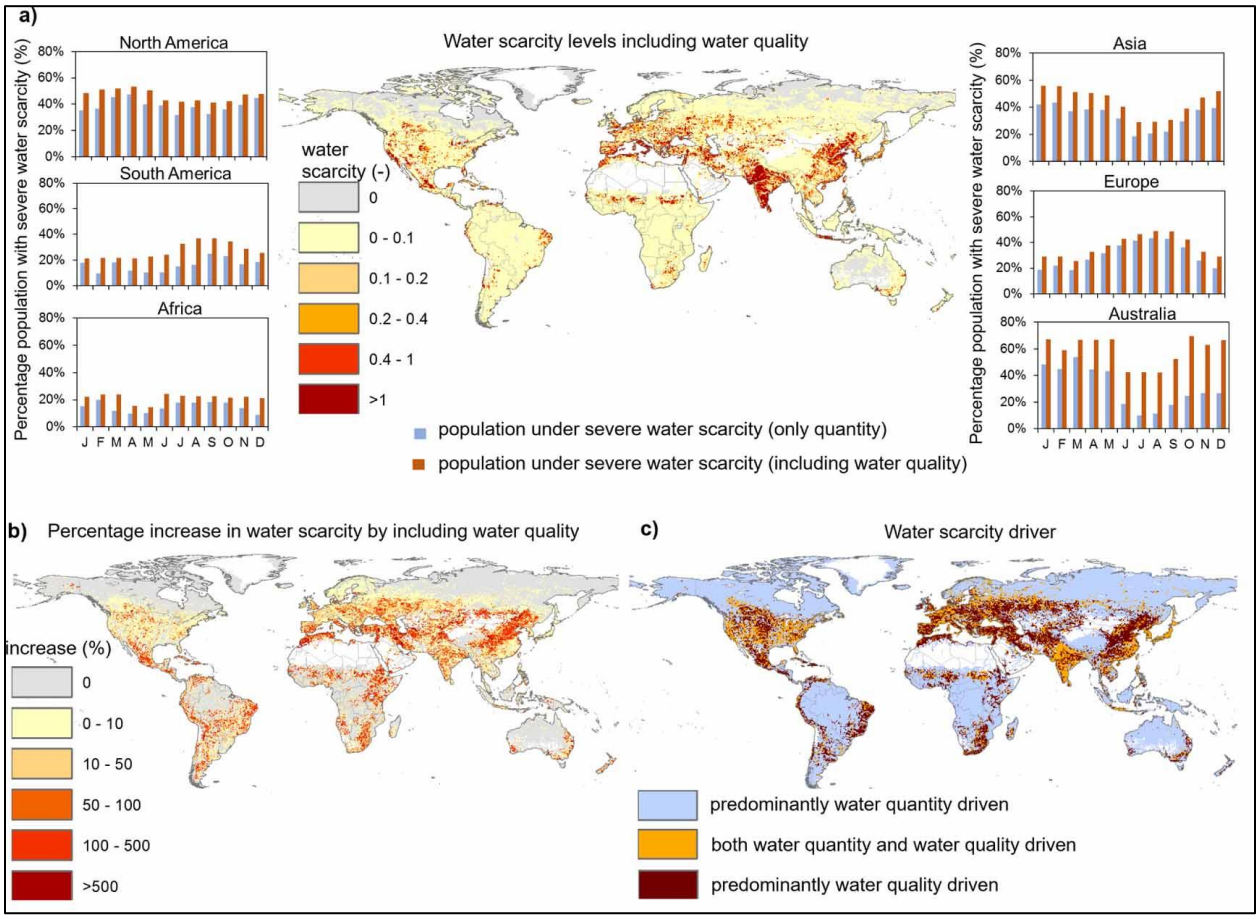

Figure 1.3: Global water scarcity map with contributing drivers. (Source: Vliet et al., (2021).

A deeper look into individual river basins is needed to understand the changes at watershed scale. River basins like Ganga and Narmada which are of extreme importance have shown high disruptions in water quantity and quality. For Ganga River basin, approximately 440 million people are directly or indirectly dependent on water that the Ganga and its tributaries provide for drinking, hydropower generation, navigation, industrial usage, ecosystem services, agriculture, and other anthropogenic activities. Among the anthropogenic activities, agricultural practices have the largest footprint in the Ganga Basin. The area of irrigated land has increased in the Ganga basin over the last 50 years, and it is estimated that presently 65% of the total catchment area in the river basin consists of agricultural land accounting for 3,61,100 km^2 of irrigated land (IIT

Consortium, 2015). It is noteworthy to mention that the Ganga River Basin also contributes to nearly 54% of the total crop production in India (*Agricultural Statistics at a Glance*, 2018). There is an emphasis on increased crop production to meet the food demand leading to a widespread application of Nitrogen (N) and phosphorus (P) based fertilizers in agricultural practices. For example, fertilizer consumption in the district levels of the Ganga River Basin has increased from 2 Gg (1 Gg = 10^9 g) in 1962-1965 to 102 Gg in 2003-2006 (IIT Consortium, 2015). In the central areas of the Ganga River Basin, the fertilizer consumption rate has increased from 300 Gg/yr (2006-2007) to 5000 Gg/yr (2019-2020), which is more than an order of magnitude (*Agricultural Statistics at a Glance*, 2019). The widespread application of fertilizer in agricultural fields leads to an increased overland flow consisting of N to the Ganga River. In addition to fertilizer consumption, the discharge of industrial and domestic effluents that has increased over the last few decades could also contribute to N and P contamination of water resources (https://www.gangaaction.org/). Moreover, the stored fertilizer in soils could also dominate the N runoff for years (Shukla et al., 2021). As a result, understanding the nutrient (N) dynamics in the Ganga River Basin is important for improved monitoring of the impact of anthropogenic activities.

Similarly, the Narmada River basin has undergone rapid changes in the past three decades with significant increase in agricultural lands, industries caused by development in this region due to the increasing population. The population in states of Gujarat and Madhya Pradesh covering majority of this river basin has increased by an average of 23% from 1991-2011 to approximately 132 million in 2011 (Census Bureau of India). Due to this increase in population, several regions in the Narmada River watershed are being polluted with point sources – sewage and industrial discharge as well as non-point sources - chemical fertilizers used in agricultural lands (Sharma et al., 2008).

In the context of Indian river basins, there are very limited studies that analyse the hydrologic fluxes and storages (Chen et al., 2014; Rodell et al., 2009a; Soni and Syed, 2015). One such study by Soni and Syed (2015) characterizes the role of hydrologic fluxes using the Total Water Storage (TWS) anomaly. The study concludes that groundwater storage is depleting in the Ganga whereas it is increasing in the Godavari and Krishna basins. A limitation to this study is that it only considers four of the major river basins of India (Ganga, Godavari, Krishna, and Mahanadi). Additionally, the study does not examine the relationship between the trends of water balance components and land cover type. Other studies (Chen et al., 2014; Rodell et al., 2009) mainly focus on North-western India where highly negative TWS anomalies have been observed thereby lacking the analysis of other parts of India.

For Ganga River basin, Whitehead et al. (2015) and Jin et al. (2015) conducted the first and only basin scale water quality study encompassing the Ganga Basin to study the impacts

of future climate and socio-economic impacts on N and P fluxes. But these studies used the INCA model for a limited past- time period of 1981-2000. For predicting the future changes in nutrient flows, Whitehead et al. (2015) and Jin et al. (2015) use RCP climate model predictions for the present century 2000-2100. Other modelling efforts in literature focus on sub-basins of Ganga River (Pathak et al., 2018). Similarly, nutrient monitoring studies which do not involve modelling have been carried out at a few select locations of the Ganga River Basin such as major cities along the banks, in Uttar Pradesh (Joshi et al., 2009; Sharma et al., 2014; Tare et al., 2003; Tiwari et al., 2016), in the delta region near the mouth of the river (Debnath et al., 2018; Mukhopadhyay et al., 2006; Sarkar et al., 2007) and a few studies focus on the Upper Ganga River (Jain, 2002; Matta, 2015). A comprehensive study of N variability through hydrological modelling using most recent in-situ observations is missing. This study is designed to help in understanding the extent and magnitude of N contamination from source to sink over a long-term record, which can aid in policymaking leading to better agricultural management practices.

For Narmada River basin, previous studies have focused solely on the components of the water cycle, viz. precipitation, evapotranspiration, soil moisture, infiltration, streamflow and total water and have not considered the transport of nutrients. Most of the studies in literature analyze nutrient contamination at specific sites inside the Narmada River basin, but there are no studies which analyse the nutrient contamination at the watershed scale (Gupta and Chakrapani, 2005; Rickards et al., 2020; Sharma et al., 2008).

In this dissertation, following broad research questions will be addressed:

i. Are the trends in hydrological variables linked to land-cover distribution for Indian river basins?
ii. For nutrient pollution in Ganga and Narmada River basin:
    a. What is the spatio–temporal variability of N concentrations across the entire Ganga and Narmada River basins through pre-monsoon, monsoon and post-monsoon seasons?
    b. What is the magnitude of increasing/decreasing trend in N fluxes exported from the Ganga Basin to Bay of Bengal and from the Narmada Basin to Arabian Sea?

Chapter 2: Estimation of land-cover linkage to trends in hydrological variables of river basins in the Indian sub-continent using satellite observation and model outputs[1]

2.1 Introduction

India has a strong monsoonal influence which implies that most of India receives over half of the annual precipitation during the four monsoon months between June and September. This likewise suggests that roughly 80% of the streamflow occurs between June and September (Kripalani et al., 2003; Krishnamurthy and Kirtman, 2009). After all the surface water has been spent, individual farmers resort to harvesting rainwater storages and pumping groundwater to meet their water demands. There is a need for management and planning of how the water will be utilized after the rainfall season, specifically with a focus on the river basins that receive low precipitation. To carry out such planning, it is necessary to monitor the changes in the seasonal patterns of the components of water balance - precipitation (P), runoff (R), evapotranspiration (ET), and water storage.

The Indian population of roughly 1.3 billion individuals relies upon agriculture for food and livelihood as cultivable land is the principal source of financial security (https://www.indiawaterportal.org/topics/agriculture). The per capita water accessibility has fallen by 400% in the past 60 years (The World Bank, 2019; World Bank, 2010). Owing to these issues, it is critical to consider the changes in accessible water (i.e., surface water and groundwater) for all the major river basins in India, which are lifelines of India's economy (Asoka et al., 2018, 2017; Misra, 2014; Wada et al., 2010). Agribusiness, a fundamental segment of the economy, represents 14% of India's Gross Domestic Product (GDP). A study by Bhanja and Mukherjee (2019) shows that despite the increasing precipitation, some regions display high rates of groundwater losses attributed due to excessive pumping. The anthropogenic impact on water utilization has triggered the impractical utilization of accessible water resources (Ashraf et al., 2017; Taylor et al., 2013b; Vörösmarty et al., 2000). Additionally, there have been studies that show the various sectors of the water usage (Aerts et al., 2006; Asoka et al., 2018; MacDonald et al., 2015; Shah et al., 2016). This has further influenced the harvest designs in various river basins (MacDonald et al., 2016; Taylor et al., 2013a). Yield patterns of crops primarily

[1] Kansara, P.; Lakshmi, V. Estimation of land-cover linkage to trends in hydrological variables of river basins in the Indian sub-continent using satellite observation and model outputs J. Hydrol. 2021, https://doi.org/10.1016/j.jhydrol.2021.126997

correspond to the seasonal precipitation cycle and sudden changes to this seasonal cycle (particularly the monsoon season) represent a threat especially to the rural communities of the country.

In the context of Indian river basins, there are very limited studies that analyse the hydrologic fluxes and storages (Chen et al., 2014; Rodell et al., 2009a; Soni and Syed, 2015). One such study by Soni and Syed (2015) characterizes the role of hydrologic fluxes using the Total Water Storage (TWS) anomaly. The study concludes that groundwater storage is depleting in the Ganga whereas it is increasing in the Godavari and Krishna basins. A limitation to this study is that it only considers four of the major river basins of India (Ganga, Godavari, Krishna, and Mahanadi). Additionally, the study does not examine the relationship between the trends of water balance components and land cover type. Other studies (Chen et al., 2014; Rodell et al., 2009) mainly focus on the North-western India where highly negative TWS anomalies have been observed thereby lacking the analysis of other parts of India. In order to examine the impact of different water balance components influencing water resources, numerous studies have been carried out in India and across the globe. These include research that have detailed the impacts of environmental change and population rise that have made water security, an important issue in the river basins of India, China, Greece, and United States (Barnett et al., 2004; Christensen et al., 2004; Fishman et al., 2011; Gemitzi and Lakshmi, 2018; Piao et al., 2010; Shah, 2009). A worldwide investigation of accessible water by Lakshmi et al. (2018) presents an extensive spatial and temporal examination of the hydrological factors related to water budget for significant river basins across various continents with different climate and ecological conditions. A study by Rodell et al. (2018) attributes the drivers of changes in total water into interannual variability, groundwater utilization, and environmental change. Because of climate change, there are more frequent extreme precipitation events and land surface and sea surface temperatures are exhibiting positive anomalies (Kingston et al., 2011; Kite, 2001; Mishra and Lilhare, 2016b; Ragab and Prudhomme, 2002). Around 5.6 million people in India will be inhabiting exceptionally water-scarce regions by 2055 (Arnell, 2004). This issue has initiated discussions around the world that are not simply restricted to India, on issues related to water security (Babovic et al., 2018; Kundzewicz et al., 2007; Nazemi and Madani, 2018). A few research studies have also called attention to the excessive usage of groundwater on a global scale (Alcamo et al., 2007; Oki and Kanae, 2006; Wada et al., 2012).

Satellite datasets indirectly measure the actual physical quantities from space and they do not matchup perfectly to in-situ observations. These hydrological variables have been validated at global scale with in-situ observations, but sufficient validation at watershed scales (especially in India) are lacking in the literature. For instance, precipitation is sufficiently validated for the Indian subcontinent (Mondal et al., 2018a). Mondal et. al (2018) found that TRMM TMPA (Tropical Rainfall Measuring Mission TRMM Multi-

Table 2.1: Information on the different datasets used in our study.

Variable		Data Sensor	Spatial resolution	Data Availability	Information
Terrestrial Water Storage Anomaly	ΔS	GRACE	0.5°	Apr 2002 – Oct 2017	Tapley et al. (2004b)
		GRACE-FO	0.5°	May 2018 - Present	
Total runoff	R	GLDAS	0.25°	1979 - Present	Mitchell et al. (2004)
Precipitation	P	TRMM	0.25°	1998 - Present	Huffman et al. (2010)
Evapotranspiration	ET	MODIS	500 m	2000 - Present (Terra) 2002 - Present (Aqua)	Mu et al. (2007)
Digital Elevation Model		SRTM	30 m	2000	Farr et al. (2007)
Land-cover		CCI	300 m	1998-2018 (annually)	Liu et al. (2018)

(PERSIANN) also shows good agreement in terms of annual and monsoonal trends with IMD in-situ observations. TMPA product showed the lowest mean Root Mean Squared Error (RMSE) of 25 to 50 mm for majority of Central, Southern, and North-Western India (Mondal et al. 2018). They reported correlation coefficients between 0.8 to 1 for all regions in India except the Northern Himalayas. The study concluded that TMPA and PERSIANN can be reliably used in hydrological and climate studies in the river basins of India. For runoff, there are no validation studies performed that are specific to the Indian subcontinent. There are two reasons for the lack of such studies: 1) Validation of GLDAS runoff requires building a land surface water routing model, and 2) There is a lack of publicly available in-situ streamflow observations in the Northern, North-Western and North-Eastern parts of India. These regions contain transboundary river basins which includes the Ganga, the Brahmaputra, and the Indus River and hence the Central Water Commission (CWC) of India does not publicly share streamflow observations for these river basins.

The fundamental objective of the current research is to address the following question: Are the trends in hydrological variables linked to land-cover distribution?

2.2 Data and Study Area

2.2.1 Indian major river basins

In our study, we analyse nine major river basins: Brahmaputra, Cauvery-Pennar, Ganga, Godavari, Indus, Krishna, Mahanadi, Narmada-Tapti, and Sabarmati-Mahi (**Figure 2.1**). We selected the river basins with an area greater than 50,000 km^2 to avoid the complexities from Gravity Recovery And Climate Experiment (GRACE) estimates due to its coarse resolution. These nine river basins represent diverse topography, land-cover distributions, size of the watershed, climate, and weather patterns across India. For the trans-boundary river basins, we only consider the areal extent inside India to observe the changes occurring in these watershed systems. A detailed list of all datasets used in this study are provided in **Table 2.1**. There have been very few previous studies (Bhuvaneswari et al., 2013; van Beek et al., 2011a) on each of the individual basins (**Table 2.2**), and a comprehensive study of all major river basins in India has not been conducted in the last decade.

2.2.2 GRACE and GRACE-FO

In our study, we use GRACE RL06 product and GRACE-FO RL06 product from NASA Jet Propulsion Laboratory (JPL), Geoforschungszentrum (GFZ), and Center for Space Research at University of Texas, Austin (CSR) for terrestrial water storage anomalies (TWSA) (Syed et al., 2008). Ensemble mean of products from all three organizations was used to reduce the uncertainty in the processing algorithms but this does not improve the resolution of the data. The data is available at a spatial grid of 0.5^o and a temporal resolution of one month (https://grace.jpl.nasa.gov/data/grace_months/) for the terrestrial water anomalies. These anomalies depict the changes in the total water column of Earth which includes surface, sub-surface, and groundwater components (Syed et al., 2008). GRACE has been used in numerous regional (Swenson et al., 2003; Swenson et al., 2009; Voss et al., 2013) and continental scale (Schmidt et al., 2006; Tapley et al., 2004a; van Beek et al., 2011) water budget studies.

2.2.3 TRMM

The Tropical Rainfall Measuring Mission (TRMM) satellite was launched in 1997 to study tropical and subtropical rainfall (Kummerow et al., 2000; Simpson et al., 1996). We used the Version – 7 TMPA (TRMM Multi-satellite Precipitation Analysis) product for our study. This product is the most widely used TRMM product and is available at 0.25° spatial resolution covering the region between 50°N - 50°S latitudes at a daily temporal repeat from 1998 to the present. Several studies have evaluated TRMM TMPA accuracy using gauge precipitation data over different parts across the world including South America (Rozante et al., 2010), Kyrgyzstan (Karaseva et al., 2012), Tibetan Plateau (Xu et

al., 2017), Indonesia (Prasetia et al., 2013), China, (Li et al., 2013) and India (Kirtsaeng et al., 2011; Mondal et al., 2018; Prakash et al., 2014; Shah et al., 2016).

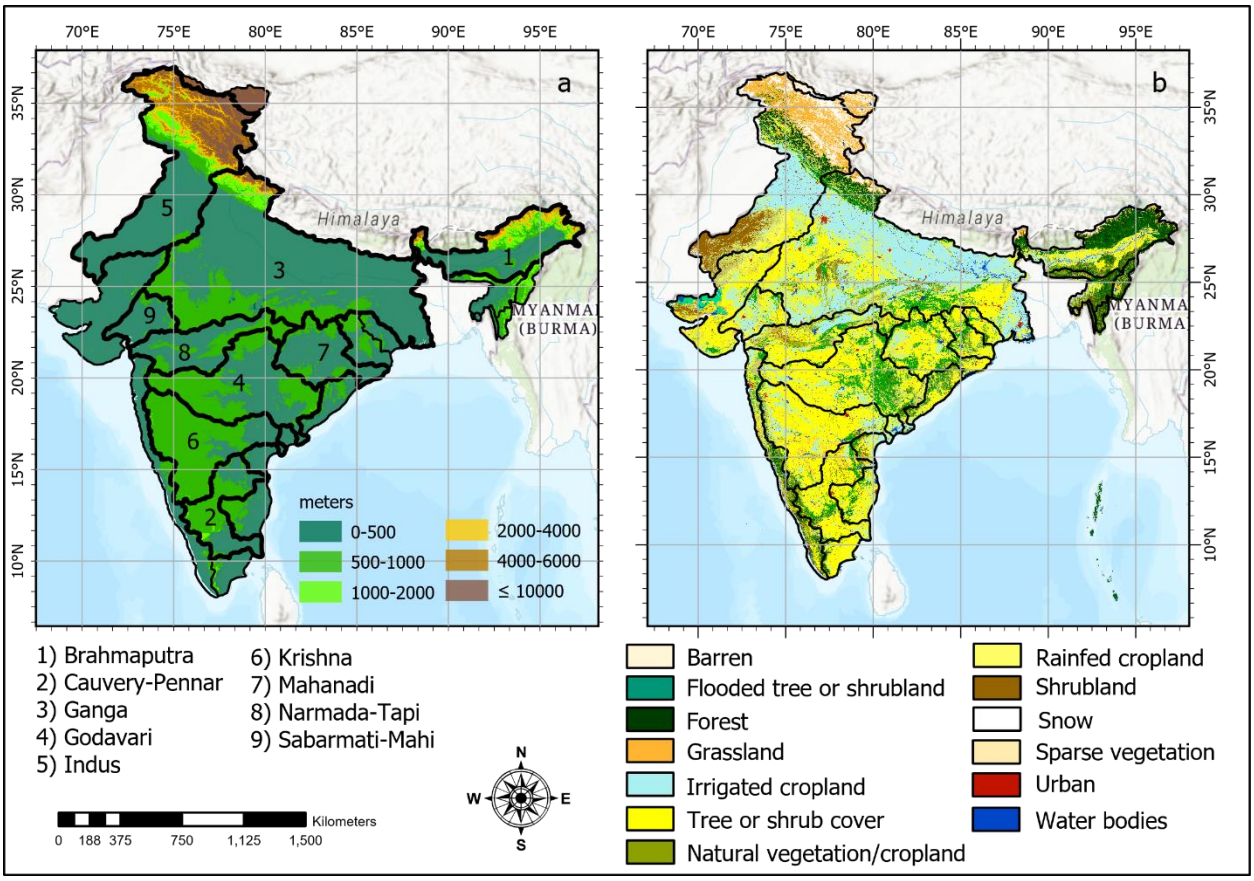

Figure 2.1 (a-b): (a) The nine major river basins in India studied in our work along with the elevation distribution. (b) Land-cover distribution map of India for 2010 (European Space Agency).

2.2.4 GLDAS

Global Land Data Assimilation System (GLDAS) is an assimilation model which combines satellite and ground-based observational data products through different land surface models to generate land surface states and fluxes at the global scale (Rodell et al., 2004). Five different land surface models - NOAH, Variable Infiltration Capacity (VIC), MOSAIC, Common Land Model (CLM), and Catchment are used for assimilation. We decided to use Noah derived runoff as it has better performance compared to the other model outputs (Bai et al., 2016; Lohmann et al., 2004; Zaitchik et al., 2010). Apart from the comparison between different GLDAS model outputs, these studies also validate it at several regional scales in different parts of the world. Since, a study does not exist which

validates GLDAS output for Indian watersheds, we performed validation with observed data in order to assess its performance. GLDAS-Noah model outputs are simulated by NASA Goddard Space Flight Center (GSFC). In this study, we only use the model outputs generated at NASA GSFC. Further information on forcing inputs to GLDAS models can be found on https://ldas.gsfc.nasa.gov/gldas/forcing-data. In this study, we use total runoff (surface runoff + baseflow) output from the GLDAS V2.1 assimilated data simulated from NOAH LSM model L4 with a spatial resolution of 0.25^{o} at a monthly time step. This dataset has been validated at different locations with in-situ observation data (Bai et al., 2016; Kim et al., 2018; Li et al., 2015); for runoff, soil moisture, ET, and several other hydrological variables. Since this dataset provides modelled outputs for 36 different hydrological variables at a global scale, it is frequently used in the studies of the data-sparse region and continental-scale studies (Lorenz et al., 2014; Zawadzki et al., 2014).

2.2.5 MODIS

Moderate Resolution Imaging Spectroradiometer (MODIS) is the main sensor on the Terra and Aqua satellites launched by NASA in 1999 and 2002, respectively. The MODIS sensor observes surface brightness temperature in 36 spectral bands which is used in imaging the atmosphere, land, and ocean. We used the MOD16A2 product which provides ET estimates, based on the Penman-Monteith method (Mu et al., 2011). MOD16A2 is available at 500 m and 8-day temporal resolution. Validation has been performed for different parts of Asia and Australia for the ET estimates based on MODIS (Cleugh et al., 2007; Kim et al., 2012).

2.2.6 Climate Change Initiative (CCI) Land-cover

European Space Agency (ESA) started the CCI program which provides land-cover maps from 1998-2018 at a native spatial resolution of 300 m (European Space Agency). These spatial maps are produced globally.

2.2.7 Uncertainties associated with satellite observations and model outputs

Satellite data uncertainties are dependent on the retrieval algorithm as well as the spatio-temporal scale affected by the cloud cover reflectance, thermal radiance, and infrequent satellite overpasses (AghaKouchak et al., 2009; Chang et al., 1997; Hossain et al., 2006; Morrissey and Greene, 1998). Precipitation data from TRMM has seasonal as well as spatial bias when compared to the rain gauge station data obtained from the Indian Meteorological Department (Le et al., 2018; Shukla et al., 2019). Topography and local climate conditions predominantly affect the uncertainties in the TRMM estimates (Bharti et al., 2015). Further, modelled data provides runoff which has been validated at global and continental scales, but these datasets underperform at the regional scale. There are issues with MODIS evapotranspiration as it underestimates the ET, as found in several studies conducted across the globe (Aguilar et al., 2018; Du et al., 2018; Tang et al., 2015).

In addition to the uncertainty in precipitation, ET, and modelled runoff, GRACE derived Total Water Storage Anomalies has errors in estimation errors. These errors are in the form of monthly gravity field solutions and the error caused by detecting mass changes other than the mass water storage changes (Swenson and Wahr, 2006; Wahr et al., 2006). These satellite datasets with coarse resolutions of the order of tens of kilometres can lead to unsatisfactory consistency issues. While precipitation and runoff data are available at 0.25˚, evapotranspiration data is available at a spatial resolution of 500 m, and the best available resolution for GRACE TWSA is 0.5˚. To reduce the uncertainty from using a single GRACE product, we have used an ensemble of all three GRACE products – GFZ, CSR, and JPL. Seo et al., (2009) concluded that the coarse resolution of GRACE can provide inaccurate results, especially for basins smaller than 90,000 km^2. In reference to our study, only the Sabarmati-Mahi River basin (the smallest river basin in our study)

Table 2.2: Characteristics of each river basin.

Basin name	**Previous Studies**	**Area inside Indian territory (km^2)**	**Climate**	**Location of Centroid (Lat, Lon)**	**Average annual rainfall (mm)**	**Average Air temperature (°C)**
Brahmaputra	Beek et al. 2011	200,677	Tropical Monsoon	27.24, 93.18	2602	22
Cauvery - Pennar	Bhuvaneswari et al. 2013	145,418	Humid rainy	14.45, 78.31	998	24
Ganga	Syed et al. 2014	840,111	Tropical Monsoon	25.87, 80.84	1062	23
Godavari	Biemans et al., 2013	312,878	Tropical Rainy	19.53, 78.87	1116	25
Indus	Hussain et al. 2011	470,262	Semi-arid	31.56, 75.07	825	23
Krishna	Bouwer et al. 2008	262,633	Tropical Rainy	16.49, 76.49	962	27
Mahanadi	Santra Mitra et al., 2015	143,971	Tropical Rainy	21.26, 83.09	1403	24
Narmada - Tapi	Shah et al 2016	161,764	Tropical Dry	22.44, 77.39	1002	28
Sabarmati-Mahi	Kumar et al. 2008	72,170	Arid	23.21,72.68	790	29

has an area of 72,170 km^2. For the Sabarmati-Mahi, sixteen pixels cover the river basin. We found that the GRACE TWSA has a fairly good correlation with P-ET-R, and the peaks and lows of the time series correlate well for the Sabarmati-Mahi River basin.

Finally, we wanted to make our study consistent by including all the major river basins of India, hence we have not excluded them from our analysis owing to issuing arising from the GRACE spatial resolution.

2.3 Methodology

Our analysis is divided into four parts: Validation of the data sets, seasonal analysis of the water budgets, seasonal singular value decomposition and trend analysis and linkage between water balance components and land cover.

2.3.1 Validation of datasets

For the analysis in this study, satellite datasets for precipitation were used in addition to modelled outputs for evapotranspiration and runoff. In this study, we performed validation of GLDAS based runoff with streamflow data obtained from Global Runoff data (Do et al., 2017). The observed in-situ data was compared with GLDAS modelled runoff output using correlation coefficients and paired significance t-test as building a runoff routing model was beyond the scope of this study. A total of 310 stations were used for the validation process which were located in Central, Western, and Southern India.

2.3.2 Seasonal analysis and water budget using P-ET-R and ΔS

To observe the seasonality in water balance components, we plotted the boxplots of each with their monthly distribution during a year. These boxplots represent the median variation of the corresponding monthly values along with its 25% and 75% distribution, and minimum and maximum values for a corresponding month.

The following equation gives the water balance of a river basin -

$$\overline{P} - \overline{ET} - \overline{R} = \overline{\Delta S} \quad (1)$$

Where $\overline{P}$, $\overline{ET}$, $\overline{R}$, and $\overline{\Delta S}$ are monthly averaged values for P (precipitation), ET (evapotranspiration), R (runoff), and changes in water (surface and sub-surface) storage, separately for each river basin. If there exists a significant anthropogenic influence in a river basin, we must incorporate this influence in Equation (1) to consider the water withdrawal for irrigation and household use (Haddeland et al., 2014; Querner, 2000; Veldkamp et al., 2017). Since the withdrawal term is small in comparison with ΔS, we have disregarded it in the water balance computation (similar to Lakshmi et al. 2018). In many cases, there would be a lag between precipitation and runoff (or changes in sub-surface), hence we perform a lagged analysis to determine the most suitable relationship between the (P-ET-R) and TWSA time series. To calculate the R-squared values, we assigned lag between 0 to 6 months to the GRACE TWSA and calculated the Pearson correlation coefficient between P-ET-R and lag-assigned TWSA.

2.3.3 Seasonal Singular Value Decomposition and trend analysis

To understand any inherent co-variability and patterns in the water balance, we performed Singular Value Decomposition (SVD) on two individual datasets: P-ET-R and TWSA for every season. SVD is used to analyze the coupled variability in these two datasets (Bretherton et al., 1992; Wallace et al., 1992). In order to perform SVD analysis, we calculate the spatial cross-covariance matrix of the whole grid. If we consider a data field A with M spatial grid points and N temporal observations (seasonal summation for each year), we can write the SVD data matrix as (Equation (2)):

$$[SVD] = [A][W] \quad (2)$$

Where [A] is an (N x M) matrix (N observations with M grid points)

[SVD] is an orthogonal projections matrix with the shape of (N x N) matrix (N SVD components with N observations), and

[W] is a weight matrix with the shape of (M x N) (N singular values with M variable weights).

The components of [SVD] matrix are orthogonal, linear projections that represent the directions of greatest variability. The singular vectors corresponding to [W] matrix are the loadings corresponding to each SVD component. The magnitude of these singular vectors represents the variance explained by the corresponding component.

As indicated by the Indian Meteorological Department (IMD), there are four seasons in India – Pre-monsoon, Southwest monsoon, Post-monsoon, and Winter. The Pre-monsoon season includes the months from March to May; the Southwest Monsoon season is from June to September; the Post-monsoon season is from October to December; and the Winter season includes the months of January and February.

In addition to the spatial patterns, we analysed the seasonal trends in each water balance components to examine the temporal variability. Since our datasets exhibit annual seasonality, we chose to use the Seasonal Mann-Kendall test (Hirsch et al., 1982) to examine monotonic patterns. The slope for the monotonic trends was determined utilizing Sen's slope estimator. The trend results are significant at $p < 0.05$. Spatial averaging was performed over the river basins for each season to conduct the test.

2.3.4 Analyze the linkage between water balance components and landcover

We classified the landcover distribution for each river basin into major land-cover types. We used land cover maps from 2002 and 2018 to compare the differences in the percentage of each land-cover type for the nine major river basins. Since the resolution of the land-cover map is much finer (300 m), we aggregate the land-cover pixels at 300 m to the GRACE pixels at 0.5°. The aggregation was done based on 'majority' statistic for land

cover types in that pixel. We further use this information to link these land-cover types with the increasing and decreasing patterns of TWSA.

The satellite datasets we use in the study have different spatial resolutions. While P and R information have the same spatial resolution of 0.25˚, MODIS ET is at 500 m, Land-

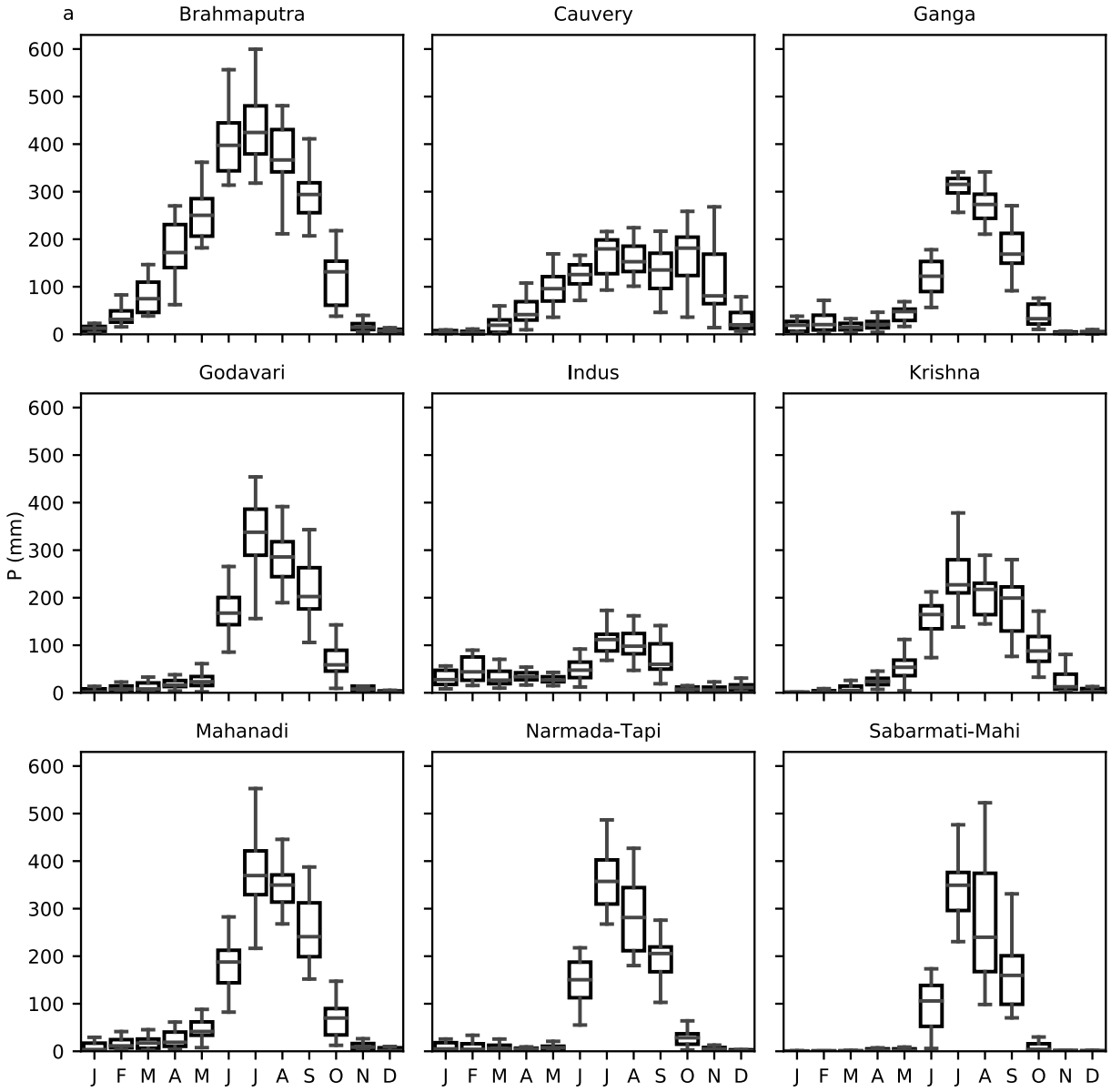

Figure 2.2 (a-c): (a) Boxplot of monthly distribution of P in the nine major river basins during a year. (b) and (c) represent monthly distribution of ET and R respectively. The annual cycle in the figure is shown from the months of January to December. The box represents the upper quartile (75%), median and lower quartile (25%) of the dataset and the whiskers extend outside of the box to represent the minimum and maximum values of that particular month during the period of analysis.

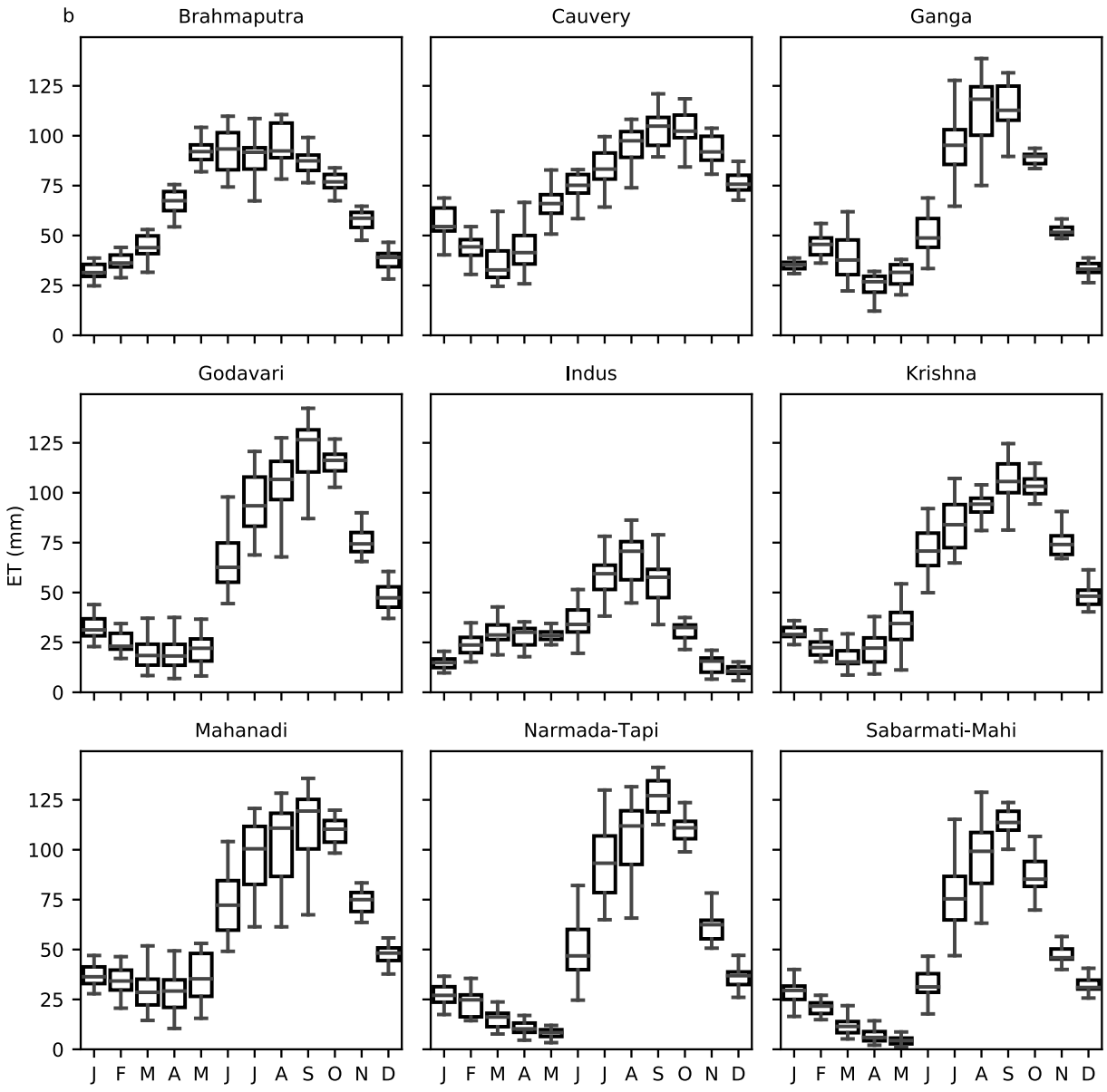

Figure 2 (continued)

cover at 300 m, DEM at 30 m, and GRACE TWSA are at a spatial resolution of 0.5°. Considering the low spatial resolution of the GRACE dataset, we upscaled the P, ET, R, land-cover, and DEM values to a spatial resolution of 0.5°. We used averaging as the aggregation method for upscaling. We used GRACE TWSA at its native resolution of 0.5°.

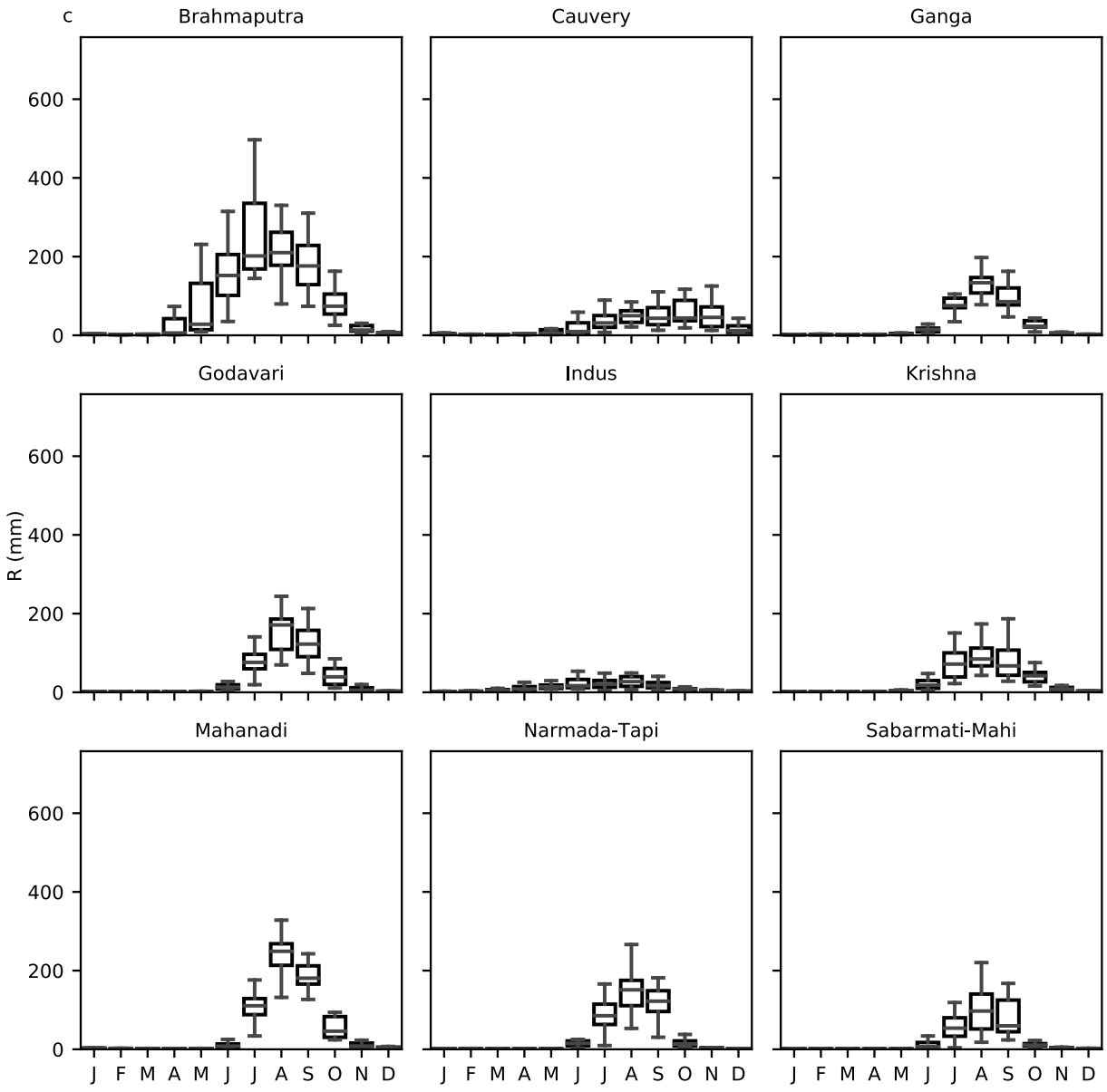

Figure 2 (continued)

2.4. Results

2.4.1 Seasonal cycle

Dominant seasonal variations are a significant characteristic of the hydrology of Indian river basins. To understand these seasonal variations, we examined the mean monthly precipitation, evapotranspiration, and runoff for the study period at their native spatial resolution (2002-2019) (**Figure 2.2**). The boxplot shows the measure of five statistics (minimum, maximum, upper (75%) and lower (25%) quartile, and the median). From the

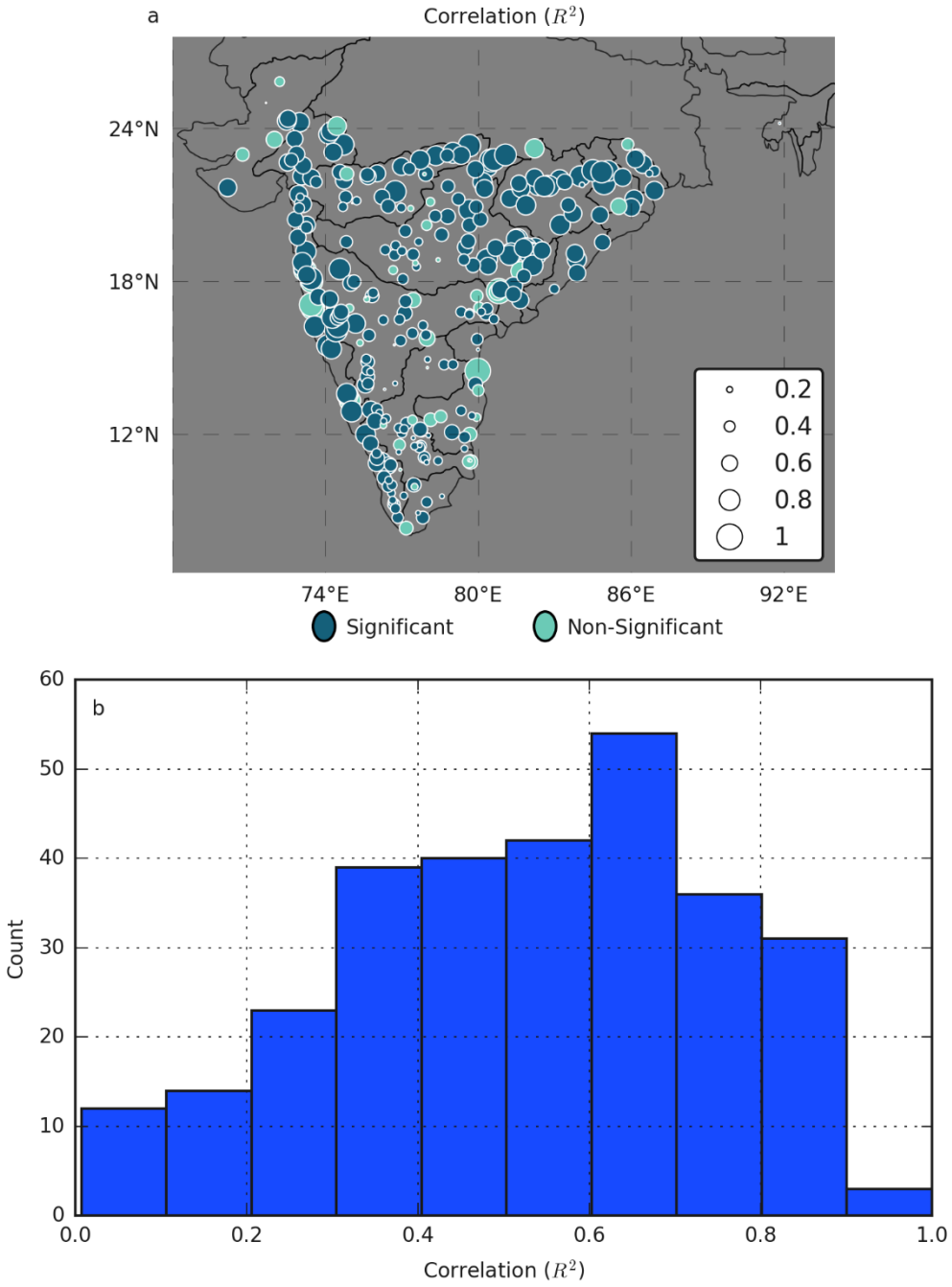

Figure 2.3 (a-b): (a) Correlation coefficient of each gauge locations for comparison of GLDAS R and in-situ streamflow measurement (Do et al., 2018). The significance level was calculated at $p \leq 0.05$. (b) Distribution of correlation coefficient across all stations.

plots, we observe that all river basins receive most of their precipitation during the months corresponding to the Monsoon i.e. June to September. The Brahmaputra River

basin receives a median precipitation of 400 mm in June, 427 mm in July, 366 mm in August, and 296 mm in September of the annual total of 2130 mm, and 1489 mm falls between June to September. On the other hand, for the Indus River basin with the lowest annual precipitation of 525 mm, it receives 51 mm in June, 108 mm in July, 103 mm in August, and 69 mm in September which amounts to 330 mm between June to September. Further, we observe that Mahanadi River and Sabarmati-Mahi River show high variability in precipitation (~300-350 mm) for July and August, respectively corresponding to the Monsoon season. Godavari and Krishna River basins receive annual rainfall of 1121 mm and 977 mm respectively with much less precipitation (<50 mm) during non-monsoon months. The Indus and Ganga River basins receive snowfall at higher elevations during the winter months which can be seen from the precipitation in January and February. Similarly, we observe that runoff for all the river basins follow the variability similar to precipitation, implying higher runoff values corresponding to monsoon months and relatively lower runoff for the rest of the year. Boxplots of ET do not follow any particular pattern although we observe relatively higher values during monsoon (summer) months.

4.2 Hydrological water balance

Firstly, GLDAS generated runoff was validated with observed streamflow (**Figure 2.3**). We found that GLDAS generated runoff had mean correlation (R2) of 0.53 across all the stations. For ET, India does not have an established flux network. Hence, we did not perform a validation for MODIS ET products. We examined the TWSA derived from GRACE and P-ET-R from individual satellite observations and model output to consider the annual cycle of the water balance components for every river basin from 2002 to 2019 (**Figure 2.4**). The time series in most of the river basins exhibit seasonality with the P-ET-R and TWSA having maximum values during the monsoon season with the exception of the Indus and Cauvery River basin where we do not observe strong seasonality. TWSA lags P-ET-R in a several of the river basins, with all river basins indicating a one-month lag except the Indus River basin which does not show any lag (**Table 2.3**). To evaluate the direct relationship between P-ET-R and TWSA, we calculated the Pearson relationship coefficients at a 5% significant level for each river basin. The Ganga River basin alongside the Southern and Western India river basins show a higher relationship (R^2 >0.5) while Indus shows a lower value (R^2 <0.3) significance at a p-value of 0.05 (**Table 2.3**). Two potential reasons that these river basins show higher correlation could be due to either low human intervention in the river basin or due to high recharge rate for the watershed which can be caused by higher precipitation. In the case of a developing country such as India with a high population density, it is unlikely for the former to be the explanation

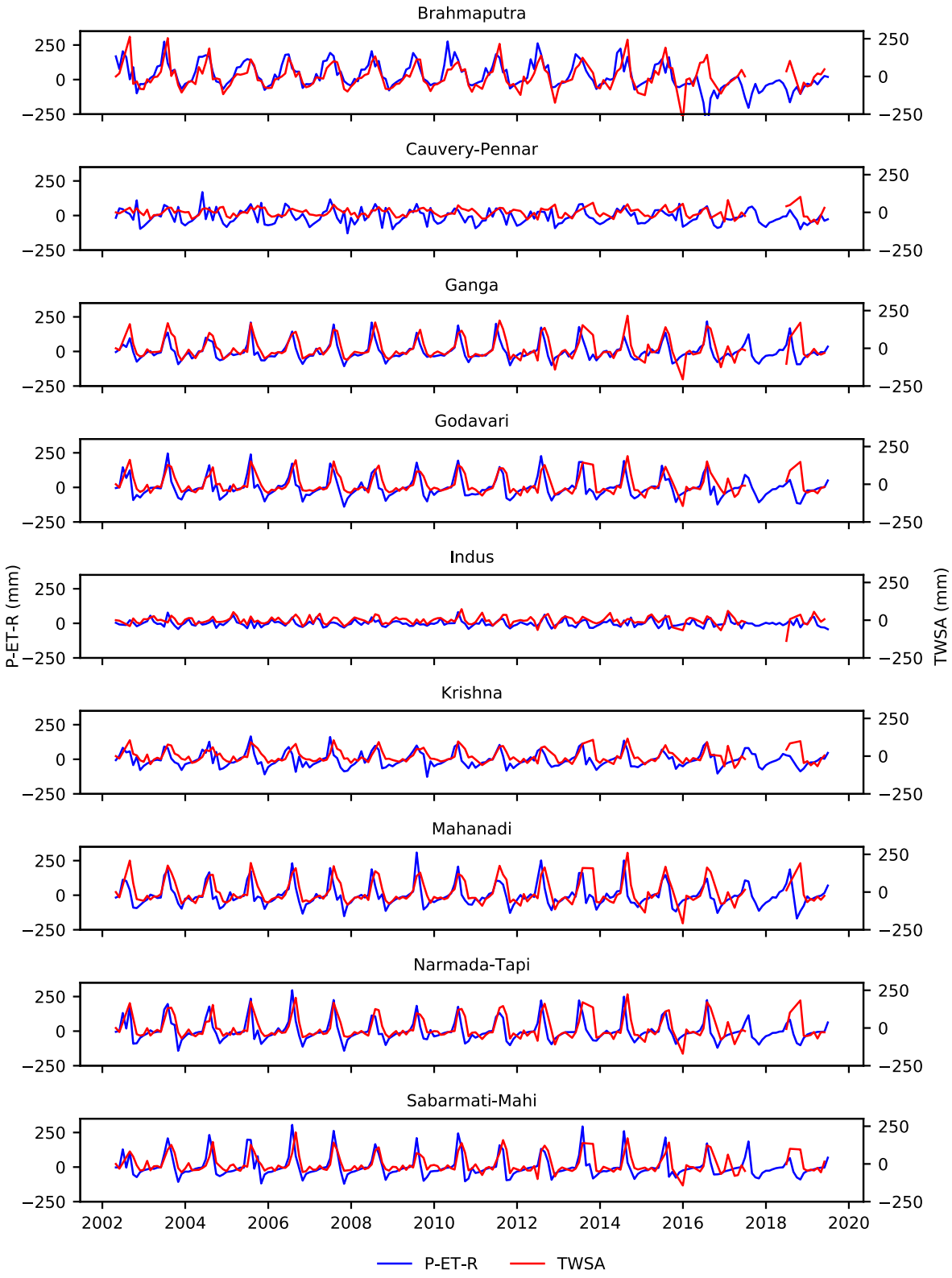

Figure 2.4: Time series of the water balance components showing the time correlation of P-ET-R with TWSA.

for the higher correlation (i.e. human intervention will exist). Normally, river basins with tropical and subtropical climatic conditions show high relationship similar to the case in our examination (Godavari (R^2 = 0.60) and Ganga (R^2 = 0.54)) while the Indus River basin shows a lower R^2 of 0.25. The two semi-arid river basins in Western India - Narmada-Tapti (R^2 = 0.59) and Sabarmati-Mahi (R^2 = 0.57), display correlation coefficients similar to the tropical river basin like Ganga (R^2 = 0.54), which can be ascribed to increased precipitation in Western India over the previous decade (Asoka et al., 2017).

Table 2.3: Correlation lag analysis results for each river basin. Average values represent the spatially averaged monthly mean values for each river basin.

Basin	**R^2**	**Lag**	**Avg. P (mm)**	**Avg. ET (mm)**	**Avg. R (mm)**
Brahmaputra	0.31	1	185	68	91
Cauvery-Pennar	0.33	1	91	73	27
Ganga	0.54	1	90	60	31
Godavari	0.60	1	98	62	36
Indus	0.25	0	46	33	12
Krishna	0.50	1	85	59	29
Mahanadi	0.57	1	116	65	52
Narmada-Tapi	0.59	1	90	56	33
Sabarmati-Mahi	0.57	1	75	46	24

4.3 Seasonal SVD analysis

We plotted the first orthogonal components obtained using singular value decomposition for determining spatial patterns in P-ET-R and TWSA (**Figure 2.5**). The dark red and dark green coloured regions in the map depict regions which explain the most variability in the corresponding seasons over entire India. For the Winter season, variability in Northern India is strongly coupled with Southern India. Since these two regions have opposite signs for their corresponding eigenvector components, increase or decrease in one region implies a corresponding decrease or increase of P-ET-R in the other region. Similarly, the Pre-Monsoon season depicts weak coupling of North-Eastern India with Central and North-Western India. For the Monsoon season, we found that the Western coast of India and Southern part of the Brahmaputra River basin have strong co-variability whereas there is weak co-variability associated with the other parts of India. It is important to note that there is strong variability in the Brahmaputra River basin during Pre-Monsoon season which dominates the water storage changes led by significant changes in precipitation. Lastly for the Post-Monsoon season, we observe that the variability can be attributed majorly to Central India. In addition, it is interesting to

note that the inherent spatial patterns in TWSA are inconsistent with the inherent spatial patterns in P-ET-R. This difference in spatial pattern is attributed to the anthropogenic interactions causing disruptions in the total water storage. For the principal components in TWSA, we observed highly negative dominant loadings for Winter, Pre-Monsoon, and Post-Monsoon seasons in North-Western India. These inherent patterns again suggest that North-Western India faces an acute problem of decreasing TWSA over the past two decades. Similar negative loadings are observed for Eastern India (states of Bihar, and West Bengal) but high positive loadings in the Pre-Monsoon season for this region offsets the negative impacts of decreasing TWSA.

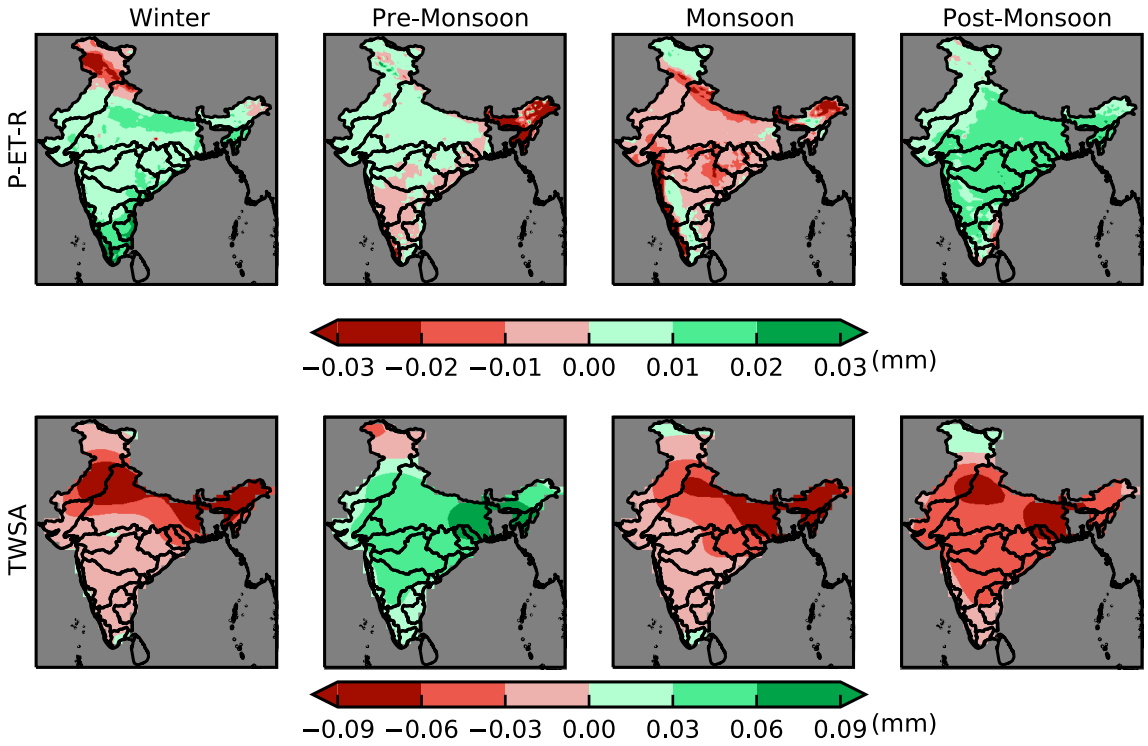

Figure 2.5: First principal component loading of P-ET-R and TWSA for whole India. These loadings represent the eigenvectors corresponding to each pixel obtained from Singular Value Decomposition of P-ET-R dataset.

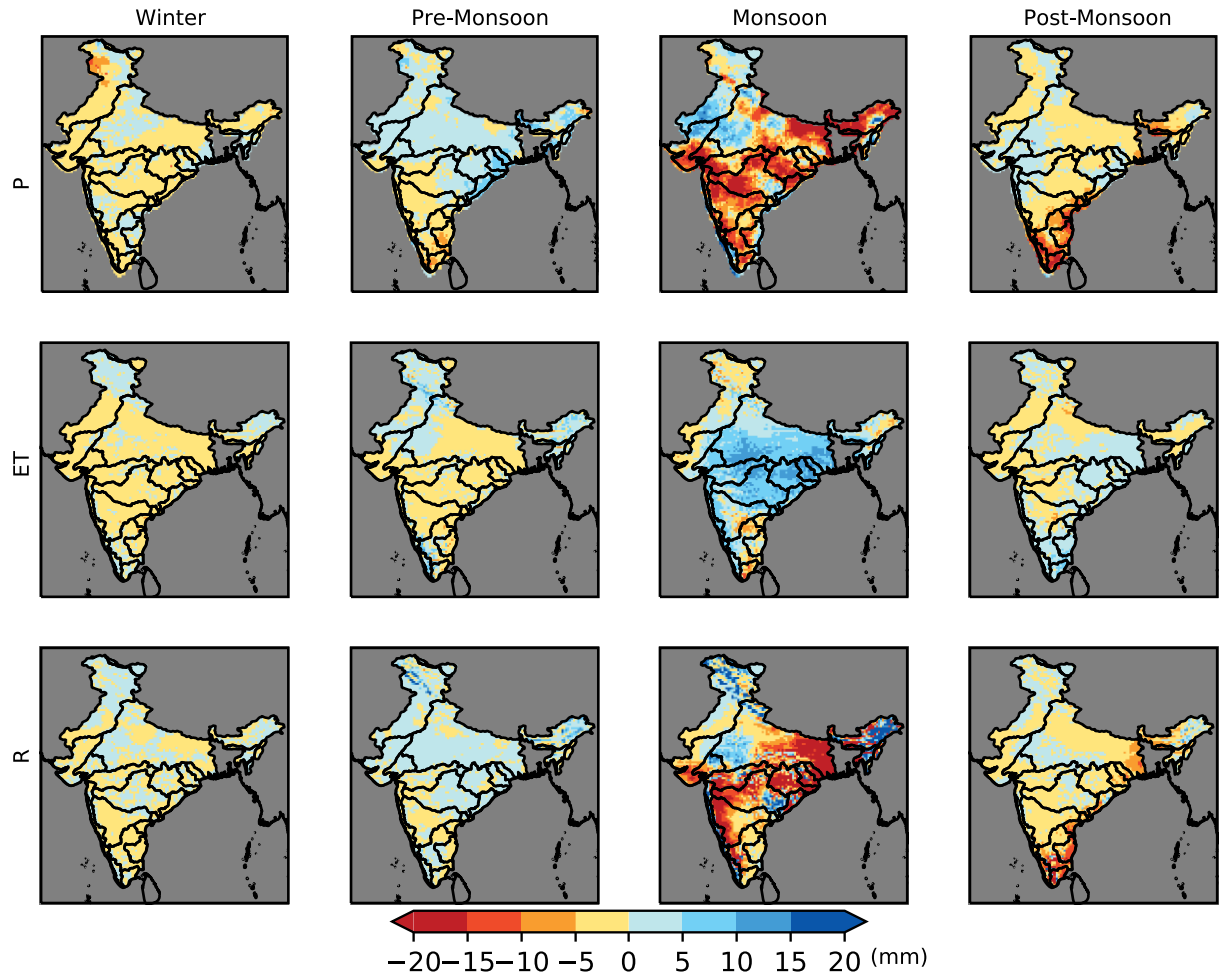

Figure 2.6: Sen's slope from Mann-Kendall non-parametric test for each season obtained from de-seasonalized data. Monsoon season prominently shows decreasing trends of precipitation and runoff for major parts of Eastern and South-western India.

4.4 Seasonal Mann-Kendall trend analysis

To understand the trends in river basins across different seasons, we used de-seasonalized data to perform Mann-Kendall (MK) test (Hirsch et al., 1982) and assessed the monotonic patterns utilizing Sen's slope estimator (**Figure 2.6**; **Table 2.4**). All the patterns estimated are significant at $p<0.05$. The spatial patterns show monotonic decrease in monsoonal P and R, whereas there is an increase in the ET. We observe that South-Western India, Central India, and Eastern India show high decreasing trends (>15 mm) for the Monsoon season corresponding to P and R, whereas ET shows increasing trends (10-15 mm) mostly in Central and Eastern India. For other seasons, there are relatively lower rates of increasing/decreasing trends. It can be further observed that Southern India shows high decreasing trends in P and R for the Post-Monsoon season

(10-15 mm) whereas the rest of India shows very little variation. Lastly, as expected, the trends in R to have very high spatial correlation with the trends in P.

From the temporal analysis (**Table 2.4**; **Figure A2.1**), we observe that for the Brahmaputra River basin, P shows a decrease of 0.56 mm/yr, an increase in ET and R by 0.01 mm/yr and 0.36 mm/yr respectively, and a large decline in TWSA of 18 mm/yr. Further, the Ganga River basin shows a decrease in TWSA with a rate of 18 mm/yr and no patterns in other components of the water balance. The Indus River basin shows a decline of 11 mm/yr in TWSA and an increase of runoff by 0.25 mm/yr. The Mahanadi River basin indicated a decreasing trend in TWSA at a rate of 9 mm/yr. However, the Krishna River basin shows an increase in runoff at 0.03 mm/yr.

Table 2.4: Seasonal MK test results for each river basin. All values are significant at $p < 0.05$. All the slope values reported in the table have units of mm/yr.

	P		**ET**		**R**		**TWSA**	
Basin	**Trend**	**Slope**	**Trend**	**S**	**Trend**	**Slope**	**Trend**	**Slope**
Brahmaputra	Decreasing	-0.56	Increasing	0.01	Increasing	0.36	Decreasing	-18
Cauvery-Pennar	No trend	-	No trend	-	No trend	-	No trend	-
Ganga	No trend	-	No trend	-	No trend	-	Decreasing	-18
Godavari	No trend	-	No trend	-	No trend	-	No trend	-
Indus	No trend	-	No trend	-	Increasing	0.25	Decreasing	-11
Krishna	No trend	-	No trend	-	Decreasing	-0.03	No trend	-
Mahanadi	No trend	-	No trend	-	No trend	-	Decreasing	-9
Narmada-Tapi	No trend	-	No trend	-	No trend	-	No trend	-
Sabarmati-Mahi	No trend	-	No trend	-	No trend	-	No trend	-

4.5 Land-cover linkage

From the comparison of the 300 m land cover map with the 50 km land cover map, we found that the 'majority' statistic realistically represents the landcover distribution inside large as well as smaller river basins (**Figure A2.2** and **Table B2.1**). For instance, for Ganga River basin, 'Agricultural' land is the major land cover type with 83.75% coverage in the 50 km resampled map whereas it is 78.5% in the original land cover map. From the land-cover comparison of 2002 and 2018, we did not find any significant percent changes in the land-use classes for any of the river basins (**Figure 2.7**, **Table 2.5**). All of the river basins show that agricultural land is the major land cover type, except for Brahmaputra and Sabarmati-Mahi River basin. These river basins with the major land cover type corresponding to agriculture belong to Northern, Central, and Southern India which comprises of the major crop production regions. For the Brahmaputra River basin, the

majority land-cover type is vegetated land whereas for the Sabarmati River basin, it is forest covered land. Since all the river basins have differences in size, we compared the percentage land-cover instead of absolute area to make observations across each of them. We detect that agricultural land has decreased by approximately 1% for all the river basins. On the contrary, forest, and urban land have increased in the range of 0.5-1% for all the river basins. It is also interesting to note the increase in water land-cover type for all the basins which corresponds to surface water stored in reservoirs.

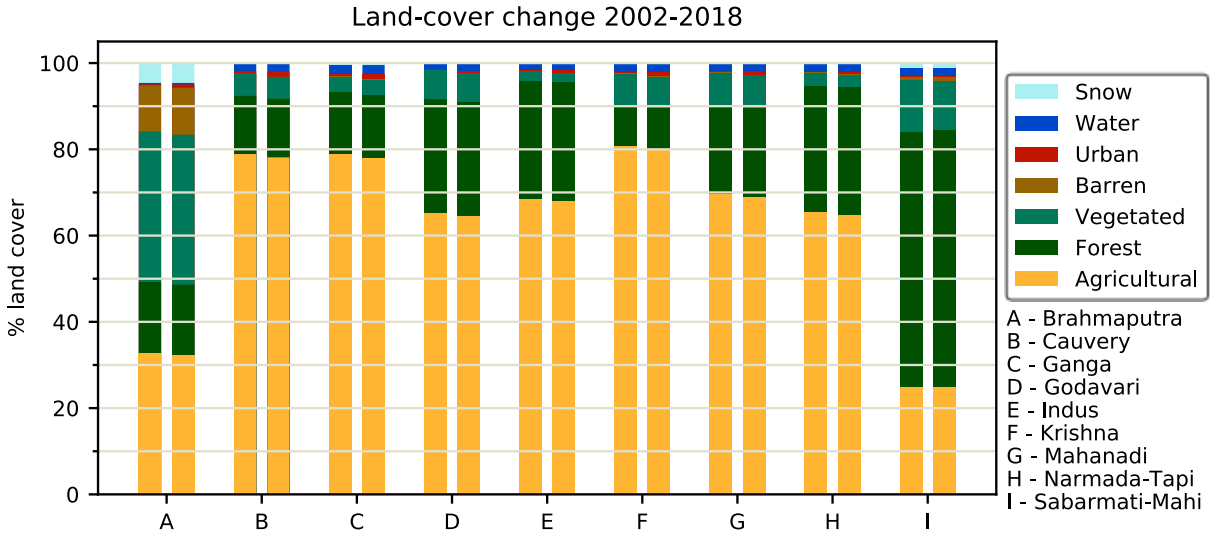

Figure 2.7: Land-cover distribution changes from 2002-2018 for all the nine major river basins. It is important to note that absolute area of these land-cover types is significantly different when we compare across all the basins due to difference in river basin sizes.

We further analysed the relation between P-ET-R and TWSA for each land-cover type for entire country (**Figure 2.8**). We observe that agricultural land and water pixels show low correlation between P-ET-R and TWSA ($R < 0.3$) whereas snow pixels show the highest amount of correlation ($R \sim 0.7$). We also observe that urban land shows high standard deviation (> 40 mm) whereas agricultural and barren land show the lowest standard deviation amongst all the land-cover types (~ 20 mm) for the difference between P-ET-R and TWSA.

2.5 Discussion and Conclusions

In this study, we analyzed nine major river basins in India utilizing publicly-available satellite and modelled dataset information for the time period from 2002 to 2019. Water balance components P, R, ET, and TWSA, were examined for each of these river basins. Time-series of the water balance components demonstrated that all the river basins exhibit strong seasonality with peaks during the Monsoon season (June – September).

Table 2.5: Percentages of each land-cover class in the river basins.

	Agricultural		Forest		Vegetated		Barren		Urban	
	2002	**2018**	**2002**	**2018**	**2002**	**2018**	**2002**	**2018**	**2002**	**2018**
Brahmaputra	25	24.9	58.9	59.5	12.2	11.6	0.8	0.9	0.1	0.3
Cauvery-Pennar	69.5	68.9	20.4	20.7	7.8	7.6	0.1	0.1	0.3	0.8
Ganga	78.9	78.1	14.4	14.6	3.5	3.4	0.3	0.3	0.5	1.1
Godavari	68.4	68.1	27.5	27.5	2.2	2.1	0.1	0.1	0.2	0.6
Indus	32.7	32.2	16.6	16.4	34.9	34.8	10.7	10.9	0.2	0.8
Krishna	80.7	79.7	9.4	9.8	7.3	7.3	0.2	0.2	0.4	0.9
Mahanadi	65.5	64.9	29.2	29.5	2.9	2.9	0.2	0.2	0.2	0.5
Narmada-Tapi	65.3	64.5	26.3	26.5	6.7	6.7	0.1	0.1	0.2	0.6
Sabarmati-Mahi	78.9	78.1	13.5	13.6	5.1	5	0	0	0.6	1.2

	Water		Snow	
	2002	**2018**	**2002**	**2018**
Brahmaputra	1.9	1.8	1.2	1.2
Cauvery-Pennar	1.9	2	0	0
Ganga	2	2.1	0.5	0.5
Godavari	1.6	1.7	0	0
Indus	0.3	0.3	4.6	4.6
Krishna	2	2.1	0	0
Mahanadi	2	2.1	0	0
Narmada-Tapi	1.4	1.8	0	0
Sabarmati-Mahi	1.8	2	0	0

The seasonal analysis demonstrated that Southern and North-Eastern parts of India experience water deficit due to decreasing monsoonal precipitation combined with increasing ET and decrease in TWSA. For example, Brahmaputra River basin shows a decline of 0.56 mm/yr in precipitation along with a decline of 18 mm/yr in TWSA whereas an increase of 0.01 mm/yr in ET and 0.36 mm/yr in R was observed. Most of the farmland in India follow cropping patterns that maximize the use of rainwater from the monsoons but any changes in this seasonal cycle represent a serious threat to food production. With changes in monsoon precipitation as seen in this study (as seen in Brahmaputra, Mahanadi, Krishna, Cauvery, and Narmada-Tapi River Basin), we believe that there is a

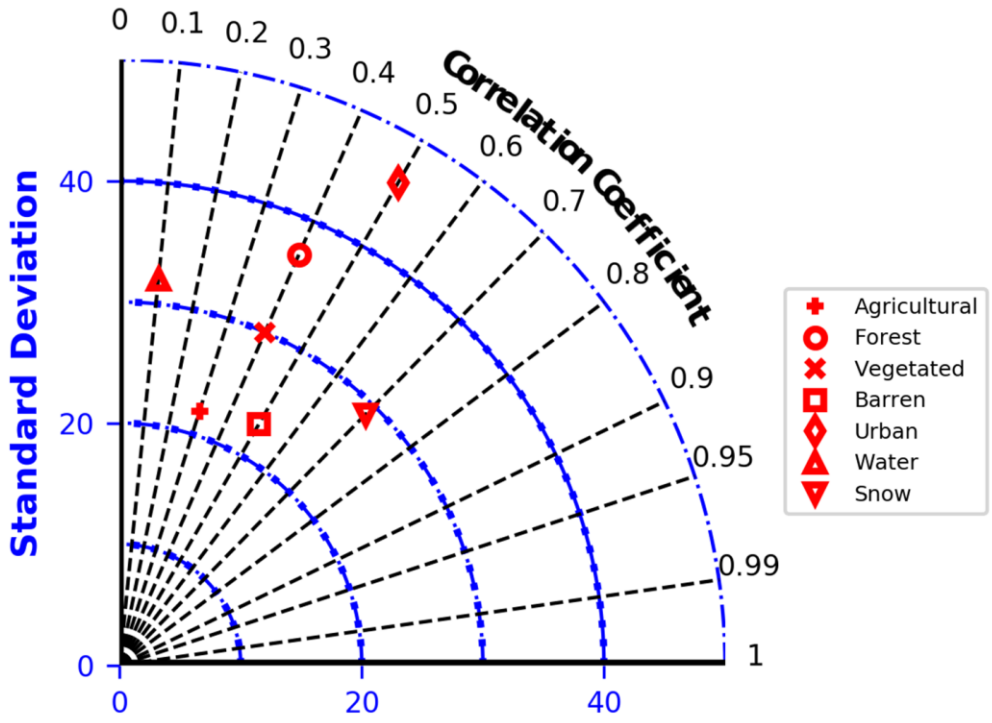

Figure 2.8: Taylor diagram for comparison between P-ET-R and TWSA for different land-cover types.

need for capacity building and effective engagement at the level of local water agencies as well as farmers about these changing seasonal patterns. While the farmers have started adapting to drip and sprinkler-based irrigation under Pradhan Mantri Krishi Sinchayee Yojana (PMKSY) scheme, but as of February 2020, only 4,300,000 hectares of land out of 68,300,000 hectares of net irrigated land has been covered under the drip and sprinkler-based irrigation schemes (Ministry of Agriculture and Farmers Welfare, 2020). This only accounts for less than 10% of the net irrigated area. Remaining agricultural land still uses groundwater wells for irrigating their lands. The net cultivated area in India is 140,000,000 hectares which implies that 71,700,000 hectares of agricultural land still depends on monsoonal rainwater. This makes the agricultural lands in the major river basins of India vulnerable to climatic changes. Further, observations from the GRACE sensor are very helpful in understanding the water status of a river basin. However, it is important to note that while GRACE TWSA is helpful to observe changes at the global scale, the spatial resolution is coarse when applied to smaller river basins. Further, we found linkage between the land-cover type of 'Agricultural' and 'Urban' with the monotonic trends in water balance components. 74% of the monotonic trends were associated with 'Agricultural' land whereas 19% were associated with 'Urban' land. Finally, from the SVD analysis for P-ET-R and TWSA, we observed that North-Western India consistently shows high negative loadings of the first principal component

explaining the most significant variability for these datasets and there does not exist synchronous co-variability between P-ET-R and TWSA.

In a study which involves the use of satellite datasets, it is important to be aware of the uncertainties associated with these datasets. The conclusions made from the analysis using satellite data should consider these limitations of the uncertainty. Aside from the errors in the datasets, in the water balance components, we assumed that TWSA is a proxy variable for changes in water storage. This assumption may not hold true as the water balance is disturbed by anthropogenic interactions. In spite of these restrictions, our outcomes are consistent with past investigations. For example, in our study, we find that average monthly ET for the Ganga River basin is generally 66% of the average monthly P (ET - 60 mm and P - 90 mm), which agrees with the report distributed by the Ganga River Basin Management Plan (http://cganga.org/wp-content/transfers/destinations/3/2018/11/057_WRM_23-09-2015.pdf).

There are numerous studies that have indicated decreasing TWSA in North-western India in parts of the Indus and the Ganga River basins (Asoka et al., 2017; Rodell et al., 2009b), yet in our investigation, we discovered that during 2019 the Brahmaputra River basin experiences a decrease in total water. This was seen as 18 mm/yr which is comparable to the magnitudes of decreasing TWSA in North-Western India. The changes in the water balance may have been influenced by land-use changes in this region.

Overall, our investigation shows that it is essential to continually monitor the water balance of these major river basin for effective management. As these river basins serve as major sources of freshwater for the population in these river basins and are drivers of the economy, it becomes fundamental to examine the seasonal and annual variability of the water budget for these river basins. Transboundary river basins, such as the Ganga, Brahmaputra, and Indus need data and analyses to settle water disputes. As the streamflow observations for these river basins are not publicly available, decision-making has to rely on methods and data (models and satellite sensors) such as those presented in this study.

2.6 Acknowledgements

This research was funded under the Applied Sciences Program (award number - 80NSSC18K0433) at NASA headquarters with the support of Dr. Bradley Doom, Program Manager in Water Resources division. The authors acknowledge this research opportunity and are grateful for the support.

Chapter 3: Application of Soil Water Assessment Tool (SWAT) model in analyzing nitrogen transport inside the Narmada River Basin[2]

3.1 Introduction

In the current times, climate change, urbanization, population growth and over-exploited unsustainable usage of water resources have exponentially increased the importance of water resource management. These problems have compounded into complex interactions with the water quantity and quality, especially in rapidly growing developing countries like India (Gosain et al., 2006; Madhusoodhanan et al., 2016; Mall et al., 2006). With the second highest population in the world (1.4 billion), India faces a major challenge in terms of the sustainable use of limited water resources that the country has, to support such a large population. In addition to the limited quantity of water, the semi-arid and arid regions in India are also facing the problem of deteriorating water quality (Gupta and Chakrapani, 2005; Saraswat et al., 2019; van Vliet et al., 2021). These studies recognise the need for an immediate perspective on the development and management of water resources to manage the diminishing and deteriorating water resources in a manner that it does not affect the routine household and industrial water usage (Rijsberman, 2006; van Beek et al., 2011b). Climate models predicting the future climatic conditions predict an increase of 1.5°C by 2050 in average temperatures across South-East India (Basha et al., 2017). With the increasing population, there will be an increase in per capita water demand in terms of irrigation, household and industrial usage. Additionally, this causes increase in food demand leading to more and more agricultural lands. This in turn leads to increased usage of fertilizers which are rich in essential nutrients like nitrogen and phosphorus which are required by crops in order to grow. Excessive use of these fertilizers over decadal time scale has led to nutrient pollution in several regions of India (Krishna et al., 2016; Sen et al., 2018). This paper estimates the potential regions of increasing nitrogen concentration and flux, causing nutrient pollution on the river system and people impacted by the water of Narmada River.

The Narmada River basin has undergone rapid changes in the past three decades with significant increase in agricultural lands, industries caused by development in this region due to the increasing population. The population in Gujarat and Madhya Pradesh covering majority of this river basin has increased by an average of 23% from 1991-2011

[2] Kansara P and Lakshmi V (2021). Application of Soil Water Assessment Tool (SWAT) Model in Analyzing Nitrogen Transport Inside the Narmada River Basin. Front. Water 3:765957. doi: 10.3389/frwa.2021.765957

to approximately 132 million in 2011 (Census Bureau of India). Due to this increase in population, several regions in the Narmada River watershed are being polluted with point sources – sewage and industrial discharge as well as non-point sources - chemical fertilizers used in agricultural lands (Sharma et al., 2008). Most of the studies in literature analyze nutrient contamination at specific sites inside the Narmada River basin, but there are no studies which analyse the nutrient contamination at the watershed scale.

Previous studies on large scale modelling using satellite and publicly-available model outputs have studied large continental river basins (Kansara et al., 2021; Lakshmi et al., 2018) or global (Kim et al., 2021; Kim and Lakshmi, 2019), models and satellite data (Billah et al., 2015; Lakshmi et al., 1997; Lakshmi and Wood, 1998; Le et al., 2020; Mohammed et al., 2018) or mainly using satellite data (Mondal and Lakshmi, 2021). Accurate and high spatial resolution mapping of precipitation (Hashemi et al., 2017; Mondal et al., 2018a) and soil moisture (Fang et al., 2020, 2019, 2018, 2013; Fang and Lakshmi, 2014) over continental regions using satellite remote sensing are instrumental for input (as in the case of precipitation) and validation/data assimilation (as in the case of soil moisture) for hydrological models. However, all of these research efforts have focused solely on the components of the water cycle, viz. precipitation, evapotranspiration, soil moisture, infiltration, streamflow and total water and have not considered the transport of nutrients.

In this study, we use SWAT (Soil Water Analysis Tool) to model hydrology of the Narmada Basin from 2001 to 2019. The model was calibrated for streamflow related parameters for the period from 2001-2010 and validated for a period from 2011-2019 using observed streamflow data from Central Water Commission (CWC). Performance metrics such as the Nash-Sutcliffe efficiency, correlation coefficient, root mean square error and percent bias were used to evaluate the model. Model simulated inorganic Nitrogen (N) - (NO_2 + NO_3) outputs were compared against in-situ nutrient measurement data from Central Water Commission India obtained from river water samples. We use the model simulated N outputs for comparison with in-situ nutrient data from CWC to analyse the spatio-temporal variability of nutrient concentrations and fluxes across the Narmada Basin from 2001-2019.

The following research questions are addressed in this study:

1) What is the spatio–temporal variability of N concentrations across the entire Narmada Basin for the monsoon season?
2) What is the spatio-temporal variability of N fluxes exported to the outlet of the Narmada Basin at the sub-basin scale for the monsoon season?

The remainder of this paper has been organized into 4 sections as follows: Section 2: Study Area and datasets - gives description of the study area and datasets used in the

study, Section 3: Methods - describes the methodology followed in building the SWAT model and the analysis of nutrients data, Section 4: Results and Discussion: discusses the important results from the analysis in this study, and finally Section 5: Conclusions: summarizes the work as well as discusses limitations of our approach and lists future questions.

3.2 Materials

3.2.1 Narmada River Basin

Narmada basin lies between longitudes 72° 38′E to 81°43′E and latitudes 21° 27′N to 23° 37′N and it spans over an area of approximately 92,000 square kilometers. The geographical location of Narmada Basin is shown in **Figure 3.1**. The basin is bounded by

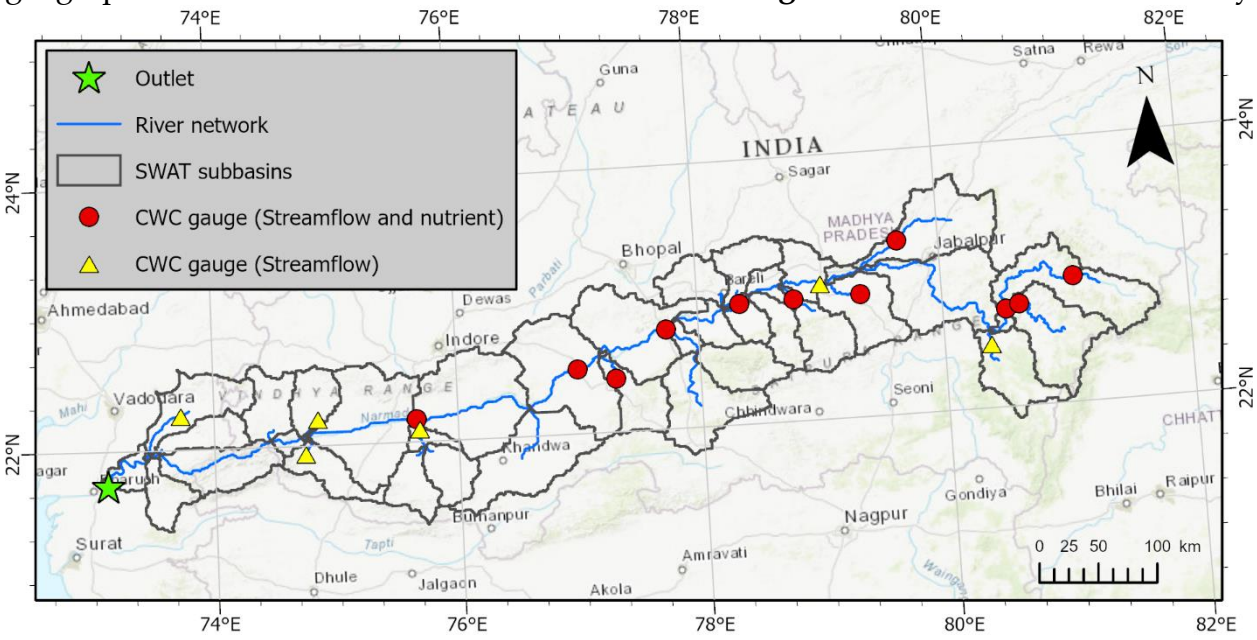

Figure 3.1: Map shows the Narmada River basin, main channel river network of Narmada, and CWC gauge locations for streamflow and nutrients. There are a total of 17 stations, out of which 11 stations have both streamflow and nutrient data and rest only have streamflow data. It is important to note that the map only shows stations for which we have used data in this study. CWC also maintains several other stations but these stations did not have enough data points, hence they were not included in the study.

the Vindhyachal mountain ranges in the north, by the Maikala range on the east, by the Satpuras on the south and by the Arabian Sea on the west. The river basin shares its area with the states of Madhya Pradesh and Gujarat majorly, while small parts of the basin also lie within Maharashtra and Chhattisgarh. The entire watershed is relatively flat with highest elevation of 1200 m in the Eastern part and slope less than 10° for the majority of

the area (**Figure 2 - a, b**). These upstream hilly regions generate more than 70% of the streamflow in the Narmada River, depositing essential nutrients and sediments for agriculture to the fertile plains in the central and downstream areas of the basin. In addition, there are two majority land cover types encompassing the watershed with agricultural land covering 53% and forests covering 42% of the basin area. Clay and clay loam are the majority soil types in the Narmada River basin. A detailed list of all datasets used in this study are provided in **Table 3.1**.

Table 3.1: Description of the datasets used in the study.

Data	**Source**	**Spatial/ Temporal resolution**
DEM	SRTM 3 arc-second void filled	90 m
Land use	Climate Change Initiative	300 m / 2015
Soil	Food and Agricultural Organization (FAO) Global Soils	7 km
Rainfall	Indian Meteorological Department (Gridded product)	0.25° / 2001-2019
Temperature	Indian Meteorological Department (Gridded product)	0.25° / 2001-2019
Discharge	Central Water Commission India (CWC)	2001 - 2019
Climatology	Climate Forecast System Reanalysis (CFSR)	2001 - 2019
Nitrite + Nitrate	Central Water Commission India (CWC)	2001 - 2019

3.2.2 Digital Elevation Model (DEM)

Elevation data was obtained using DEM from the Shuttle Radar Topography Mission (SRTM) (Farr et al., 2007). SRTM generated high-resolution topographical data from its mission conducted in 2000. It is a global dataset with high-resolution (30 m) as well as low-resolution (90 m) products extending from 60° N to 60° S (Berry et al., 2007). This dataset is distributed by the United States Geological Survey (USGS) and is available from the Earth explorer platform. The SRTM system consisted of two radar antennas to obtain interferometric imagery of the topography of the Earth's surface. This dataset has been assessed using non-oceanic Ground Control Points (GCPs) measured from kinematic GPS (Rodríguez et al., 2005) and displays good performance of DEM specifically for regions with low gradients. In this study, we use the 30 m void filled product.

3.2.3 Land-cover

In this study, we used the land cover data from European Space Agency (ESA) Climate Change Initiative (CCI) land cover products. CCI provides global annual land-cover maps for 1992-2018 at a spatial resolution of 300 m. The land cover map for 1992-1999 were obtained from AVHRR, for 1998-2012 were obtained from SPOT Vegetation, and for 2013 onwards were obtained from PROBA-V and Sentinel-3 OLCI. The product classifies the imagery into 22 distinct land-cover classes. We use the Version 2.0.7 land cover product from 2010 which accurately classifies irrigated cropland, rainfed cropland, forested areas, urban and barren areas validated using the Globcover 2009 validation dataset (ESA, 2017). There are 6 major land cover types in the Narmada River basin with 'Agricultural land' being the most common type (**Table 3.2**) with 53.7% of the geographical area inside the watershed. Following specific crops were used for the 'Agricultural' land-cover type: Rice, sorghum, soybean, and wheat. And for the 'Forest' land-cover type, 'Broadleaved Deciduous' and 'Needleleaved Deciduous' were the specific forest types used. This study does not take into account crop rotation patterns inside the river basin. We have updated the manuscript text with this information.

Table 3.2: Land cover class distribution in the Narmada River basin.

Land-cover	Area (%)
Agricultural	51.7
Forest	42.77
Grass/shrub	3.29
Urban	0.01
Wetland	0.27
Water	1.96

3.2.4 Soils

The soils data from the Food and Agriculture Organization (FAO) is used for this study. The soil map was available at a scale of 1:5000000 at global level. This dataset was produced as a collaboration of FAO and UNESCO in 1961 and it took twenty years to compose the global dataset (http://www.fao.org/soils-portal/data-hub/soil-maps-and-databases/faounesco-soil-map-of-the-world/en/).

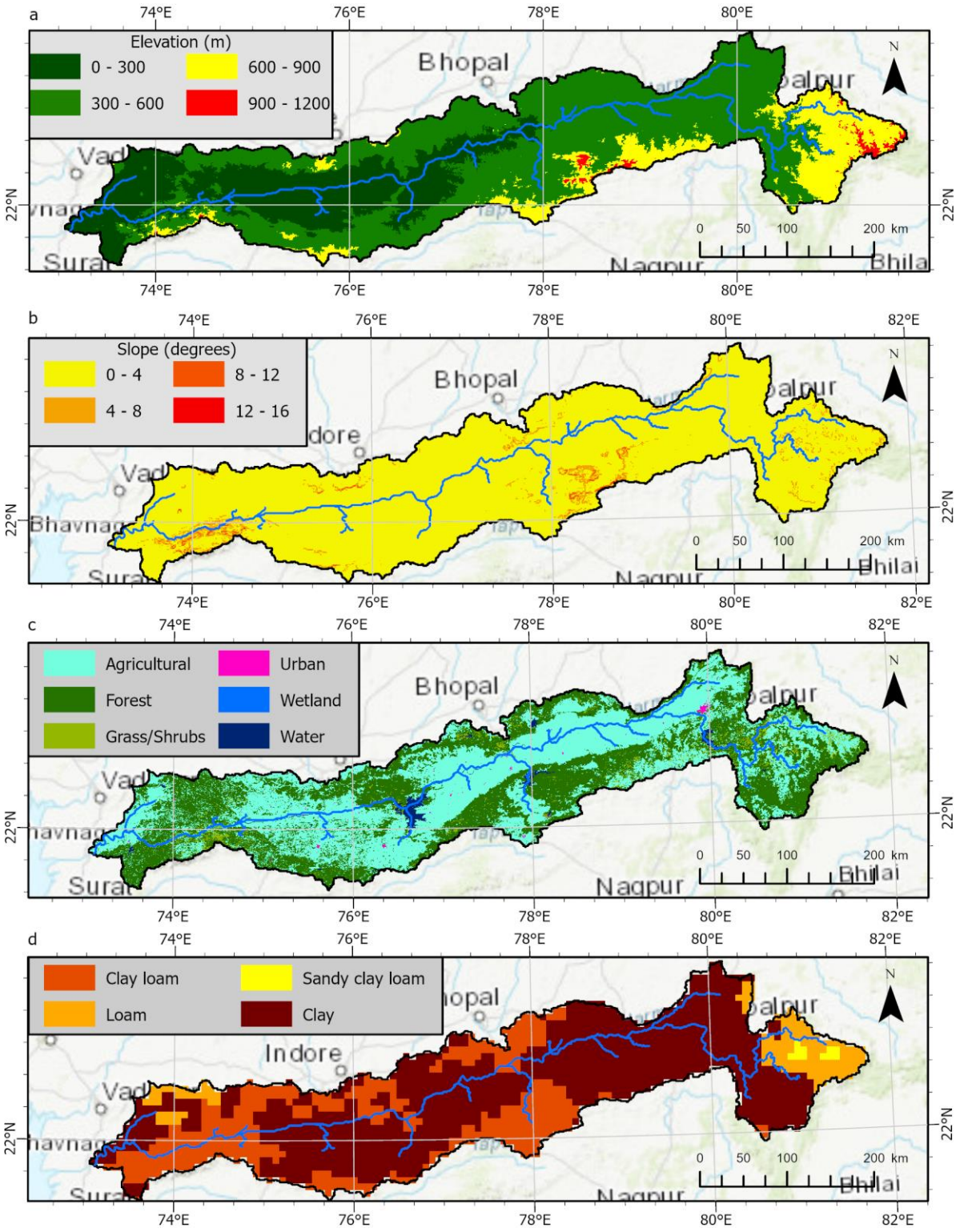

Figure 3.2 (a-d): 'a' – Digital Elevation Model (DEM) map; 'b' – Slope map; 'c' – Land cover map. 'd' – Soil map used as topographical and spatial input forcing for setting up the SWAT model.

3.2.5 Meteorological data (Rainfall, air temperature, solar radiation, wind speed and relative humidity)

Rainfall and air temperature data were obtained from the Indian Meteorological Department (IMD). IMD provides gridded rainfall and minimum and maximum air temperature at 0.25° spatial resolution. IMD maintains rainfall records from a network of approximately 6,329 rain gauges and 395 temperature gauges across different parts of India with varying time spans of data collection. The data collected by these in-situ stations had been interpolated to the latitudinal and longitudinal grids using Shepard's interpolation technique (Rajeevan et al., 2006; Srivastava et al., 2009). In this study, we used the gridded rainfall and temperature product from 2001-2019. The remaining meteorological datasets – solar radiation, wind speed, and relative humidity were obtained from the global Climate Forecast System Reanalysis (CFSR) system (Saha et al., 2010).

Table 3.3: Table shows the streamflow and nutrients data available at each gauge location in the Narmada River basin.

Site	Latitude	Longitude	Available Data Points (Daily streamflow – 2001 to 2019)	Available Data Points (Monthly (NO_2 + NO_3) – 2001 to 2019)
Bamni	22.48	80.37	4618	182
Barmanghat	23.03	79.01	6077	182
Belkhedi	22.92	79.33	6594	180
Chhidgaon	22.40	77.30	6492	180
Dhulsar	22.20	74.85	4870	179
Dindori	22.94	81.07	6324	179
Gadarwara	22.92	78.79	6191	167
Garudeshwar	22.26	73.72	6401	167
Handia	22.49	76.99	6581	182
Hoshangabad	22.75	77.73	6634	182
Mandleshwar	22.17	75.66	6592	182
Manot	22.73	80.51	6630	182
Mohgaon	22.76	80.62	6657	180
Patan	23.31	79.66	6377	180
Pati	21.94	74.74	5203	179
Sandia	22.91	78.34	6640	179
Kogaon	22.10	75.68	5242	178

3.2.6 Observed streamflow

The observed streamflow data required for the SWAT hydrological model calibration was obtained from the Central Water Commission (CWC) - the central water resource management body of the Government of India. CWC maintains a network of 29 surface water measurement locations. Out of these 29 stations, only 17 locations had adequate streamflow observations (**Figure 3.1**). These stations were selected on the basis of more than 50% observational data points for the study time period of 2001-2019 (**Table 3.3**).

3.2.7 Nutrients

CWC monitors nutrients in water at 29 different locations inside the Narmada River Basin. Out of 29, only 11 stations had adequate (NO2 + NO3) observations (**Figure 3.1**). These stations were again selected on the basis of more than 50% observational data points for the study time period of 2001-2019. The study utilizes only (NO2 + NO3) data out of the 24 nutrient parameters given. **Table 3.3** provides a comprehensive list of all the streamflow and nutrient measurement observations collected from the stations. This data can be downloaded from the Water Resources Information System (WRIS) India website. Further information about this data can be found at https://indiawris.gov.in/wiki/doku.php.

3.3 Methods

This section describes the methods used in our study - the hydrological model and analysis of the nutrients. The section is divided into three sub-sections. The first sub-section explains the SWAT model setup and the pre-processing of the input data for the model. The second sub-section describes the calibration and validation process for the SWAT model. In the final sub-section, we describe the analysis performed on the comparison of simulated with the observations for the nutrients.

3.3.1 SWAT model setup

Soil Water Assessment Tool (SWAT) is a semi-distributed, continuous daily timestep hydrological model developed by the United States Department of Agriculture (USDA) in collaboration with Texas A&M University. This model can simulate the hydrology of small to river-basin scale watersheds (Abbaspour et al., 2015; Neitsch et al., 2011). The SWAT model has application that range from soil erosion to analysing non-point source pollution (Arnold et al., 1998a). This model can simulate quality and quantity of surface water and can assess the impact of environmental change due to land-use and agricultural management practices (Jayakrishnan et al., 2005). The inputs to this model are spatial data which includes DEM, land-use/land cover, soils and meteorological data including precipitation, temperature, solar radiation, wind speed and relative humidity (**Figure 3.2**). The model divides the watershed into sub-basins and further divides them

into Hydrological Response Units (HRUs) which are a combination of slope class, land cover type, and soil type. The modelling of the watershed is done in two phases: land phase and routing phase. The land phase estimates the runoff for each of these HRUs using the water balance equation:

$$SW_t = SW_0 + \sum_{i=1}^{t}(R_{day} - Q_{surf} - E_a - W_{seep} - Q_{gw}) \quad (1)$$

Where SW = Soil Moisture content, R = Precipitation, Q = Surface runoff, E = Evapotranspiration, W = Infiltration, and Q = Groundwater, and the subscripts represent: *0* = intial time step, *t* = time step t, *day* = total daily precipitation, *surf* = surface runoff, *a* = evapotranspiration into the atmosphere, *seep* = Seepage into the soil, *gw* = groundwater storage

Penman-Monteith method was used for estimation of the potential evapotranspiration. The generated runoff is then routed through the stream network to the outlet of the watershed in the routing phase. The Muskingum routing method was used for the routing of water in the streams. The percentage distribution of each land-cover type has changed marginally over the study period (**Table B3.1**). Hence, we use a single land-use land-cover map for the study.

3.3.2 SWAT model calibration and validation

The model is then calibrated using the software called SWAT Calibration and Uncertainty Procedures (SWAT-CUP). For model calibration, the Sequential Uncertainty Fitting (SUFI2) method was used (Abbaspour et. al, 2004). The model was run with warm up

Table 3.4: Calibrated SWAT parameter ranges for the Narmada River basin. Calibration was performed using the SUFI-2 algorithm inside SWAT-CUP.

No	Parameters	Method	Fitted value	Min	Max
1	CN2.mgt	Relative	-0.157169	-0.272422	-0.147824
2	ALPHA_BF.gw	Replace	0.567571	0.558718	0.57558
3	GW_DELAY.gw	Replace	144.065659	136.819458	169.024811
4	GWQMN.gw	Replace	0.258918	0.238288	0.329978
5	ESCO.hru	Replace	0.268123	0.074944	0.3091
6	EPCO.hru	Replace	0.346514	0.279924	0.52207
7	GW_REVAP.gw	Relative	0.117352	0.102548	0.168342
8	REVAPMN.gw	Replace	192.265594	138.030182	208.011353
9	SOL_K(..).sol	Relative	0.091695	-0.014808	0.170414
10	OV_N.hru	Replace	0.155736	0.093178	0.173898
11	SOL_AWC(..).sol	Replace	0.340161	0.074277	0.580723
12	CANMX.hru	Replace	68.216423	43.828438	95.171562
13	CH_N2.rte	Replace	0.048607	-0.147896	0.226396
14	HRU_SLP.hru	Relative	-0.184803	-0.205714	0.630714

period of 3 years (1998-2000), then was calibrated for streamflow from 2001-2010, and finally validated for 2011-2019. (Pandey et al., 2019) used 14 parameters associated with streamflow to calibrate their SWAT model for the Upper Narmada basin. In this study, those 14 parameters were used with 10 iterations of 500 simulations to perform multi-site calibration of the model for entire Narmada River basin (**Table 3.4**). The 14 parameters were calibrated for streamflow at 5 different locations along the main channel and tributaries of Narmada River basin (**Table 3.5**). Simulated streamflow was compared with observed streamflow using the statistical metrics: Nash-Sutcliffe Efficiency (NSE), correlation coefficient (R^2), percent bias (p-bias), and Root Mean Squared Error (RMSE) (**Table 3.5**).

3.3.3 Nutrient analysis

An average value of fertilizer obtained from the Department of Fertilizers, India at district level was used as input to the SWAT model. The average fertilizer consumption in Narmada River basin was for 42 kg/hectares in 2010 as per the Ministry of Agriculture and Farmers Welfare of India. This was used a constant input to all the agricultural land-cover types in the study. We analyze the performance of SWAT model simulated (NO_2 + NO_3) using three statistical measures – Correlation coefficient (R^2), Root mean squared error (RMSE), and Percent Bias (P-Bias). We study the spatial variability of nitrogen concentration and flux as simulated by the SWAT model in monsoon months (June-September). In a river channel, a majority inorganic/mineral nitrogen is present in the form of nitrites (NO_2) and nitrates (NO_3). Since, the concentration of nitrite is very less in water (not more than 7% of total dissolved nitrogen), nitrogen is reported as (NO_2 + NO_3). In addition to the spatial variability of mean monsoon concentration and mean monsoon flux, trends in concentration and flux were estimated using Mann-Kendall trend test and Sen's slope estimator (Lettenmaier, 1988).

3.4 Results

3.4.1 SWAT model performance

In the calibration phase, the SWAT model achieved a mean NSE of 0.72 and a mean R^2 of 0.78 (**Table 3.5**). These values indicate that the model performs well in the calibration phase. Similar studies conducted for Ganga River Basin also show comparable performance (Mishra and Lilhare, 2016c; Pandey et al., 2019). Multi-site calibration by Pandey et al. (2019) had NSE in of 0.77 for the streamflow locations inside the Narmada River Basin whereas Mishra and Lilhare (2016) had NSE of 0.96 and correlation coefficient of 0.98 for the calibration period of 1973-77. The model was only calibrated for the streamflow related parameters (**Table 3.4**). We found CN2 and ESCO as the most important parameters in the calibration of the SWAT model. CN2 represents the curve number for corresponding HRU which is a function of antecedent soil moisture

conditions and soil's permeability. ESCO represents the Soil Evaporation Compensation Factor which allows the user to modify depth distribution for evaporative demand. These two factors combined represent primary HRU characteristic affecting overland flow for the Narmada River Basin. For the validation phase, the SWAT model achieved a NSE of 0.63 and R^2 of 0.76 (**Table 3.5**). The literature on hydrological model building suggests NSE > 0.5 as a good model (Anand et al., 2018; Mishra and Lilhare, 2016c; Moriasi et al., 2015; Pandey et al., 2019). Since the model showed NSE > 0.5 for both the calibration and validation phase, we used this model to compare the observed and simulated nutrients (N). We evaluate the time series of calibrated and validated streamflow data (**Figure 3.3**). We observe that the simulated streamflow peaks match the observed streamflow peaks and the low flows have been captured well in the calibration as well as the validation phase for all 5 calibration sites. The extreme flow values are also correctly simulated as observed from 2013 high flow peak for all sites except for Barmanghat. In addition to this, the Narmada basin experiences several extreme flood events every decade which are captured sufficiently well in the calibrated model. For instance, from 2001-2010, there were two significant flood events in 2003 and 2005 respectively and for 2011-2019, there was one significant flood event in 2013. After calibration and validation of the parameters, the SWAT model was run for the entire time period of 2001-2019 using calibrated parameter values. The performance of streamflow at 17 stations and of N at 11 stations were estimated using hydrological model evaluation statistics (**Figure 3.4 and Figure 3.5**). Eight stations had NSE < 0.5 and 11 stations had R^2 > 0.75 for streamflow comparison. No patterns were observed in terms of the presence of biased model performance in upstream or downstream part of the river basin. For nutrient comparison, only four out of eleven stations had R^2 > 0.2. These stations belong to the mainstream channel of Narmada River whereas rest of the stations with lower R^2 with most of them located along the tributaries of the Narmada River.

Table 3.5: Performance of the SWAT model for streamflow calibration and validation at the five calibration sites. Calibration period is from 2001-2010 and validation period is from 2011-2019.

Station	**R^2**		**NSE**		**RMSE (m^3/s)**	
	Cal	**Val**	**Cal**	**Val**	**Cal**	**Val**
Patan	0.75	0.74	0.68	0.62	56.56	67.82
Sandia	0.8	0.81	0.78	0.74	294.95	360.55
Handia	0.84	0.85	0.77	0.66	469.04	678.23
Mandleshwar	0.7	0.69	0.61	0.61	600	871.77
Barmanghat	0.8	0.7	0.75	0.5	249	289.82
Mean	**0.78**	**0.76**	**0.72**	**0.63**	**333.8**	**453.64**

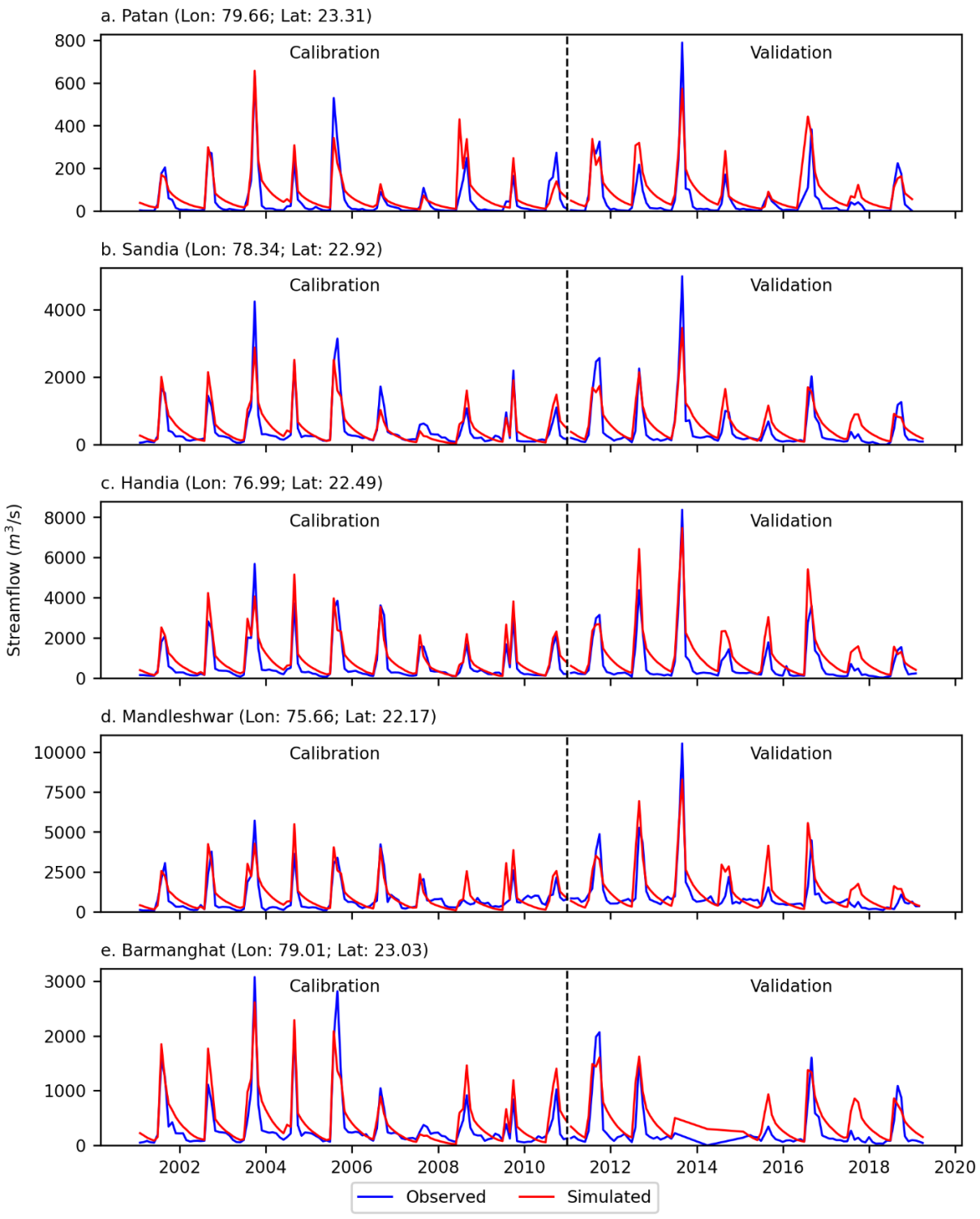

Figure 3.3 (a-e): Time series of streamflow comparison between simulated and observed (CWC) streamflow for calibration and validation phase. Calibration was performed for 2001-2010 and validation was performed for 2011-2019. Black dotted line represents the end of calibration period and start of validation period for simulation.

3.4.2 Temporal distribution of N

3.4.2.1 N - Concentration

To understand the temporal variations, we examine the time-series of N (NO_2 + NO_3) concetration at a few selected reach locations (**Figure 3.6**). Three sites – Handia, Mandleshwar and Sandia were selected for the time series analysis. Mandleshwar is located towards the downstream end whereas Sandia is located at the upstream end and Handia is between these two locations along the main chanel. For the upstream locations of Handia and Sandia, we observe that there exists low correlation between the simulated and observed nutrient concentration which is significant at a p-value of 0.05. Sandia shows the highest correlation amongst the upstream locations with $R^2 = 0.36$. For all three locations, there was no observation data for (NO_2 + NO_3) after 2016. For the early simulation period (2001-2005), it is seen that the simulated and observed time-series are highly correlated. Additionally, the peaks for the simulated nutrient load were underestimated by the model for all the upper reach locations for a major portion of the 2005 -2015 period. The extreme values of nutrient concentrations were underestimated by the model. For instance, the bias for extreme event ranges up to 7 mg/L for Handia as observed in the monsoon of 2013. Bias for Mandleshwar is relatively less (3 mg/L) as compared to Handia and Sandia. High values of nutrient concentrations were observed during the monsoon than pre-monsoon or post-monsoon season for both upstream and downstream stations. In Mandleshwar and Sandia, (NO_2 + NO_3) concentrations vary between 0 – 1.5 mg/L, during the pre-monsoon and 0.3 – 2.0 mg/L during the post-monsoon season. During monsoon months, Handia showed higher (NO_2 + NO_3) (2 – 10 mg/L) concentrations. The reason for high concentration of (NO_2 + NO_3) during monsoon season is due to the fact that higher precipitation during monsoon season causes the surface runoff to increase and this washes out fertilizer and sewage wastes from the overland locations and moves it to the stream network and then to the river.

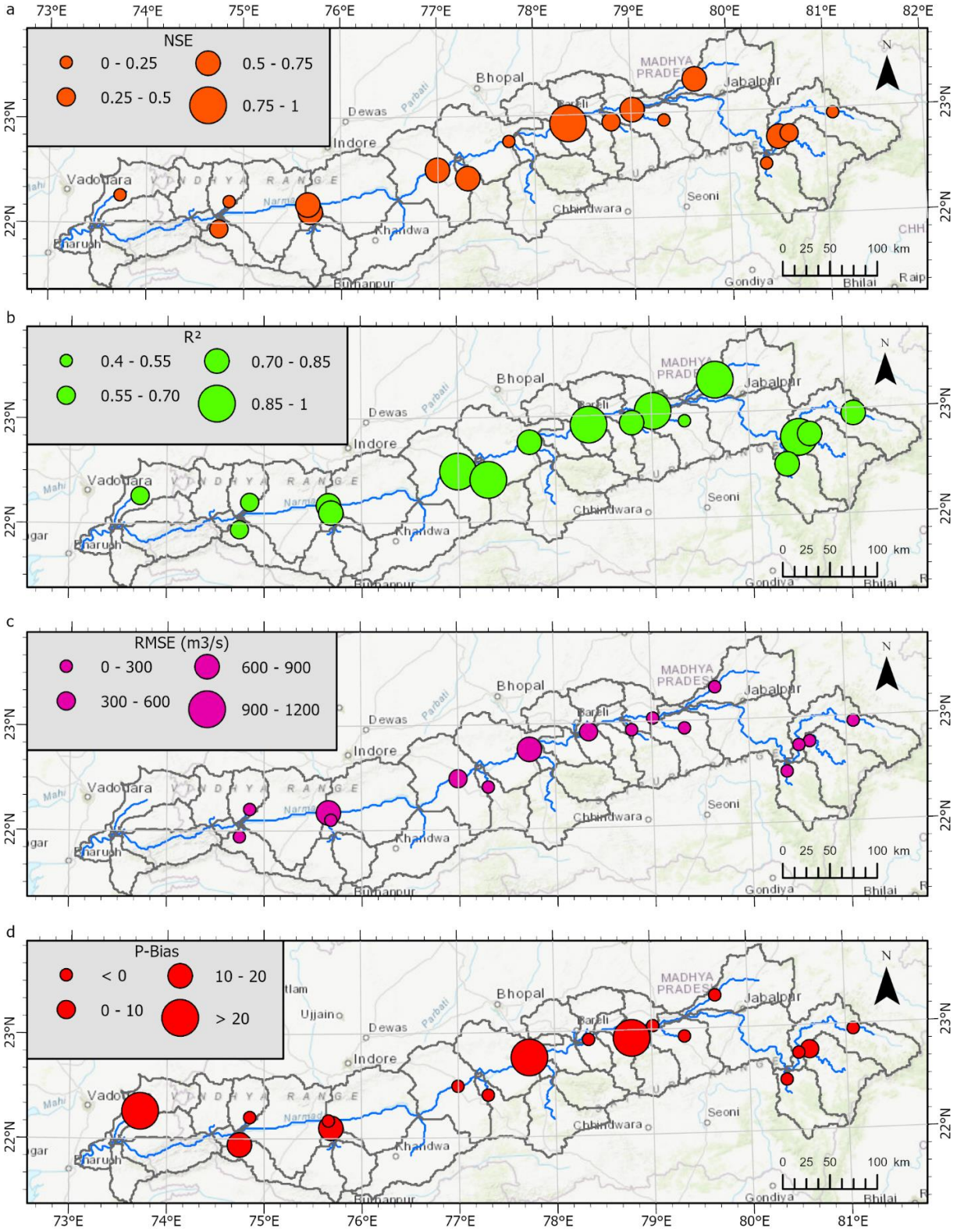

Figure 3.4 (a-d): SWAT Model performance statistics – 'a': Nash-Sutcliffe efficiency, 'b': Correlation coefficient squared, 'c': Root mean squared error, and 'd': Percent bias, for 17 gauge locations inside the Narmada River basin.

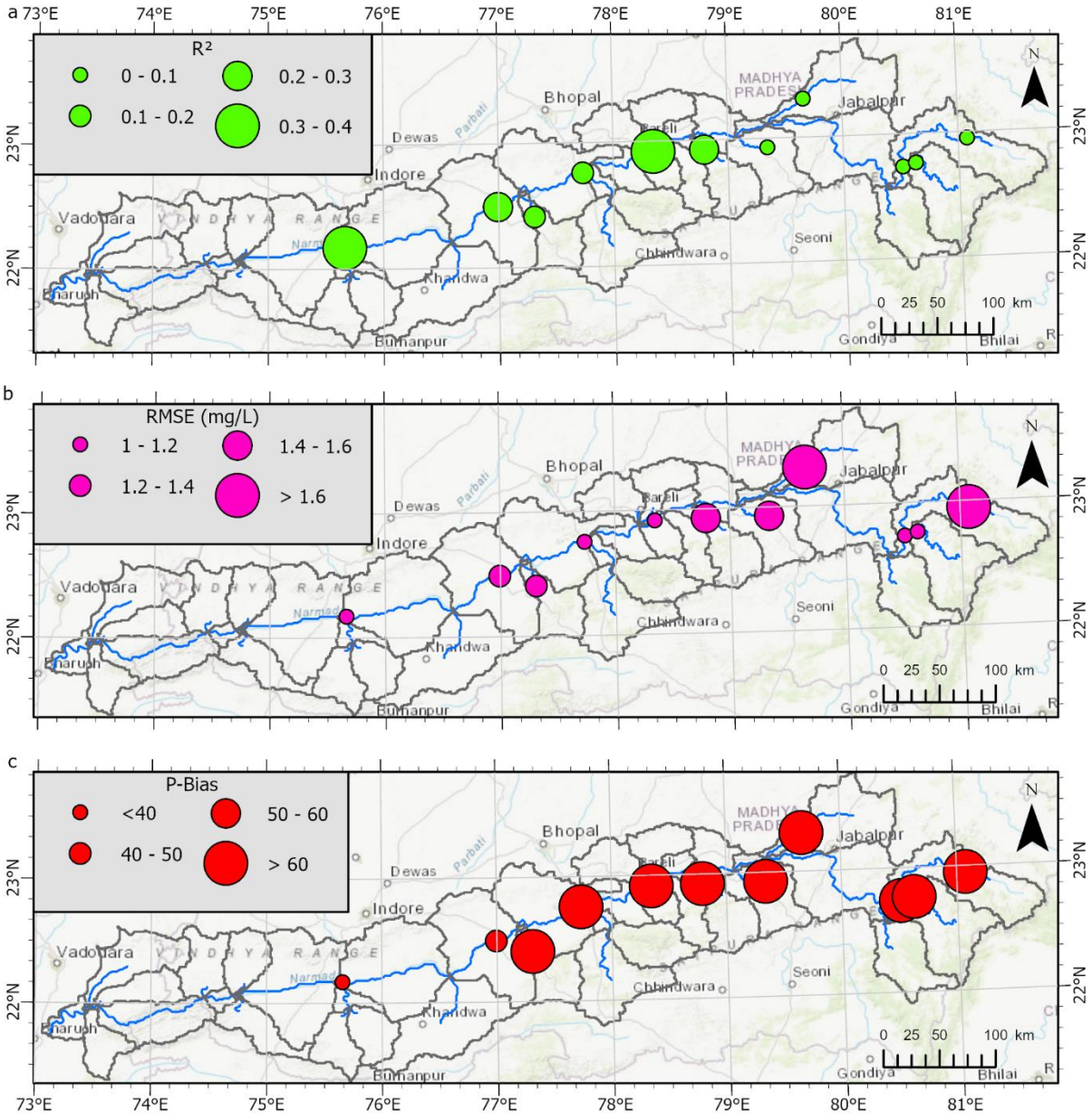

Figure 3.5 (a-c): SWAT Model performance statistics – 'a': Correlation coefficient squared, 'b': Root mean squared error, 'c': Percent bias, for 11 gauge locations inside the Narmada River basin.

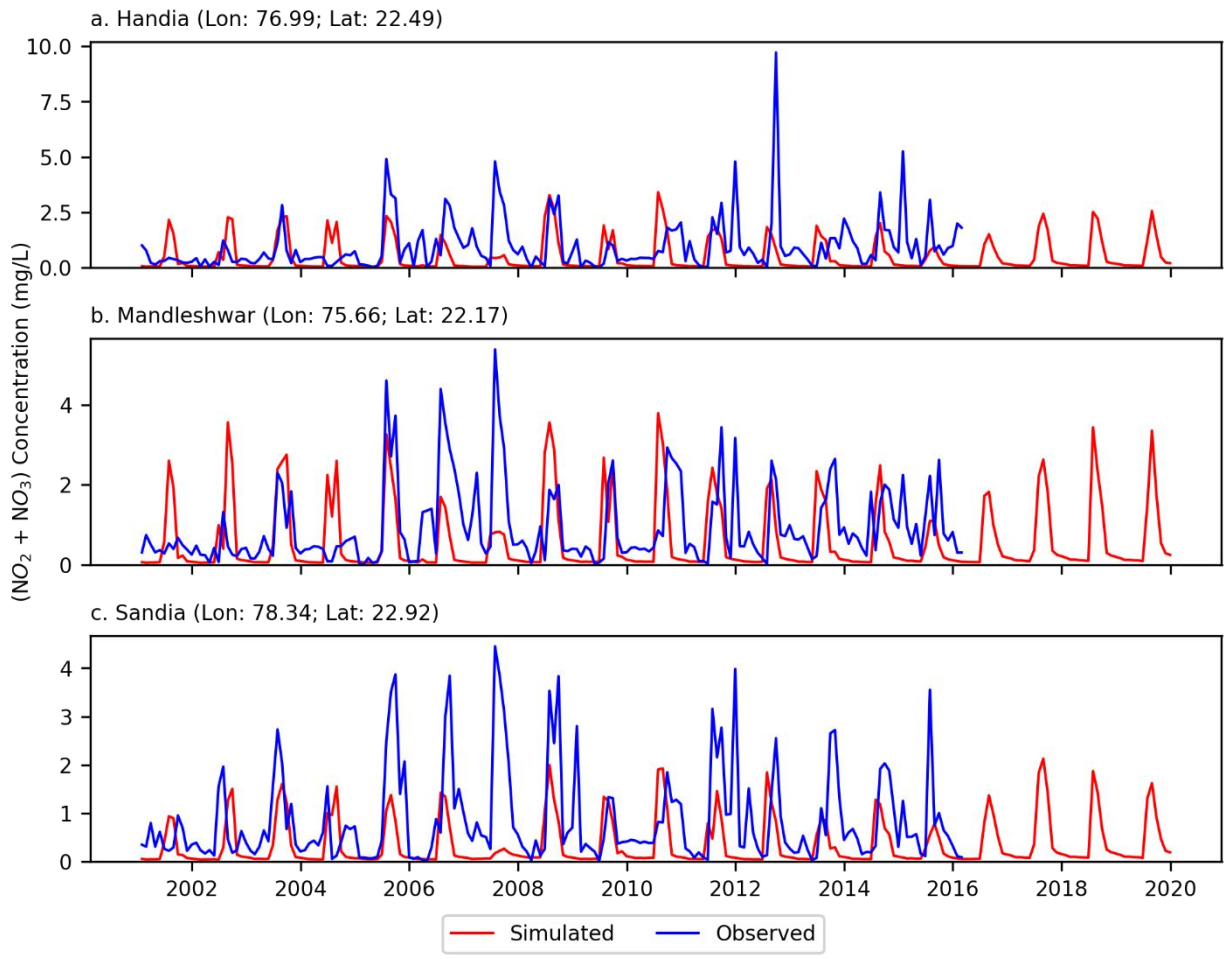

Figure 3.6 (a-c): Time series of (NO2 + NO3) concentration for comparison between SWAT simulated nutrients and CWC observed nutrient data.

3.4.2.2 N - Flux

We also examine the time-series of N (NO_2 + NO_3) flux at three sites – Handia, Mandleshwar and Sandia (**Figure 3.7**). For the upstream locations of Handia and Sandia, we observe that there exists fairly good correlation between the simulated and observed nutrient flux after 2008. For all three locations, there was no observation data for (NO_2 + NO_3) after 2016. For the early simulation period (2001-2005), it is seen that the simulated and observed time-series are poorly correlated. Additionally, the peaks for the simulated nutrient load were overestimated by the model for all the upper reach locations for normal events of the 2001 -2008 period but significantly underestimated during the extreme events of high concentration. For instance, the bias for extreme event ranges up to 40 Kilo Tonnes (KT) for Handia as observed in Monsoon 2013. Bias for Mandleshwar is relatively less (20 KT) as compared to Handia and Sandia. High values of nutrient flux

were observed during the monsoon than pre-monsoon or post-monsoon season for both upstream and downstream stations.

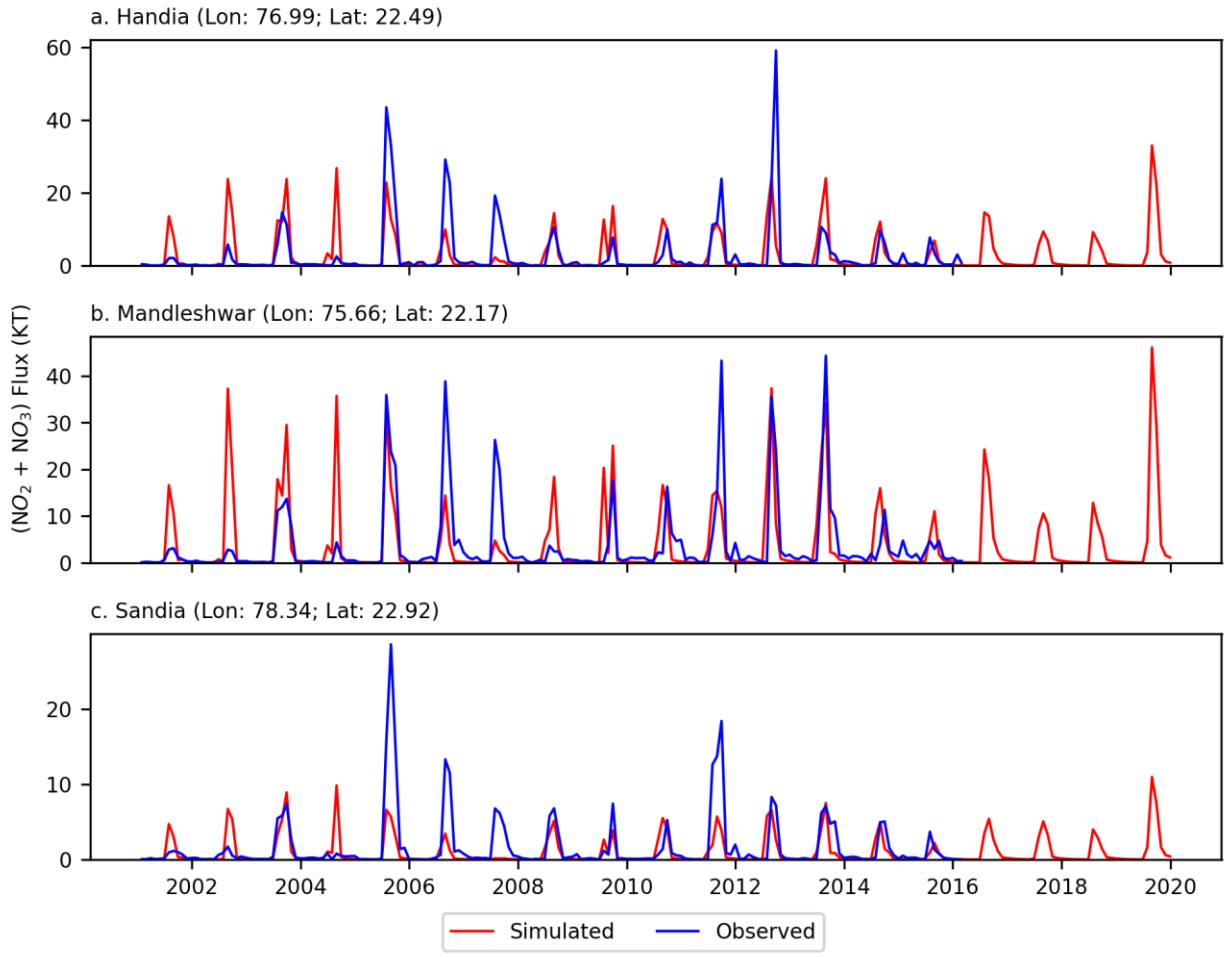

Figure 3.7 (a-c): Time series of (NO2 + NO3) flux for comparison between SWAT simulated nutrients and CWC observed nutrient data. The unit of flux is Kilo Tonnes (KT).

3.4.3 Spatial distribution of nutrient concentration and flux

The mean monsoonal concentration (mg/L) and flux (Kilo Tonnes - KT) for each subbasin of the Narmada River Basin for nitrogen are shown in **Figure 3.8**. From the distribution, it is observed that nutrient concentration and flux map spatially correlate very well. The downstream locations have high nutrient concentration along the main channel in the range of 0.4 – 0.8 mg/L for the entire subbasin. Similarly, the downstream locations have high nutrient flux along the main channel with a range of 200 – 500 KT. One possible reason for high concentrations and fluxes in the main channel is due to the presence of a large area of agricultural land in these regions where N based fertilizer is utilized. From

the land use map (**Figure 3.2**), it can be observed that all the agricultural land are present only near the main channel leading to overland flow washing the soil and carrying nutrients to the main channel. Further, we also observe that in terms of absolute quantities, the nutrient concentration in main channel is 6-8 times higher than that tributary subbasins.

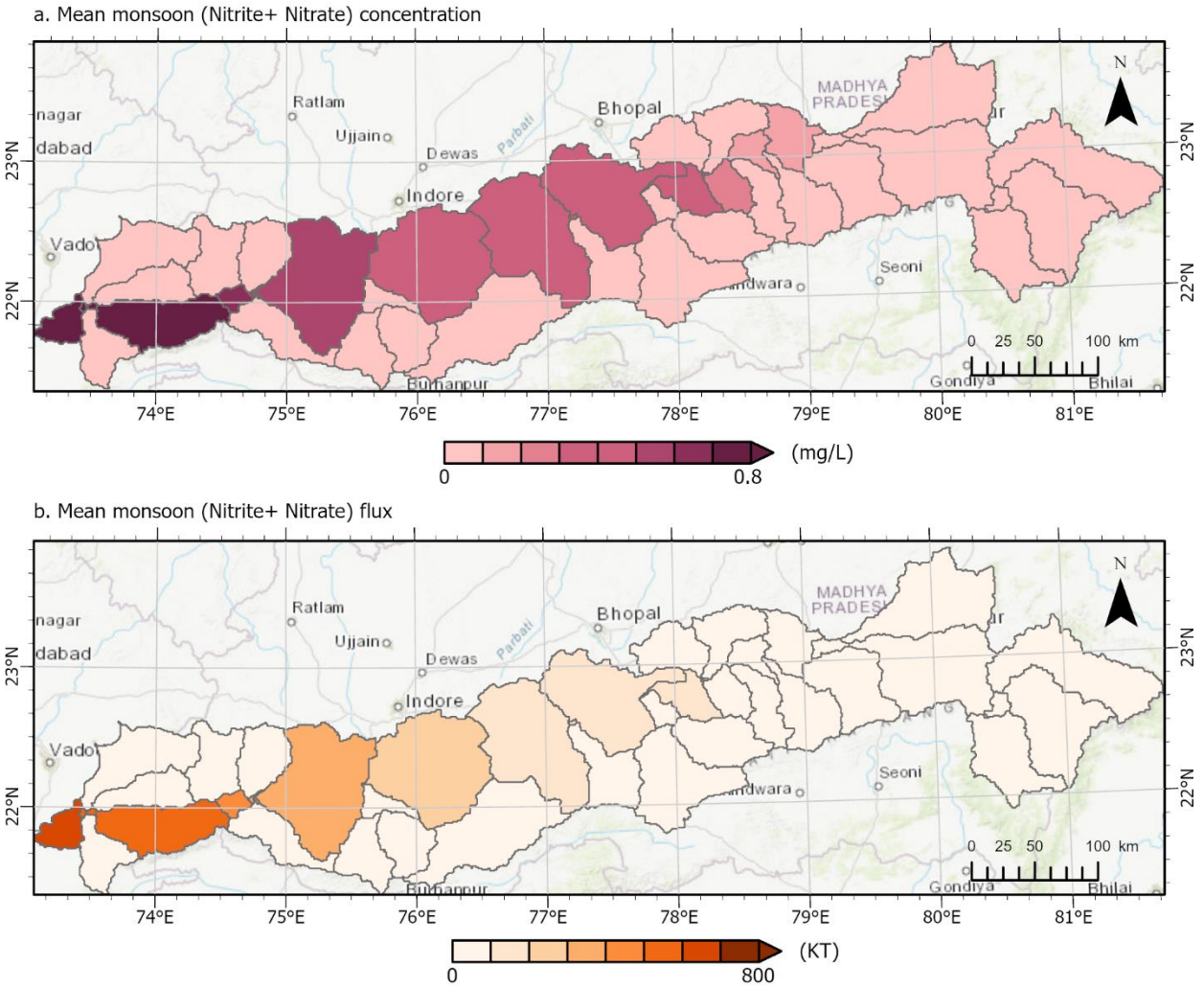

Figure 3.8 (a-b): 'a' Mean monsoonal (NO2 + NO3) concentration spatial variation across the subbasins in the Narmada River basin. 'b' Mean monsoonal (NO2 + NO3) flux spatial variation across the subbasins in the Narmada River basin. The flux values are in the order Kilo Tonnes (KT). Monsoonal concentration was obtained by taking mean of concentration values for individual months from June-September. Monsoonal flux was obtained by summation of flux values for individual months from June-September.

In addition to spatial comparison of mean concentration and mean flux, we estimated the monotonic trends in subbasins for monsoon season using Mann-Kendall non-parametric trend test from 2001-2019 (**Figure 3.9**). It is interesting to note that for concentration trends, we only found increasing concentration trends which are significant at 95% confidence level. Tributary subbasins lying on the outer boundaries of the Narmada watershed showed an increasing trend in N concentration. One possible reason is that these subbasins have undergone land cover changes from forest to agricultural lands leading to more usage nitrogen containing fertilizers and hence leading to pockets of increasing nitrogen concentrations. Rest of the subbasins showed neither increasing nor decreasing trends in nutrient concentration. Additionally, we also estimated the trends in nutrient

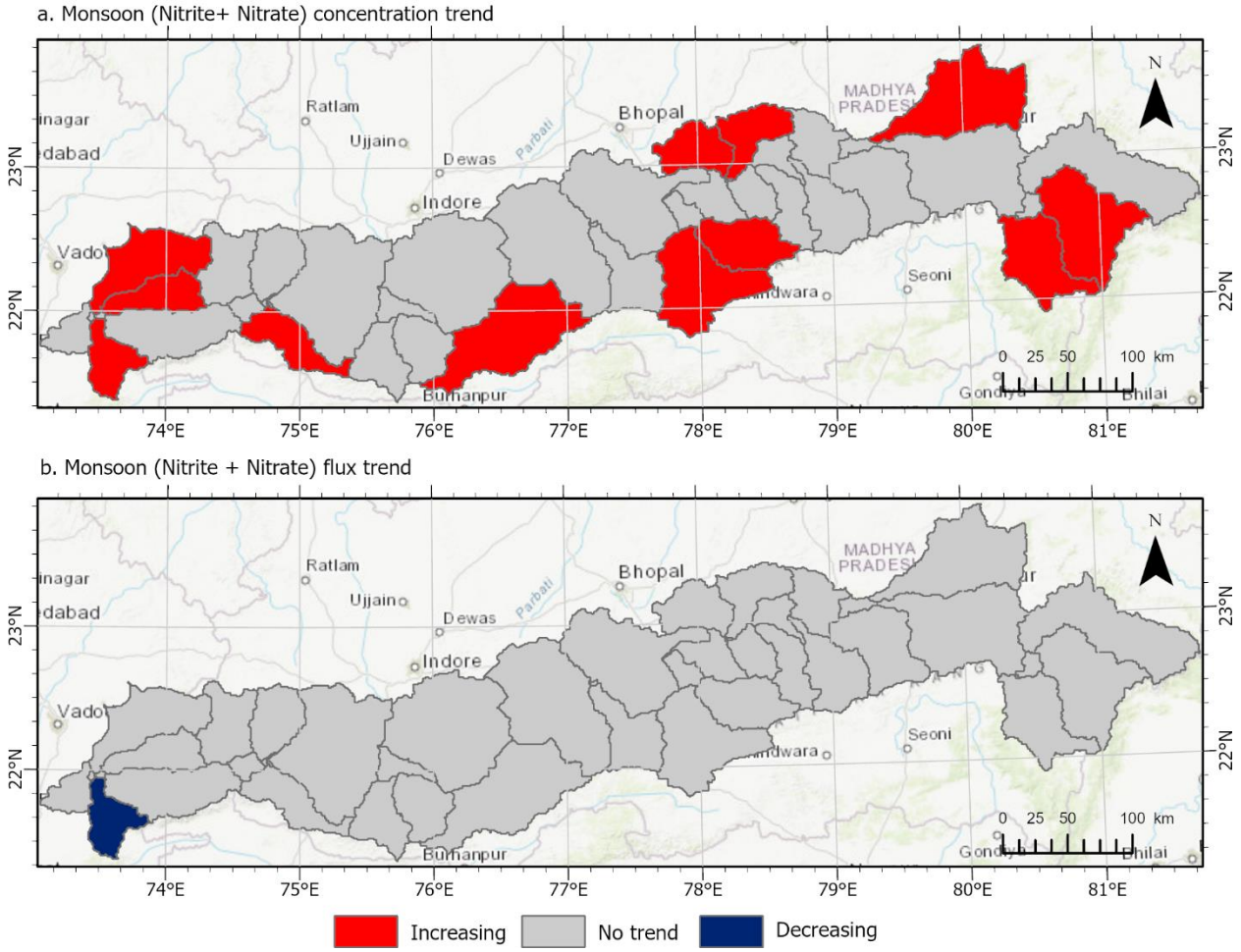

Figure 3.9 (a-b): 'a' Monsoonal (NO2 + NO3) concentration trend spatial variation across the Narmada River basin. 'b' Monsoonal (NO2 + NO3) flux trend spatial variation across the Narmada River basin. Mann-Kendall trend test was used to estimate the monotonic trends for each subbasin. All trends are significant at $p < 0.05$.

flux for all the subbasins of Narmada River basin. We found only one subbasin with a decreasing trend in nutrient fluxes. This subbasin belong to the area where outlet of the Narmada River basin is present. In spite of increasing concentration trend in this subbasin, it depicts decreasing flux of nitrogen. The only possible explanation for this observation is that the streamflow has decreased over this subbasin (Flux = Concentration * Discharge). Rest of the subbasins showed neither increasing nor decreasing trend of nutrient flux.

3.5 Discussion and Conclusions

This study builds a semi-distributed physically based hydrological model (SWAT) to characterize the catchment hydrology and nutrient transport for the Narmada River Basin. Using the flow calibrated hydrological model, we compare simulated and observed nutrients flows (N) at 17 locations inside the Ganga River Basin.

The SWAT model proved to be a useful hydrological model especially for an agriculture dominant watershed like the Narmada River Basin. Through the calibration of flow parameters, we obtain mean R^2 of 0.77 during the calibration phase (2001-2010) and mean R^2 of 0.76 during the validation phase (2011-2019) for streamflow at the five calibration sites. The analysis shows that the SWAT model adequately captures the hydrologic characteristics of the Narmada River basin. This model can be effectively used for water resource and land use management.

The capabilities of the SWAT model that facilitate extensive modelling of nutrient fluxes also has certain limitations. The SWAT model requires forcing data, which involves significant pre-processing of the input datasets which is computationally expensive for a large river basin. There are also problems in modeling reservoir processes as well as point and non-point source pollution due to the absence of adequate observation data, required data for input parameters, and lack of technical understanding pertaining to the Narmada River Basin. The SWAT model is a semi-distributed model which implies all the spatial variability within a HRU is ignored in the model, which limits applications at high spatial resolution. Finally, constant land use was assumed for the period of analysis which might influence the results of the model. The study does not account for major reservoirs and their operations as there was a lack of consistent operational data available for reservoirs inside the river basin.

The time series and spatial plots of total N reveal that the main channel of the Narmada River basin have 4-8 times higher concentration and fluxes of N as compared to the other regions. The mean monsoonal N concentration at reach locations such as Sandia and Patan are in the range of 2-6 mg/L, whereas upper reach locations such as Mandleshwar are in the range of 6-12 mg/L. This is due to the fact that anthropogenic activities -

specifically farming, are more extensive near the main channel of the basin (compared to the tributaries), and these activities use large amounts of N and P based fertilizers, excess of which is drained into the river through run-off. An average value of fertilizer input for all the agricultural land cover type for our SWAT model was used. In addition, the SWAT model was calibrated for streamflow related parameters only. This led to a significant mismatch in observed and simulated nutrient concentration. But the nutrient fluxes simulated by our model match up quite well. We conclude that our SWAT model can be used for accurate analysis for fluxes.

From our land-cover change analysis, we find that the agricultural land increased from 62.1% to 66.7% from 2000 to 2018. An average value of fertilizer input for all agricultural land inside the river basin obtained from Department of Fertilizers India at district level was used. Since the focus of this study was to account for the non-point sources of pollution mainly caused by fertilizers, we did not include any point source pollution inside our model simulations. Inclusion of point sources involves tremendous amount of work with preparing the list of industries and sewage treatment plants inside the river basin. Also, there is no central platform which reports the amount of effluents discharged into the river. Hence, this was out of scope for this study and this inspires future work which can build on this study.

Nitrogen concentration during Kharif season was observed to be more than two times higher as compared to the Rabi season. In Narmada River basin, the agricultural lands are cultivated for both Kharif and Rabi seasons with different crop cycles around the year. Due to this reason, we observe high concentrations of nitrogen for the whole year with concentration being highest in Monsoon season. The highest concentration in Monsoon season is due to the fact that this river basin lied in a temperate climate and it receives majority of rainfall during Monsoon season. Farmers in this region try to maximise the usage of rainwater to cultivate their lands causing high nitrogen concentration and flux in monsoon season.

The study attempts to analyse the impact of farming on river flow by comparing the nutrient changes from the in-situ measured data with the simulated data from the SWAT model. The analysis shows that in the tributary subbasins, which predominantly remain unexploited, there are lower absolute concentration of N but, there is a noticeable increase in their nutrient concentration over the study period of 2001-2019. This study establishes the general understanding of nutrient pollution using non-point sources mainly caused by fertilizer usage in agriculture. With future work focusing on crop cycles and incorporating LULC changes in SWAT model simulations, we can further identify the crop cycling patterns affecting the concentrations of nitrogen inside the river basin. This will further help in planning of crop cycles for the region for the most efficient and sustainable use of land.

The results of this and similar studies can help water resources planners. As the main channel contains higher concentrations of nitrogen, this water may need to be treated for domestic consumption to ensure safe health. Higher concentration of nitrogen in water may have implications in agricultural and/or industrial water use as well. Water resources planning using these results can help in controlling the agricultural application of fertilizers (specifically in the pre-monsoon/monsoon periods) when a higher rate of flux of nutrients may reach the main channel. Through the implementation of SWAT model, it is now possible to monitor the nitrogen levels in the regions of Narmada River Basin where there are very less nitrogen monitoring stations as these regions have shown changing N dynamics over the past two decades.

3.6 Conflict of Interest

The authors declare that the research was conducted in the absence of any commercial or financial relationships that could be construed as a potential conflict of interest.

3.7 Author Contributions

Conceptualization - P.K., V.L.; data analysis - P.K.; methodology - P.K., V.L.; validation - P.K.; writing (original draft) - P.K.; writing (review and editing) - P.K., V.L. All authors have read and agreed to the published version of the manuscript.

3.8 Acknowledgments

I would like to acknowledge Mr. Hung Manh Le for his critical insights and feedback in the preparation of this manuscript.

Chapter 4: Analyzing Nitrogen Transport through non-point sources in the Ganga River from Source to Sink using a hydrological model[3]

4.1 Introduction

The Ganga River Basin is one of the most densely populated (around 400 people/km^2) regions in the world. The river is of extreme importance as approximately 440 million people are directly or indirectly dependent on water that the Ganga and its tributaries provide for drinking, hydropower generation, navigation, industrial usage, ecosystem services, and agriculture. Among the anthropogenic activities, agricultural practices have the largest footprint in the Ganga Basin. The area of irrigated land has increased in the Ganga basin over the last 50 years, and it is estimated that presently 65% of the total catchment area in the river basin consists of agricultural land accounting for 3,61,100 km^2 of irrigated land (IIT Consortium, 2015). It is noteworthy to mention that the Ganga River Basin also contributes to nearly 54% of the total crop production in India (*Agricultural Statistics at a Glance*, 2018). There is an emphasis on increased crop production to meet the food demand leading to a widespread application of Nitrogen (N) based fertilizers in agricultural practices. For example, fertilizer consumption in the district levels of the Ganga River Basin has increased from 2 Gg (1 Gg = 10^9 g) in 1962-1965 to 102 Gg in 2003-2006 (IIT Consortium, 2015). In the central areas of the Ganga River Basin, the fertilizer consumption rate has increased from 300 Gg/yr (2006-2007) to 5000 Gg/yr (2019-2020), which is more than an order of magnitude (*Agricultural Statistics at a Glance*, 2019). The widespread application of fertilizer in agricultural fields leads to an increased overland flow consisting of organic and inorganic N to the Ganga River. It is estimated that smaller floodplain tributaries (< 1500 km^2) of the Ganga River that drain predominantly through agricultural lands could potentially export 0.8 ± 0.1 Gg/yr of Dissolved Inorganic Nitrogen (DIN) (nitrate + nitrite + ammonium) to the Ganga River accounting for 0.1% of the total DIN fluxes to the Bay of Bengal (Sen et al., 2018). In addition to fertilizer consumption, the discharge of industrial and domestic effluents that has increased over the last few decades could also contribute to N and P contamination of water resources (https://www.gangaaction.org/). Moreover, the stored fertilizer in soils could also dominate the N runoff for years (Shukla et al., 2021). As a result, understanding the nutrient (N) dynamics in the Ganga River Basin is important for improved monitoring of the impact of anthropogenic activities.

---

[3] Kansara Prakrut; Chatterjee Nikitasha; Sen Indra; Lakshmi Venkataraman, Analyzing Nitrogen Transport through non-point sources in the Ganga River from Source to Sink using a hydrological model. (In preparation for submission)

In this study we use the SWAT model and in-situ observations to model the nutrient transport from source to sink for the Ganga River Basin. The SWAT model is a semi-distributed model used to characterize hydrology of predominantly agricultural watersheds (Arnold et al., 1998b). Physical process based hydrological models such as SWAT, INCA (Whitehead et al., 1998), and regression based hydrological models like SPARROW (Smith et al., 1997) provide a comprehensive understanding of the dominant hydrological processes as well as nutrient transport in a watershed which can lead to key insights on historic trends and spatial distribution of nutrient contamination distribution over the entire basin. For the entire Ganga River Basin, however, there exist very limited modelling studies. Whitehead et al. (2015) conducted the first and only basin scale water quality study encompassing the Ganga Basin to study the impacts of future climate and socio-economic impacts on N fluxes. But these studies used the INCA model for a past-time period of 1981-2000. For predicting the future changes in nutrient flows, Whitehead et al. (2015) and Jin et al. (2015) use RCP climate model predictions for the present century 2000-2100. Other modelling efforts in literature focus on sub-basins of Ganga River (Pathak et al., 2018). Similarly, nutrient monitoring studies which do not involve modelling have been carried out at a few select locations of the Ganga River Basin such as major cities along the banks, in Uttar Pradesh (Joshi et al., 2009; Sharma et al., 2014; Tare et al., 2003; Tiwari et al., 2016), in the delta region near the mouth of the river (Debnath et al., 2018; Mukhopadhyay et al., 2006; Sarkar et al., 2007) and a few studies focus on the Upper Ganga River (Jain, 2002; Matta, 2015). A comprehensive study of N concentration and flux variability through hydrological modelling using most recent in-situ observations is missing. This study is designed to help in understanding the extent and magnitude of N-based contamination from source to sink over a long-term record, which can aid in policymaking leading to better agricultural management practices.

In this study, we use SWAT to model catchment hydrology of the Ganga Basin from 1998 to 2016. The model was calibrated for streamflow and nitrogen concentration related parameters for the period from 2001-2010 and validated for a period from 2011-2016 using observed streamflow data from Central Water Commission (CWC). Performance metrics such as the Nash-Sutcliffe efficiency, correlation coefficient, root mean square error and percent bias were used to evaluate the model. Model simulated N outputs were compared against two in-situ nutrient measurement data datasets – 1) CWC and 2) In-situ data obtained from river water samples collected during this study. We use the model simulated N outputs for comparison with in-situ nutrient data from CWC and data collected for this study to analyse the spatio-temporal variability of nutrient concentrations and fluxes across the Ganga Basin from 1998-2016.

The following research questions are addressed in this study:

1) What is the spatio–temporal variability of N concentrations across the entire Ganga Basin through pre-monsoon, monsoon and post-monsoon seasons?
2) What is the magnitude of increasing/decreasing trend in N fluxes exported from the Ganga Basin to Bay of Bengal at sub-basin scale?

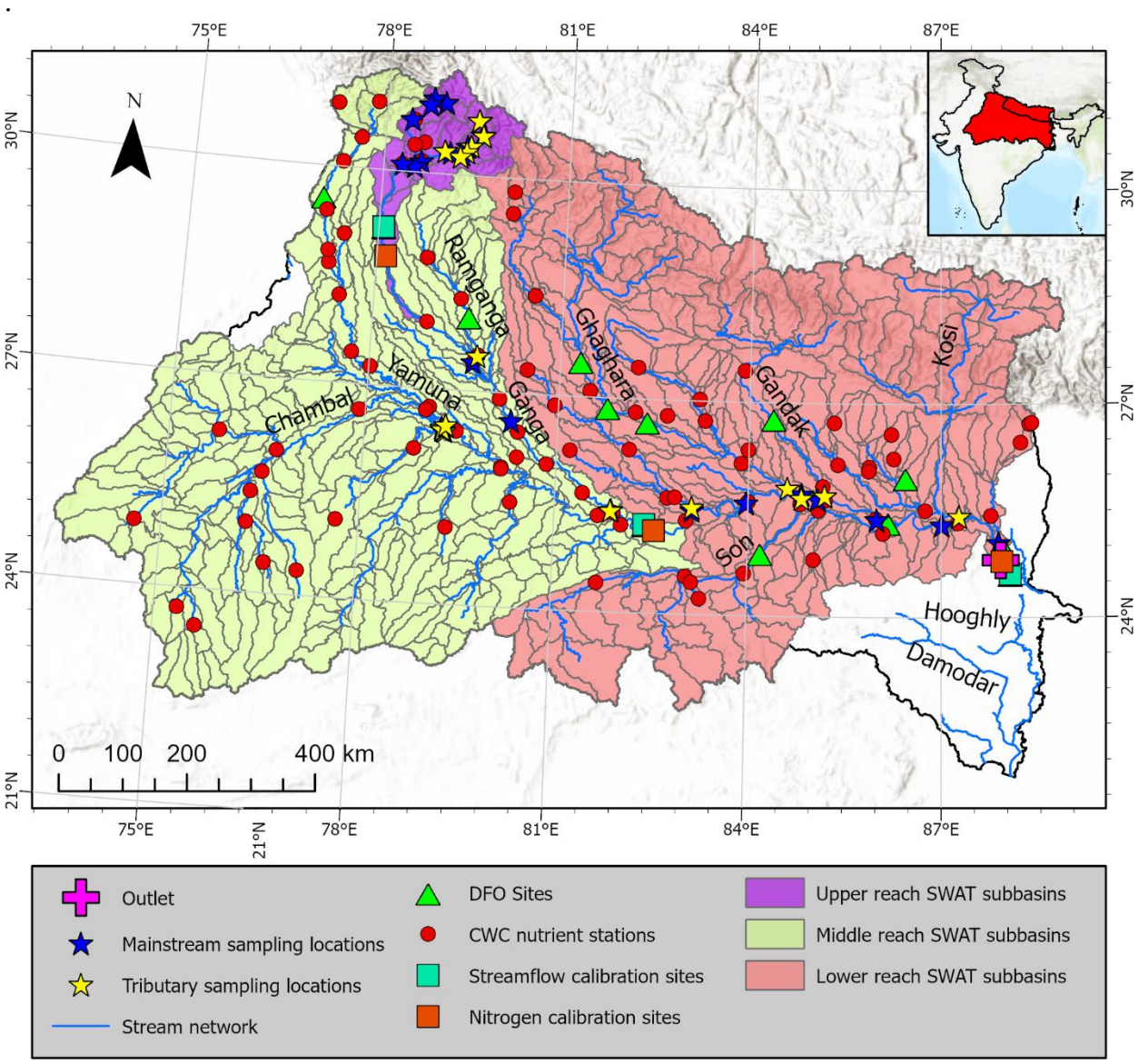

Figure 4.1: Study area showing the locations of gauge network measuring nutrients inside the Ganga River Basin. The Himalayan Mountain ranges forms the northern boundary of the watershed whereas rest of the watershed largely remain flat. The map also shows 38 in-situ sampling locations on mainstream and tributary channel of River Ganga where nutrient data was collected. DFO sites represent the locations at which SWAT model was calibrated and validated.

The remainder of this paper has been divided into 4 sections as follows: Section 2: Study Area and datasets - gives description of the study area and datasets used in the study, Section 3: Methods - describes the methodology followed in building the SWAT model and the analysis of nutrients data, Section 4: Results and Discussion: discusses the important results from the analysis in this study and limitations of our study, and finally Section 5: Conclusions: summarizes the work as well as discusses future questions

4.2 Study Area and Datasets

The section provides a description of the Ganga River basin. In addition, we describe the datasets utilized in this study (**Table 4.1**).

Table 4.1: Description of the datasets used in this study.

Data	**Source**	**Spatial/ Temporal resolution**
DEM	SRTM 3 arc-second void filled	90 m / -
Land use	Climate Change Initiative	300 m / 2008
Fertilizers	ICRISAT	Per district / 1956-2008
Soil	Food and Agricultural Organization (FAO) Global Soils	7 km / -
Rainfall	Indian Meteorological Department (Gridded product)	0.25° / 1951-2019
Temperature	Indian Meteorological Department (Gridded product)	0.25° / 1951-2019
Discharge	Central Water Commission India (CWC)	- / 1951 - 1973
Climatology	Climate Forecast System Reanalysis (CFSR)	- / 1998 - 2017

4.2.1 Ganga River Basin

The Ganga River is a 2,525 km long perennial river originating from the Gangotri glacier in the Himalayas in the Indian state of Uttarakhand (**Figure 4.1**). The catchment of the river extends across India, Nepal, Tibet and Bangladesh encompassing an area of 1.08 million square kilometres. Inside India, the river traverses from Uttarakhand to Himachal Pradesh, Haryana, Union Territory of Delhi, Rajasthan, Madhya Pradesh, Uttar Pradesh, Bihar, Jharkhand, Chhattisgarh, West Bengal and finally it flows into the Bay of Bengal covering approximately 26% of the geographical area and 47 % of the net irrigated land area of the country (https://indiawris.gov.in/wiki/doku.php?id=ganga) (**Figure 4.2**). This region also suffers from excessive nitrogen pollution due to more and more usage of

fertilizers. It forms one of the most fertile flood plains of the world providing for large scale agricultural activities. In this paper, we have defined the upper reach of the Ganga River basin as the watershed region upstream of Bijnor, middle reach as the watershed region between Bijnor and Mirzapur, and lower reach as the downstream region of Mirzapur (Mirzapur to Farakka).

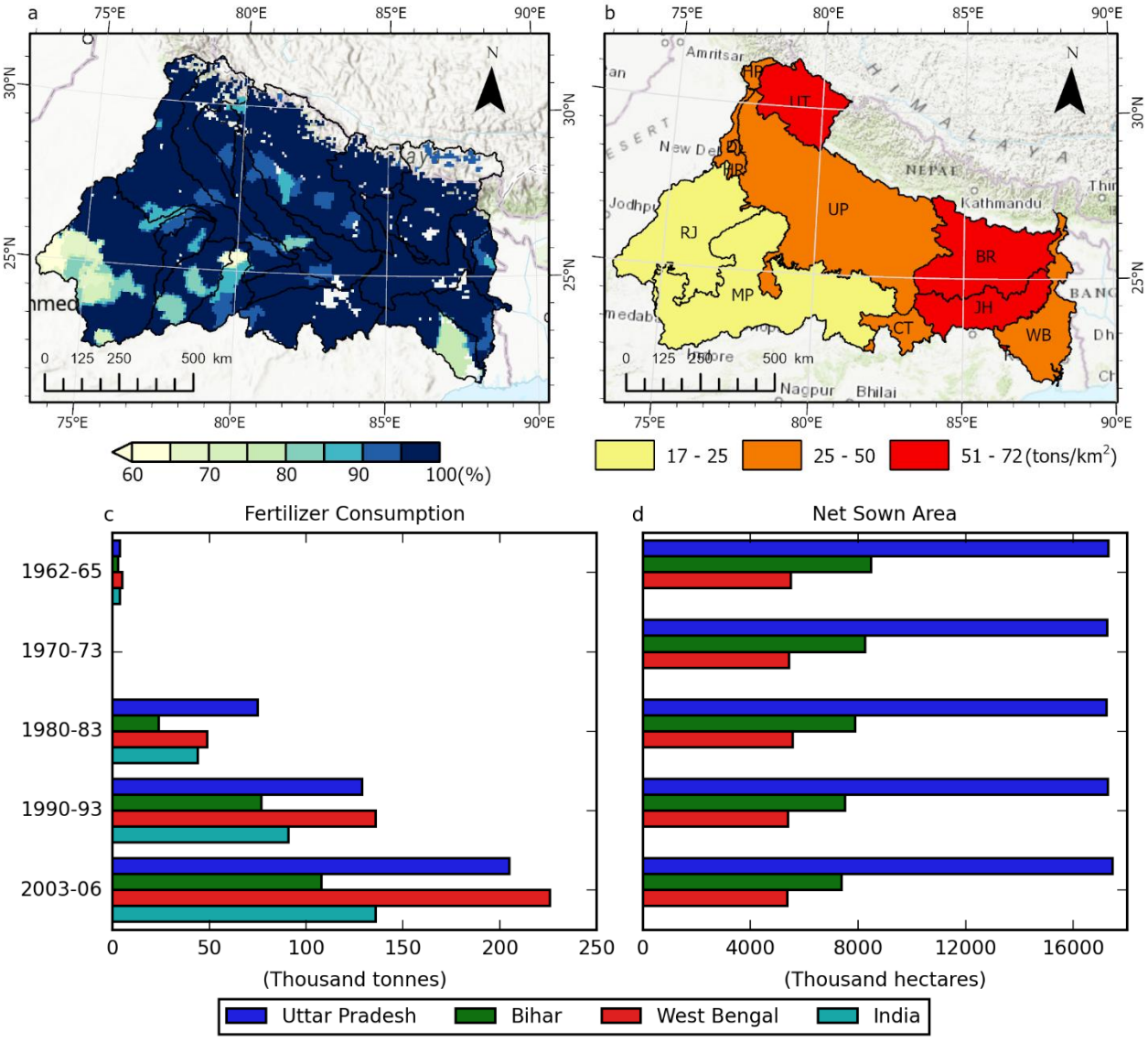

Figure 4.2 (a-d): (a) Irrigated land map depicting percentage of land being irrigated for crop production. Western part of watershed highlights less irrigation (<60%) as compared to the other parts which show very high extent of irrigation (>90%). (b) State-wise mean fertilizer consumption area across Ganga River Basin. (c) Average state-wise fertilizer consumption per district in Ganga Basin. (d) State-wise mean net sown area in the Ganga River Basin.

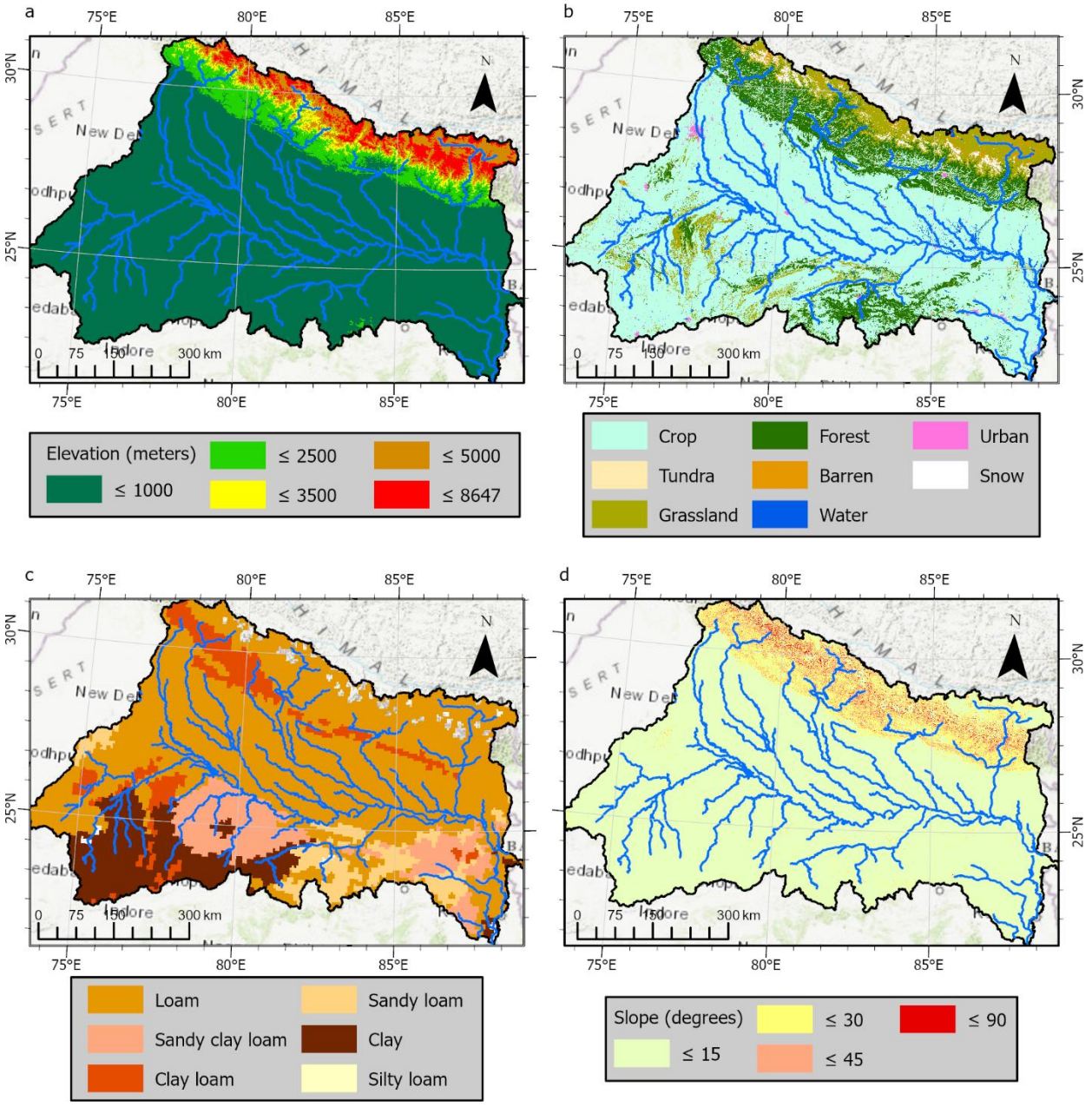

Figure 4.3 (a-d): Spatial data input for the SWAT model. (a) DEM of the Ganga River Basin. The Gangetic floodplains has relatively flat terrain with elevation less than 1000 m from the mean sea level. (b) Land-cover map of the Ganga River Basin. It is important to note that the most dominant land cover type is 'Cropland' as it feeds from the fertile floodplains covering more than 70% of the watershed area. (c) Soils map of the Ganga River Basin. Loamy soil is the most dominant soil type. (d) Slope map of the Ganga River Basin. Slope map correlated with the DEM map with less than 15% slope in majority of the watershed (Gangetic floodplains).

4.2.2 Digital Elevation Model (DEM)

Elevation data was obtained using DEM from the Shuttle Radar Topography Mission (SRTM) (Farr et al., 2007b). SRTM generated the high-resolution topographical data from its mission conducted in 2000. It is a global dataset with high-resolution (30 m) as well as low-resolution (90 m) products extending from 60° N to 60° S (Berry et al., 2007). This dataset is distributed by the United States Geological Survey (USGS) and is available from the Earth explorer platform. The SRTM system consisted of two radar antennas to obtain interferometric imagery of the topography of the Earth's surface. This dataset has been assessed using non-oceanic Ground Control Points (GCPs) measured from kinematic GPS (Rodríguez et al., 2005) which displays good performance of DEM specifically for regions with low gradients. In this study, we use the 90 m void filled product to reduce the processing complexity of the SWAT model considering the size of the Ganga River Basin is approximately 1.6 million km^2 (~ 197 million pixels of 90 m * 90 m) (**Figure 4.3a**).

4.2.3 Land-cover

In this study, we used the land cover data from European Space Agency (ESA) Climate Change Initiative (CCI) land cover products. CCI provides global annual land-cover maps for 1992-2018 at a spatial resolution of 300 m. The land cover map for 1992-1999 were obtained from AVHRR, for 1998-2012 were obtained from SPOT Vegetation, and for 2013 onwards were obtained from PROBA-V and Sentinel-3 OLCI. The product classifies the imagery into 22 distinct land-cover classes. We use the Version 2.0.7 land cover product which accurately classifies irrigated cropland, rainfed cropland, forested areas, urban and barren areas validated using the Globcover 2009 validation dataset (ESA, 2017b) (**Figure 3b**). There are 8 major land cover types in the Ganga River basin with 'Agricultural land' being the most common type with 69.7% of the geographical area inside the watershed. A new detailed land cover map was prepared using the ESA land cover map. 'Agricultural land' was further classified into distinct crop types to produce the new detailed land cover map, which was used as input to the SWAT model. District wise annual crop data for India was available for a period of 1956-2008 through - http://www.lib.utexas.edu/maps/middle_east_and_asia (Ross et al., 2018).

4.2.4 Soils

For this study, we used soils data from the Food and Agriculture Organization (FAO) (**Figure 3c**). The soil map was available at a scale of 1:5000000 at global level. This dataset was produced as a collaboration of FAO and UNESCO in 1961 and it took twenty years to prepare the global dataset (http://www.fao.org/soils-portal/data-hub/soil-maps-and-databases/faounesco-soil-map-of-the-world/en/).

4.2.5 Meteorological data (Rainfall, air temperature, solar radiation, wind speed and relative humidity)

Rainfall and air temperature data were obtained from the Indian Meteorological Department (IMD). IMD provides gridded rainfall at 0.25° and minimum and maximum air temperature at 0.5° spatial resolution. IMD maintains rainfall records from a network of approximately 6,329 rain gauges and 395 temperature gauges across different parts of India with varying time spans of data collection. The data collected by these in-situ stations had been interpolated to the latitudinal and longitudinal grids using Shepard's interpolation technique (Rajeevan et al., 2006; Srivastava et al., 2009). In this study, we used the gridded rainfall and temperature product from 1951-2016. The remaining meteorological datasets – solar radiation, wind speed, and relative humidity were obtained from the global Climate Forecast System Reanalysis (CFSR) system (Saha et al., 2010).

4.2.6 Streamflow

The observed streamflow data required for the SWAT hydrological model calibration was obtained from the Dartmouth Flood Observatory (DFO) - https://floodobservatory.colorado.edu/, as a part of Global Flood Detection System (GFDS) program. This program is developed and run at the Joint Research Centre of the European Commission in collaboration with the DFO at Colorado University. The data is available from 1998 at a daily time scale. There are 11 locations inside the Ganga River Basin where data from DFO was available. For this study, we use data for only 3 locations for calibration and validation of SWAT model. These locations are: 1) Bijnor (downstream of Haridwar), 2) Mirzapur, and 3) Farakka (**Figure A4.1**).

Table 4.2: CWC nutrient gauge station data information.

Site	Lat	Lon	Data availability	# of observ-ations	Min	Max	Mean	Std	Trend slope	p-value
	(°N)	((°E)			(mg/L)	(mg/L)	(mg/L)	(mg/L)	(mg/L/ yr)	
Agra	27.26	78.02	1976-2017	1669	0.00	44.38	1.90	3.24		
Aklera	24.43	76.6	1993-2016	208	0.00	65.86	4.15	5.68	0.00	0.91
Ankinghat	26.91	80.07	1973-2017	628	0.00	44.38	3.35	4.07	0.16	0.00
Auraiya	26.43	79.42	1981-2017	578	0.00	29.20	2.67	3.30	0.07	0.00
Ayodhya	26.81	82.21	1998-2017	341	0.00	5.75	2.67	1.87	0.00	1.00
Azamabad	25.33	87.26	2001-2015	40	0.18	10.40	8.82	2.30		
Balrampur	27.44	82.23	1998-2017	317	0.00	22.33	2.63	2.12	0.01	0.69
Baltara	25.5	86.75	2005-2015	119	0.01	10.40	4.07	4.52	0.89	0.00
Banda	25.48	80.31	1982-2015	313	0.00	17.30	2.77	3.02	0.23	0.00
Bareilly	28.28	79.38	1973-2017	564	0.00	44.38	4.68	5.99	0.19	0.00
Barod	25.4	76.32	1993-2016	217	0.00	22.00	4.10	3.91	0.09	0.02
Basti	26.78	82.71	1998-2017	314	0.00	5.75	2.68	1.78	0.01	0.91
Berhampore	26.33	83.99	2001-2015	166	0.00	5.00	3.52	0.97	0.20	0.00
Bhatparani	26.03	80.85	1998-2006	543	0.00	44.38	3.52	4.63	0.18	0.00
Bhitaura	26.72	83.3	1976-2017	299	0.00	5.94	2.70	1.93	-0.02	0.65
Birdghat	25.6	84	1998-2017	60	5.74	11.12	9.02	1.87		
Buxar	25.4	81.91	2009-2015	1024	0.00	17.30	1.13	2.16	0.01	0.00
Chapra	24.53	83.05	2001-2015	1215	0.00	44.38	0.80	2.49	0.00	0.00
Chhatnag (Allahabad)	27.5	79.7	1972-2017	430	0.00	33.34	3.54	6.12	0.14	0.00
Chopan	28.66	77.25	1963-2017	482	0.07	78.56	9.33	9.58	0.25	0.00
Dabri	30.16	78.6	1985-2017	493	0.00	44.38	0.59	2.58		
Delhi Rly Bridge	26.73	85.33	1993-2016	67	0.01	10.40	4.59	4.71	2.13	0.00

Deoprayag (G)	26.65	77.9	1976-2016	1099	0.00	126.12	1.75	4.64	0.01	0.00
Dheng Bridge	24.23	83.27	2005-2015	246	0.01	10.40	0.68	1.65	0.01	0.00
Dholpur	26.11	85.88	1976-2017	112	0.01	10.40	4.65	4.76	0.49	0.00
Duddhi	27.09	81.48	2004-2017	339	0.00	6.73	2.72	1.90	0.02	0.69
Ekmighat	26.75	78.98	2006-2015	1669	0.00	44.38	1.90	3.24		
Elginbridge	24.79	87.94	1998-2017	208	0.00	65.86	4.15	5.68	0.00	0.91
English Bazar	24.81	87.92	2001-2015				5.35			
Etawah	27.4	79.62	1972-2017	1054	0.00	1387.20	2.65	42.74	0.02	0.00
Farakka	29.07	77.46	2001-2015	174	3.14	11.12	6.28	2.47	0.38	0.00
Farakka (Feeder)	25.64	85.2	2001-2015	169	0.02	10.40	5.35	3.30		
Fatehgarh	28.8	78.14	1976-2017	573	0.00	44.38	3.45	4.71	0.15	0.00
Galeta	25.08	79.34	1993-2016	272	0.07	37.83	5.96	4.73	0.38	0.00
Gandhi ghat	24.8	85.02	2009-2015	60	0.01	10.40	6.67	4.80		
Garhamukteshwar	29.51	80.13	1976-2017	557	0.00	44.38	3.48	3.94	0.17	0.00
Garrauli	25.96	80.15	1982-2016	494	0.00	28.02	3.17	3.88	0.10	0.00
Gaya	25.38	85.99	2006-2014	59	5.03	10.40	7.83	2.22		
Ghat	26.05	85.87	1995-2017	140	0.01	10.00	0.79	1.89	0.02	0.00
Hamirpur	26.57	86.22	1981-2017	584	0.00	65.86	1.77	3.98	0.02	0.00
Hanskhali	24.59	83.95	2001-2015	59	0.84	10.40	7.38	3.97		
Hathidah	26.23	86.26	2009-2015	118	0.07	10.40	4.91	3.91	0.00	0.31
Hayaghat	27.93	78.86	2005-2015	68	0.01	10.40	4.54	4.87	2.47	0.00
Islampur	30.07	77.35	2005-2005	36	0.04	23.86	6.36	5.61		
Jainagar	26.46	80.38	2005-2015	117	0.01	10.40	3.96	4.48	0.59	0.00
Jamtara	25.68	76.48	1980-2001	498	0.00	17.30	2.21	2.99		
Japla	25.58	84.81	2009-2015	231	0.00	11.89	2.82	3.69	0.10	0.00
Jhanjharpur	26.11	80.38	2005-2015	642	0.00	44.38	3.17	4.06	0.13	0.00
Kachlabridge	24.45	83.14	1982-2017	217	0.00	24.00	3.43	3.52	0.07	0.01
Kalanaur	24.41	81.69	1993-2016	35	0.01	10.40	5.93	4.62		
Kalna(Ebb)	25.43	87.77	2001-2015	585	0.00	11.89	1.60	2.15	0.06	0.00
Kanpur	25.18	86.1	1970-2017	226	0.05	1.21	0.10	0.15	0.00	0.00
Katwa	25.83	85.16	2001-2015	804	0.00	44.38	0.65	2.53		
Khatoli	26.86	80.94	1993-2016	169	0.07	10.40	5.32	3.36	-0.69	0.00
Koelwar	23.48	75.63	2009-2015	76	0.01	10.40	3.51	4.08	1.29	0.00
Kora	25.64	82.86	1981-2016	58	0.01	10.40	3.70	4.57		
Kota	26.72	88.38	1995-2004	596	0.00	126.15	2.77	6.95	0.05	0.00

Kuldah bridge	29.38	77.15	1981-2017	204	0.00	21.00	4.53	3.88	0.11	0.03
Labha	25.23	82.04	2001-2015	923	0.00	44.38	1.19	2.85	0.00	0.00
Lakhisarai	25.16	82.55	2006-2015	12	3.60	4.22	3.91	0.20		
Lalganj	28.22	77.45	2005-2015	273	0.07	15.29	5.22	3.51	0.38	0.00
Lucknow	28.82	78.8	1973-2017	900	0.00	394.00	1.28	13.34	0.00	0.00
Mahidpur	27.34	80.48	1993-2016	911	0.00	9.26	0.59	1.02	0.01	0.00
Maighat	25.1	77.65	1963-2017	274	0.00	49.08	5.43	7.99	0.36	0.00
Matigara	28.38	80.55	2006-2007	542	0.00	44.38	4.91	6.34	0.19	0.00
Mawi	28.83	77.22	1993-2016	478	0.00	44.38	1.51	3.34	0.02	0.00
Mejja Road	30.43	77.62	1976-2017	408	0.00	36.47	2.13	3.48	0.06	0.00
Mirzapur	25.35	81.67	1976-2017	357	0.00	5.94	2.76	1.89	0.04	0.15
Mohana	26.24	81.21	1993-2016	111	0.06	38.23	8.35	5.17	0.46	0.00
Moradabad	27.02	83.21	1980-2017	176	0.52	19.51	5.01	3.17	0.38	0.00
Neemsar	30.1	78.3	1977-2016	12	0.07	0.94	0.62	0.25		
Pachauli	30.3	78.99	1980-2017	576	0.00	34.37	2.58	4.78	0.06	0.00
Paliakalan	24.97	76.29	1998-2017	327	0.00	5.94	2.74	1.93	0.03	0.50
Palla	26.16	78.78	2007-2016	560	0.00	44.38	0.53	2.35	0.01	0.00
Paonta	25.94	80.15	1998-2016	487	0.00	44.38	0.63	2.64	0.01	0.00
Pratappur	25.66	81.43	2014-2017	196	0.00	22.00	3.69	3.22	0.22	0.00
Raibareli	26.14	85.39	1973-2017	633	0.00	16.27	1.74	2.44	0.04	0.00
Regauli	26.74	88.42	1998-2017	616	0.00	20.35	1.88	2.60	0.05	0.00
Rishikesh	26.46	88.24	1971-2016	735	0.00	44.38	1.87	3.50	0.00	0.00
Rudraprayag	25.5	85.09	1976-2016	119	0.01	10.40	4.11	4.54	0.89	0.00
Sangod	26.29	82.13	1993-2016	18	0.06	5.54	1.58	1.92		
Seondha	23.72	75.35	1972-2017	399	0.00	34.47	3.57	4.12	0.14	0.00
Shahijina	30.38	78.48	1981-2017	62	0.01	10.40	3.94	4.44	1.91	0.00
Shahjadpur	29.81	80.13	1980-2016	481	0.00	19.54	1.57	2.23	-0.03	0.00
Sikander Pur	26.21	75.77	2005-2015	230	0.00	35.94	3.44	5.09	0.01	0.54
Silliguri (Champa)	27.44	83.91	2006-2007	476	0.00	44.38	0.45	2.37		
Sonapur	30.94	77.85	1989-2015	65	0.01	10.12	1.23	1.90	-0.09	0.17
Sripalpur	26.14	83.88	2006-2015	204	0.00	12.00	3.65	2.92	0.06	0.13
Sultanpur	26.7	78.93	1994-2017	81	0.01	10.40	5.32	4.17	1.31	0.00
Tal	30.73	78.45	1993-2016	232	0.07	15.15	4.44	3.10		
Tehri - Zero point	25.32	83.04	1972-2013	350	0.00	5.75	2.63	1.88	0.01	0.78
Thal	30.88	77.21	1998-2007	713	0.00	17.94	1.67	2.59	0.03	0.00
Tonk	27.26	78.02	1993-2016	335	0.00	10.40	0.56	1.84	0.01	0.00
Tribeni	24.43	76.6	2005-2015	1200	0.00	322.29	1.35	9.59	0.00	0.00
Tuini (T)	26.91	80.07	1993-2016	231	0.07	23.86	4.55	3.33	0.38	0.00

Turtipar	26.43	79.42	1998-2017	1054	0.00	1387.20	2.65	42.74	0.02	0.00
Udi	26.81	82.21	1972-2017	174	3.14	11.12	6.28	2.47	0.38	0.00
Uttarkashi	25.33	87.26	1989-2016	169	0.02	10.40	5.35	3.30		
Varanasi	27.44	82.23	1963-2017	573	0.00	44.38	3.45	4.71	0.15	0.00
Yashwant Nagar	25.5	86.75	1993-2016	272	0.07	37.83	5.96	4.73	0.38	0.00

4.2.7 Nutrients data

We have used two nutrient datasets: 1) From CWC and 2) In-situ data collected for this study.

4.2.7.1 CWC nutrients data

CWC monitors constituents present in water at 109 different locations inside the Ganga River Basin. There are a total of 109 in-situ stations that collect the nutrient observations out of which 9 stations had inconsistent data as a result data from the 92 stations were used in this study. Amongst these 92 stations as well, there were inconsistencies with no data at several time points. **Table 4.2** provides a comprehensive list of all the water quality and nutrient measurement data collected from the stations. The availability of data for each in-situ station varies but lies within 1963-2017. This data can be downloaded from the Water Resources Information System (WRIS) India website. Further information about this data can be found at https://indiawris.gov.in/wiki/doku.php.

4.2.7.2 In-situ nutrient data

Upstream water samples were collected from the bank of the river and downstream water samples were collected from the centre of the rivers by using a boat or from a bridge. Samples were collected at 38 locations in total, out of which 22 are from the main stem of Ganga River and 16 are from its major tributaries. In the headwater region of the Ganga River (from Gangotri, 30° 59′ 41.1″ N, 78° 56′ 16.9″ E, altitude 3053 m above mean sea level (amsl) to Haridwar (29° 56′ 44.5″ N, 78° 09′ 51.1″ E, altitude 314 m amsl) samples were collected in the pre-monsoon, monsoon, and post-monsoon season corresponding to 2014, 2015, and 2016 and in the downstream of Haridwar up to Manikchak (25° 03′ 32″ N, 87° 53′ 41″ E, altitude 19 m amsl), samples were collected for only three seasons of 2016. In addition to seasonal sampling, a monthly time-series sampling was carried out at Manikchak between June 2016 and April 2017.

4.2.8 Fertilizers data

All India district level fertilizer consumption information was obtained from the International Crops Research Institute for the Semi-Arid Tropics (ICRISAT) (http://data.icrisat.org/dld/src/support.html). The dataset consists district-wise fertilizer

consumption per year from 2000-2017. There are 185 districts lying completely or partially inside the Ganga River Basin. Fertilizer data was analyzed for district-wise mean consumption and consumption trends. This mean fertilizer consumption rates from this data were also provided as an input to the SWAT model to assign appropriate fertilizer rates based on crop types.

4.3 Methodology

This section describes the methods used in our study - the hydrological model and analysis of the nutrients. The section is divided into four sub-sections. The first sub-section explains the steps performed to create a detailed land use map with crop type. The second sub-section describes the analysis performed on nutrient data. The third sub-section describes the SWAT model setup and the pre-processing of the input data for the model. And, the fourth sub-section describes the calibration and validation process for the SWAT model.

4.3.1 Detailed land use preparation

The land use data from ESA only classifies agricultural land as a single class of generic cropland. Since the purpose of this study is to perform nutrient analysis, a more detailed land use data with crop type distribution was required. To prepare the detailed land use map, three auxiliary datasets were used – District polygons, Annual crop distribution per district, and ESA land use raster. 'Majority' crop type was extracted per district for 2008 from the annual crop distribution per district data. This provided us with the crop type with largest sown area per district. This information was then attributed to the corresponding district polygons. This district polygon shapefile was then rasterized to the spatial resolution of ESA land use map (i.e. 300 m). The rasterized district polygons which contain 'majority' crop type per district was overlaid on original ESA land use map. Information was extracted from the rasterized district polygons only for the locations where ESA land use raster map had a pixel value corresponding to 'Cropland' type. An important thing to note here is that we only had access to crop distribution data for the districts in India only. For the regions of the Ganga River Basin lying outside of India, 'Cropland' land use type remains the same, which is generic cropland. A flow chart of the steps followed in detailed land use preparation is provided in **Figure A4.1**. In addition, the 'majority' crop type per district is also shown in **Figure A4.2**. Also, for few districts in India, the data was inconsistent. Hence, for these regions again, 'Cropland' type remains the same (generic cropland). The detailed land use map finally prepared is shown in **Figure A4.3**.

4.3.2 Nutrient data analysis

For the in-situ sampling data collected, physio-chemical parameters (pH, temperature, dissolved oxygen (DO), specific conductance (μS/cm)) of stream water were measured with a handheld PCSTestr 35 Multi-parameter instruments. Nutrient concentrations (nitrate + nitrite) were analysed using a Seal Analytical continuous-flow Auto Analyzer 3 (AA3) instrument. Since, the concentration of nitrite is very low in water (not more than 7% of total dissolved nitrogen), nitrogen is reported as nitrate + nitrite.

CWC nutrient data was analyzed using Mann-Kendall non-parametric trend test and boxplots. We use the original Mann-Kendall test (Hirsch et al., 1982) to examine monotonic patterns. The slope for the monotonic trends was determined utilizing Sen's slope estimator. The trend results are considered significant if $p < 0.05$.

4.3.3 SWAT model setup

Soil Water Assessment Tool (SWAT) is a semi-distributed, continuous daily timestep hydrological model developed by the United States Department of Agriculture (USDA) in collaboration with Texas A&M University. This model can simulate the hydrology of small to river-basin scale watersheds (Abbaspour et al., 2015; Neitsch et al., 2011). The SWAT model has application that range from soil erosion to analysing non-point source pollution (Arnold et al., 1998a). This model can simulate quality and quantity of surface water and can assess the impact of environmental change due to land-use and agricultural management practices (Jayakrishnan et al., 2005). The inputs to this model are spatial data which includes DEM, land-use/land cover, soils and meteorological data including precipitation, temperature, solar radiation, wind speed and relative humidity. The model divides the watershed into sub-basins and further divides them into Hydrological Response Units (HRUs) which are a combination of slope class, land cover type, and soil type. The modelling of the watershed is done in two phases: land phase and routing phase. The land phase estimates the runoff for each of these HRUs using the water balance equation:

$$SW_t = SW_0 + \sum_{i=1}^{t}(R_{day} - Q_{surf} - E_a - W_{seep} - Q_{gw}) \quad (1)$$

Where SW = Soil Moisture content, R = Precipitation, Q = Surface runoff, E = Evapotranspiration, W = Infiltration, and Q = Groundwater, and the subscripts represent: *0* = intial time step, *t* = time step t, *day* = total daily precipitation, *surf* = surface runoff, *a* = evapotranspiration into the atmosphere, *seep* = Seepage into the soil, *gw* = groundwater storage

Penman-Monteith method was used for estimation of the potential evapotranspiration. The generated runoff is then routed through the stream network to the outlet of the watershed in the routing phase. The Muskingum routing method was used for the routing of water in the streams. Detailed land use map prepared as described in Section

3.1 was used as the input for the SWAT model. Fertilizer rates based on individual crop types were applied to the HRUs corresponding to those crop types.

4.3.4 SWAT model calibration and validation

An initial model was built using SWAT 2012 (QSWAT) using the catchment attributes inputs and climatic inputs. The model is then calibrated using SWAT Calibration and Uncertainty Procedures (SWAT-CUP) (**Figure A4.4**). For model calibration, the Sequential Uncertainty Fitting (SUFI2) method was used (Abbaspour et al., 2015). Nash-Sutcliffe Efficiency (NSE) was used as the objective function for calibrating streamflow as well nitrogen concentration and flux. Next, we create two separate models for calibration. The purpose of creating two separate models is because high flows dominate the nutrient fluxes whereas low flows contribute more to the variability of nutrient concentrations. For the purpose of this paper, we name them model A and B. For model A, the calibration aim is to first calibrate the model for high flows and then for nutrients. For model B, the calibration aim is to first calibrate the model for low flows and then for the nutrients. These models were calibrated for 2001-2010, with 3 years (1998-2000) as the warm-up period. The models were calibrated at three locations for streamflow and nitrogen concentration each (**Figure 4.1**). A workflow depicting the process model building, calibration and validation for this study is shown in **Figure A4.4**. Parameters for both streamflow and nitrogen concentration were included in the calibration process. The SWAT model allows for elevation corrections for precipitation and temperature which can be calibrated using the lapse rate parameter. Using Anand et al. (2018), we used a value of −3 to −6.5 °C/km as the temperature lapse rate and 100–250 mm/km as the precipitation lapse rate in sub-basins where the elevation changes are significant. After multiple simulations to calibrate the model, we validated the model from the time period 2011-2017. Simulated streamflow and nitrogen concentration were compared with observed streamflow using the statistical metrics: NSE, correlation coefficient (R^2), and percent bias (p-bias).

4.4 Results and Discussion

4.4.1 Fertilizer consumption and crop distribution

Ganga River Basin is a pre-dominantly agricultural watershed with agricultural lands as 67% of the total watershed area. These agricultural lands consume tonnes of fertilizers to produce crops. These fertilizers are rich in nitrogen and phosphorus which are the two most essential nutrients for crop growth. These nutrients eventually get transported by the surface runoff and sub-surface runoff causing non-point source nutrient pollution in the watershed. To understand the transport of these nutrients, we need to first analyze the non-point sources of pollution caused by fertilizer applications – their amounts and their spatial distribution over the entire watershed. First, we analyze the spatial

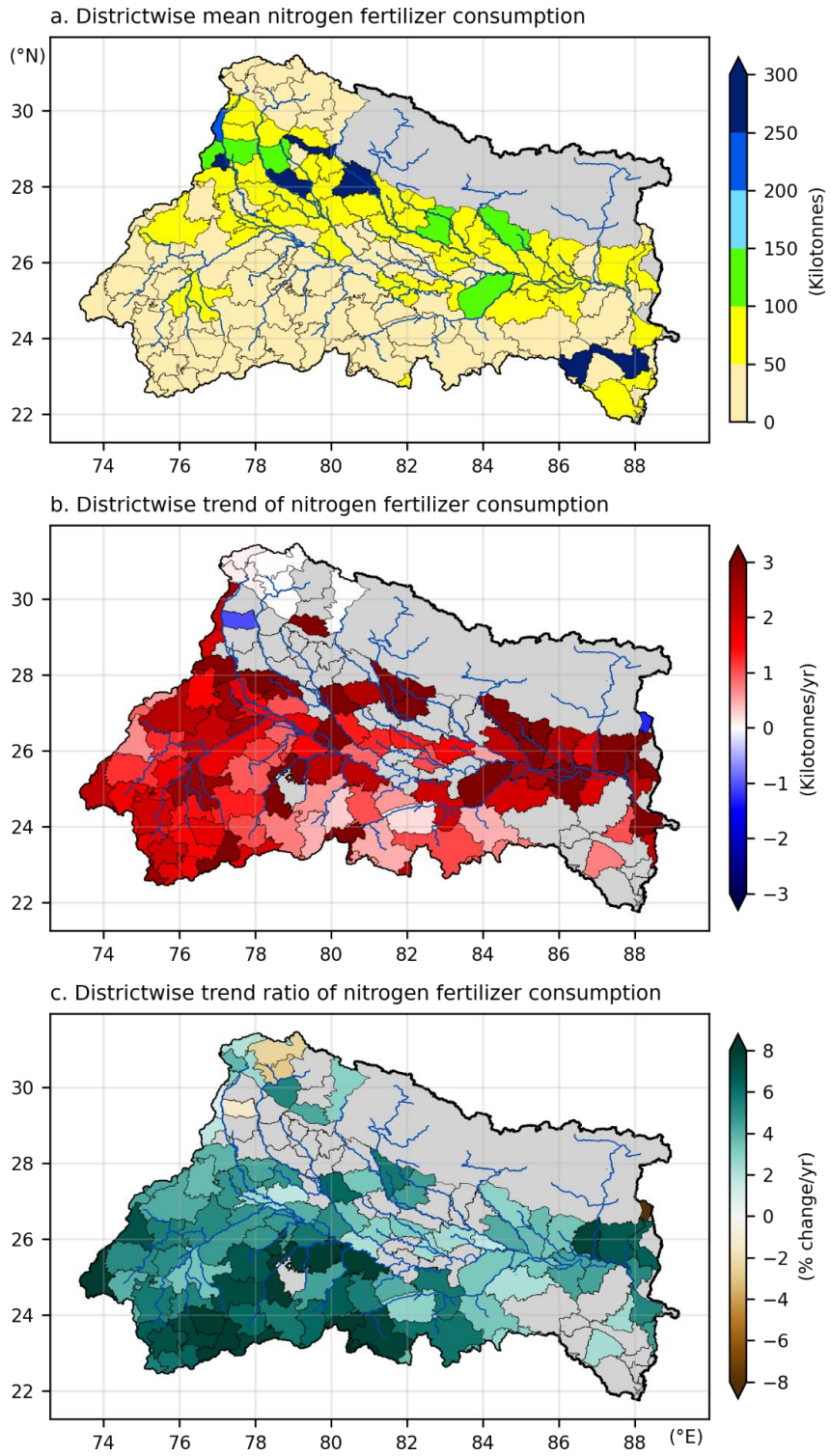

Figure 4.4 (a-c): (a)Mean fertilizer consumption, (b) trend map for fertilizer, and (c) trend ratio map for fertilizer from 2000-2017. Grey areas in the figures represent the following in each subfigure: (a) no data (b) no data and no statistically significant trend and (c) no data and no statistically significant trend.

distribution of average nitrogen-based fertilizer consumption per district from 2000-2017 (**Figure 4.4a**). The fertilizer consumption is higher for the Northern districts closer to the sources of tributaries of River Ganga. Average fertilizer consumption for the Indian districts in the Ganga River Basin is 73 Kilotonnes (KT) per hectare. Higher fertilizer consumption in the northern districts is because agricultural lands in these districts are not as fertile as compared the regions in middle of Gangetic floodplains in the central and southern part of the watershed where there is lot more nutrient deposition from the main channel of River Ganga. Next, we performed a Mann-Kendall trend test for the nitrogen-based fertilizer data per district (**Figure 4.4b**). A contrasting spatial trend was observed where the districts with higher mean fertilizer consumption are showing no statistically significant trend especially in North-western part of the watershed. The southern districts showed positive trends ranging from 0-3 KT/yr. The fertilizer consumption is more stressed in the Eastern districts where not only mean consumption is high but the districts show high rates of increase in fertilizer consumption (> 3 KT/yr). Since the magnitudes of fertilizer consumption for districts vary a lot, we also analyzed the trend ratio which is trend values normalized by their corresponding mean fertilizer consumption (**Figure 4.4c**). The map shows percentage trend ratio of positive and negative trends. Based on this map, we find that the southern districts are experiencing a lot more rapid increase in fertilizer consumption as compared to even the Eastern districts.

Rice, wheat and soybean are the three major crops grown in the Ganga River Basin based on net sown area – covering more than 70% of the agricultural lands (**Figure 4.5b**). Most of the North-western and central districts majorly grow wheat whereas eastern districts majorly grow rice. South-western districts majorly grow a mix of maize, mustard, soybean, millet and others (**Figure A4.2**). If we consider the fertilizer consumption per each crop type – wheat, rice and soybean consume 86% of the total fertilizer consumption (**Figure 4.5c**). Amongst the three, wheat crop consumes 4 MT/yr, rice crop consumes 3 MT/yr and sugarcane consumes 1 MT/yr.

4.4.2 CWC nutrients analysis

CWC nutrients data using Mann-Kendall trend test and boxplots (**Figure 4.6**). From the Mann-Kendall trend test, we found that lower reach regions in the Eastern part of watershed show high rates of increasing N concentration trends. In addition, the Yamuna tributary in the North-western region of watershed also shows high rates of increasing N concentration trends. Several stations did not have enough data to perform an annual trend test whereas several station in the north western part of lower reach show no statistically significant trends. Trend slope and their corresponding p-values as estimated from the Mann-Kendall trend test and Sen's slope estimator for each CWC nutrient gauge location is given in **Table 4.2**. Overall, 53 stations show increasing trends whereas two stations show decreasing trends of N concentration. For the boxplots, we grouped the

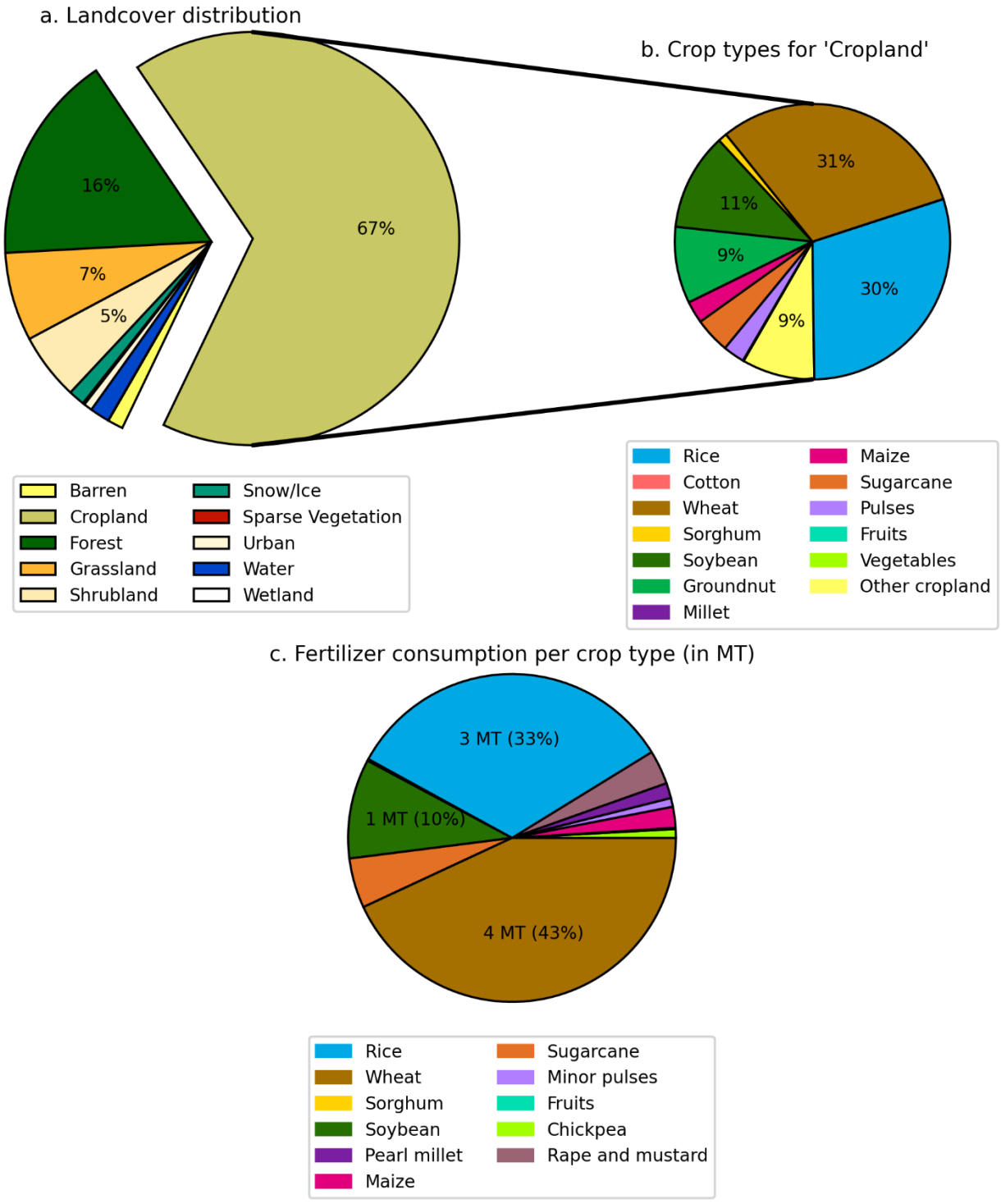

Figure 4.5 (a-c): Pie charts for (a) ESA landcover distribution, (b) Crop distribution under 'Cropland' land cover type, and (c) Fertilizer consumption per crop for aggregated over districts in Ganga River Basin. (MT = Mega Tonnes)

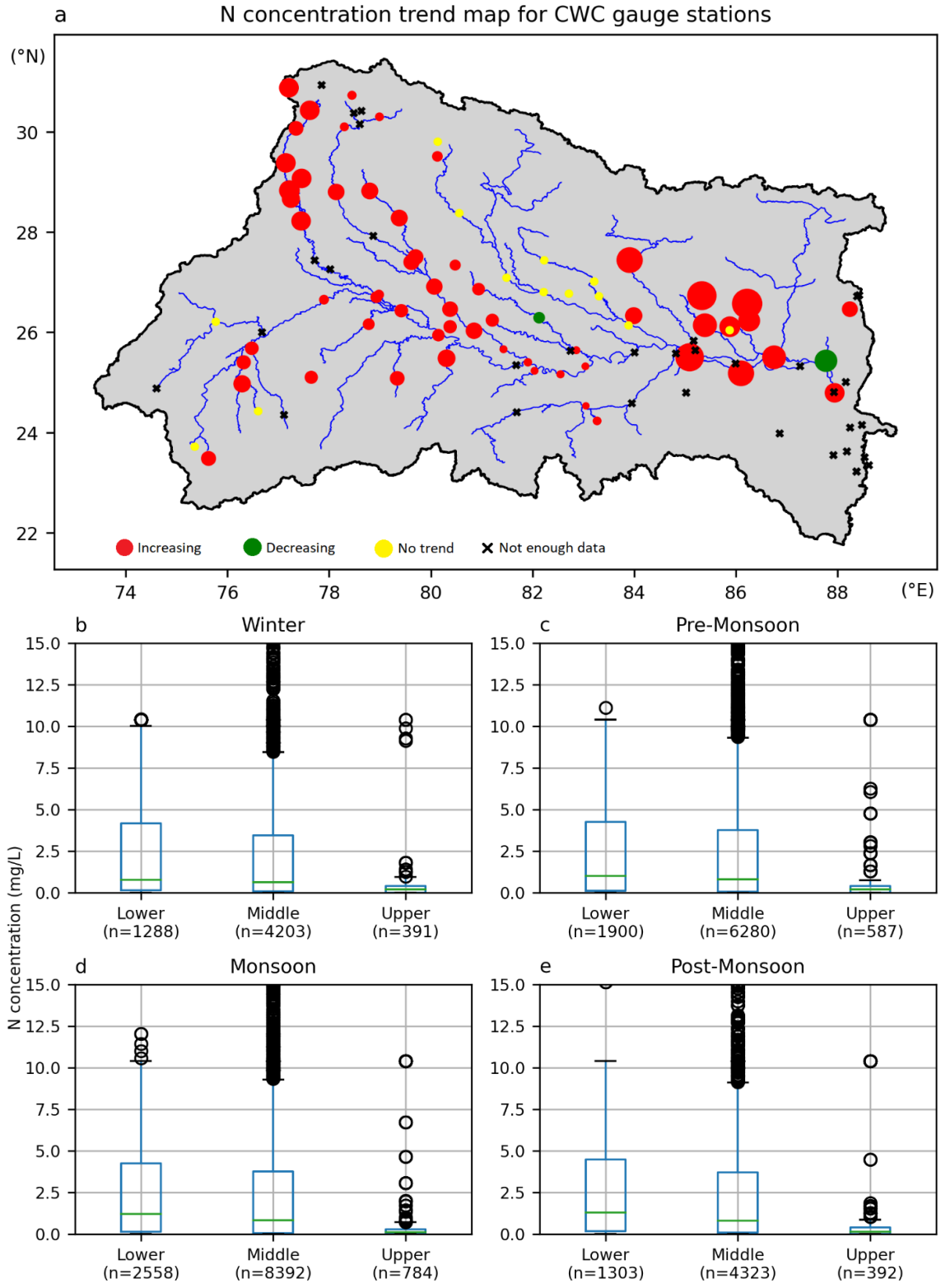

Figure 4.6 (a-e): (a) Map of CWC gauge stations with Mann-Kendall trend results. (b-e) Boxplots of upper reach, middle reach and lower reach stations for N concentration for each season in Ganga River Basin.

stations based on their locations into upper, middle and lower reach stations. Further, we isolated the concentrations based on four seasons (Monsoon, Pre-Monsoon, Post-Monsoon, and Winter). Monsoon season is from June to September, Pre-Monsoon from March to May, Post-Monsoon from October to December, and Winter from January to February. Based on this, we found that median N concentration for lower reach is marginally higher as compared to middle reach for all four seasons. Further, median concentrations for middle and lower are significantly higher as compared to upper reach locations for all four seasons.

4.4.3 SWAT model performance

The SWAT model calibration was performed for the period of 2001-2010 with a 3-year warm-up period (1998-2000) at a monthly timestep. In the calibration phase, the SWAT model achieved an average NSE of 0.68 and an average R^2 of 0.76 (**Table 4.3**) across all three streamflow calibration sites for streamflow. These values indicate that the model performs well in the calibration phase. Similar studies conducted for Ganga River Basin also show comparable performance (Anand et al., 2018; Mishra and Lilhare, 2016c). Multi-site calibration by Anand et al. (2018) had NSE in the range of 0.7-0.9 for the streamflow locations inside the Ganga River Basin whereas Mishra and Lilhare (2016) had NSE of 0.91 and correlation coefficient of 0.97 for the calibration period of 1965-69. The model was calibrated for the streamflow and nutrient related parameters (**Table 4.4**). A global sensitivity analysis was performed using SWATCUP to identify the important parameters. SWATCUP software uses multiple linear regression technique which regresses over the generated parameters against the objective function. NSE was used as the objective function for all parameters. Through the global sensitivity analysis of parameters along with statistical significance level of $p < 0.05$, we found CN2 and ESCO as the most important parameters for calibrating streamflow whereas SOLNO3 as the most important parameter for N concentration and flux. CN2 represents the curve number for corresponding HRU which is a function of antecedent soil moisture conditions and soil's permeability. ESCO represents the Soil Evaporation Compensation Factor which allows the user to modify depth distribution for evaporative demand.

These two factors combined represent primary HRU characteristic affecting overland flow for the Ganga River Basin. In addition, SOLNO3 is the parameter for initial NO3 concentration in soil layers. For the validation phase, the SWAT model achieved a NSE of 0.68 and R^2 of 0.73 (**Table 4.3**). The literature on hydrological model building suggests NSE > 0.5 as a good model (Nash and Sutcliffe, 1970; Anand et al., 2018; Mishra and Lilhare, 2016). Since the model showed NSE > 0.5 for both the calibration and validation phase, we used this model to perform analysis on transport of N concentration and fluxes.

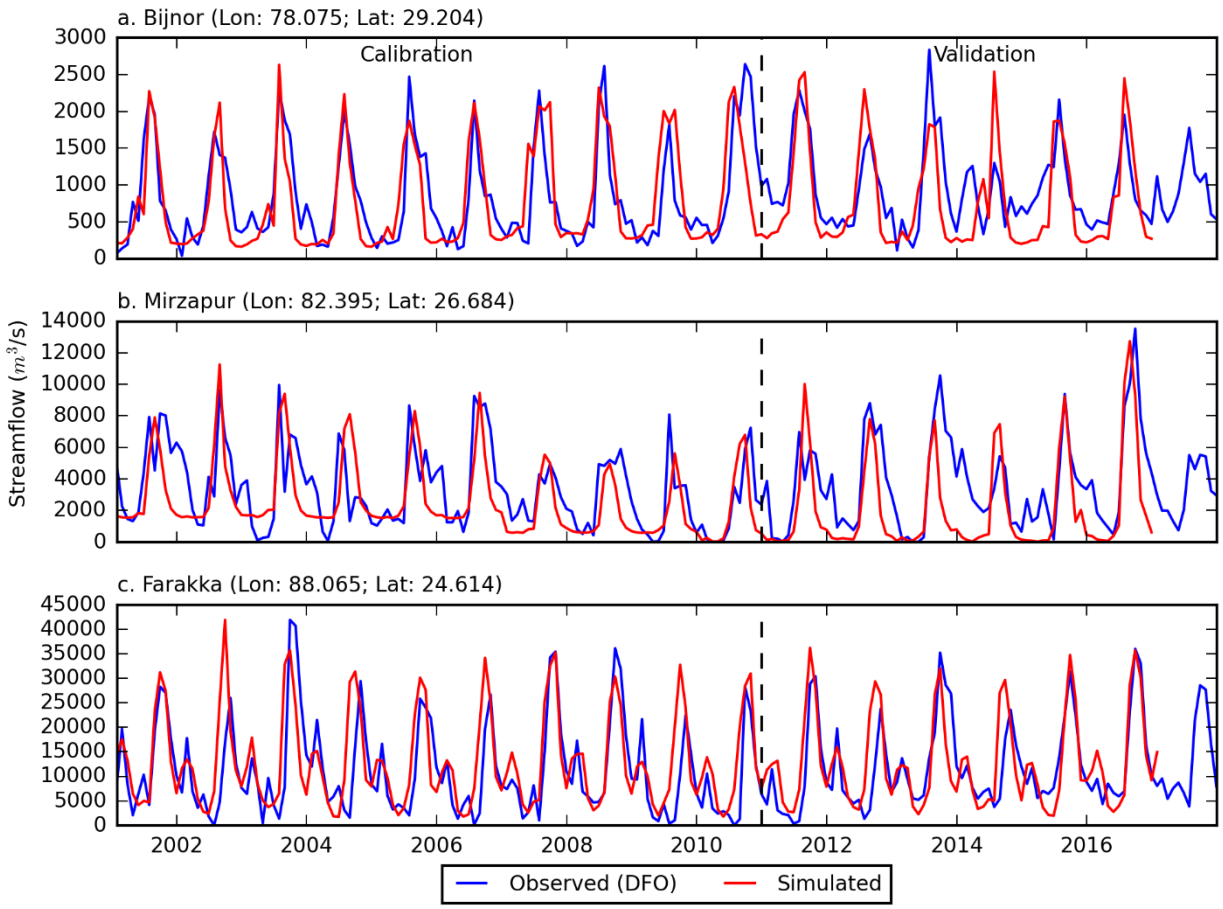

Figure 4.7 (a-c): Calibration and validation results for streamflow at three locations in Ganga River Basin, where data shown in (a) is for a location which is the outlet for upper reach inside the Ganga River Basin. Similarly, (b) and (c) are for location which are at the outlet of middle reach and lower reach respectively.

From the comparison of observed and simulated streamflow time series (**Figure 4.7**), we see that upper reach location of Bijnor is closely correlated for observed and simulated streamflow especially in the calibration phase. From 2010 onwards, we observe an increase in the baseflow at all three locations. The middle reach location of Mirzapur again shows good correlation by capturing peak and low flows in calibration phase. For the Farakka location in lower reach, we observe an overall fair correlation with underestimation of peak and low flows.

Table 4.3: Performance of the SWAT model for streamflow calibration and validation at the three outlet locations.

	Streamflow					
Location	**Bijnor**		**Mirzapur**		**Farakka**	
	Cal		**Cal**		**Cal**	
R^2	0.82	**R^2**	0.82	**R^2**	0.82	**R^2**
NSE	0.74	**NSE**	0.74	**NSE**	0.74	**NSE**
p-bias	-3.1	**p-bias**	-3.1	**p-bias**	-3.1	**p-bias**
	N flux (Model A)					
Location	**Bijnor**		**Mirzapur**		**Farakka**	
	Cal		**Cal**		**Cal**	
R^2	0.69	**R^2**	0.69	**R^2**	0.69	**R^2**
NSE	0.65	**NSE**	0.65	**NSE**	0.65	**NSE**
p-bias	-7.4	**p-bias**	-7.4	**p-bias**	-7.4	**p-bias**
	N concentration (Model B)					
Location	**Bijnor**		**Mirzapur**		**Farakka**	
	Cal		**Cal**		**Cal**	
R^2	0.64	**R^2**	0.64	**R^2**	0.64	**R^2**
NSE	0.61	**NSE**	0.61	**NSE**	0.61	**NSE**
p-bias	-9.7	**p-bias**	-9.7	**p-bias**	-9.7	**p-bias**

Table 4.4: Ranked calibrated SWAT parameter ranges for the Ganga River basin.

Rank	**Parameters**	**Method**	**Description**	**Min**	**Max**
1	CN2	Replace	SCS runoff curve number f	79.68	85.57
2	ESCO	Replace	Soil evaporation compensation factor	0.43	0.6
3	SOLNO3	Relative	Initial NO3 concentration in soil layers (mg/kg)	2.58	3.87
4	GW_Revap	Relative	Groundwater "revap" coefficient	0.1	0.5
5	NPERCO	Replace	Nitrogen percolation coefficient	0.001	1
6	CMN	Relative	Rate factor for mineralization of active organic nutrients	0.001	0.003
7	REVAPMN	Relative	Threshold depth of water in the shallow aquifer for "revap" to occur	-0.03	0.2
8	GW_Delay	Replace	Groundwater delay time (days)	80	100
9	RSDIN	Relative	Initial residue cover (kg/ha)	0	100000

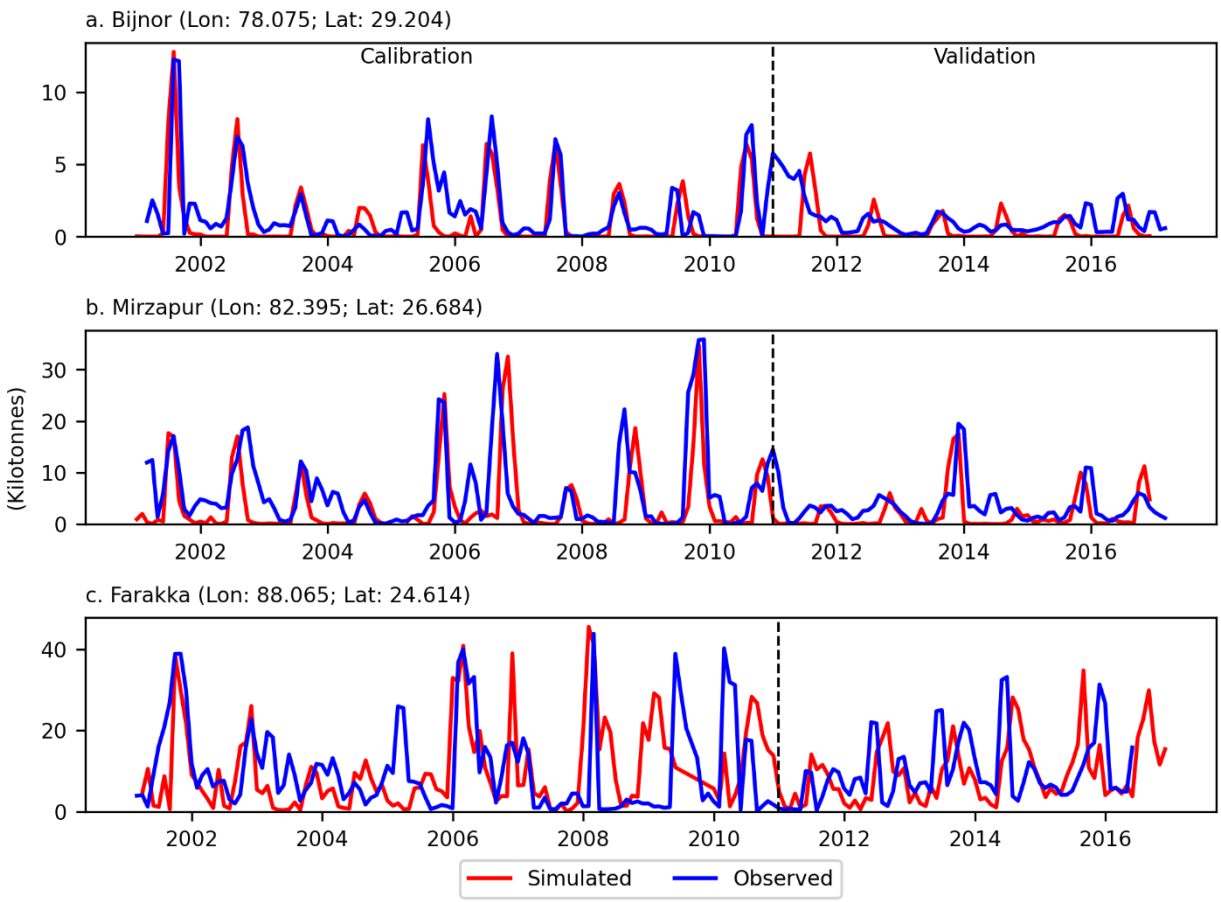

Figure 4.8 (a-c): Calibration and validation results for nutrient concentration at three locations in the Ganga River Basin. (a) Bijnor lies in the upper reach, whereas (b) Mirzapur lies in the middle reach, and (c) Farakka lies in the lower reach of watershed. N fluxes show much better performance as compared to the N concentration for both calibration and validation phase.

For model A, which was calibrated for nutrient flux, shows good correlation with an average R^2 of 0.62 and average NSE of 0.61 across all three locations (**Table 4.3**) for the calibration phase. The model performed fairly well in the validation phase with an average R^2 of 0.62 and average NSE of 0.61 across all three locations. The time series of simulated and observed nitrogen flux shows that for Bijnor in upper reach, the model accurately simulates the mean annual flows but underestimates the nitrogen concentration during years when it is much higher than the mean annual flow (**Figure 4.8a**). For middle reach location of Mirzapur, the model accurately simulates the peak and mean annual flows. The model overestimates the concentration during initial years of simulation (2001-2005) when the observed concentration was much lower (**Figure 4.8b**). For lower reach location of Farakka, the model accurately simulates the low mean

annual flows but underestimates for the years when observed concentration is significantly higher (**Figure 4.8c**).

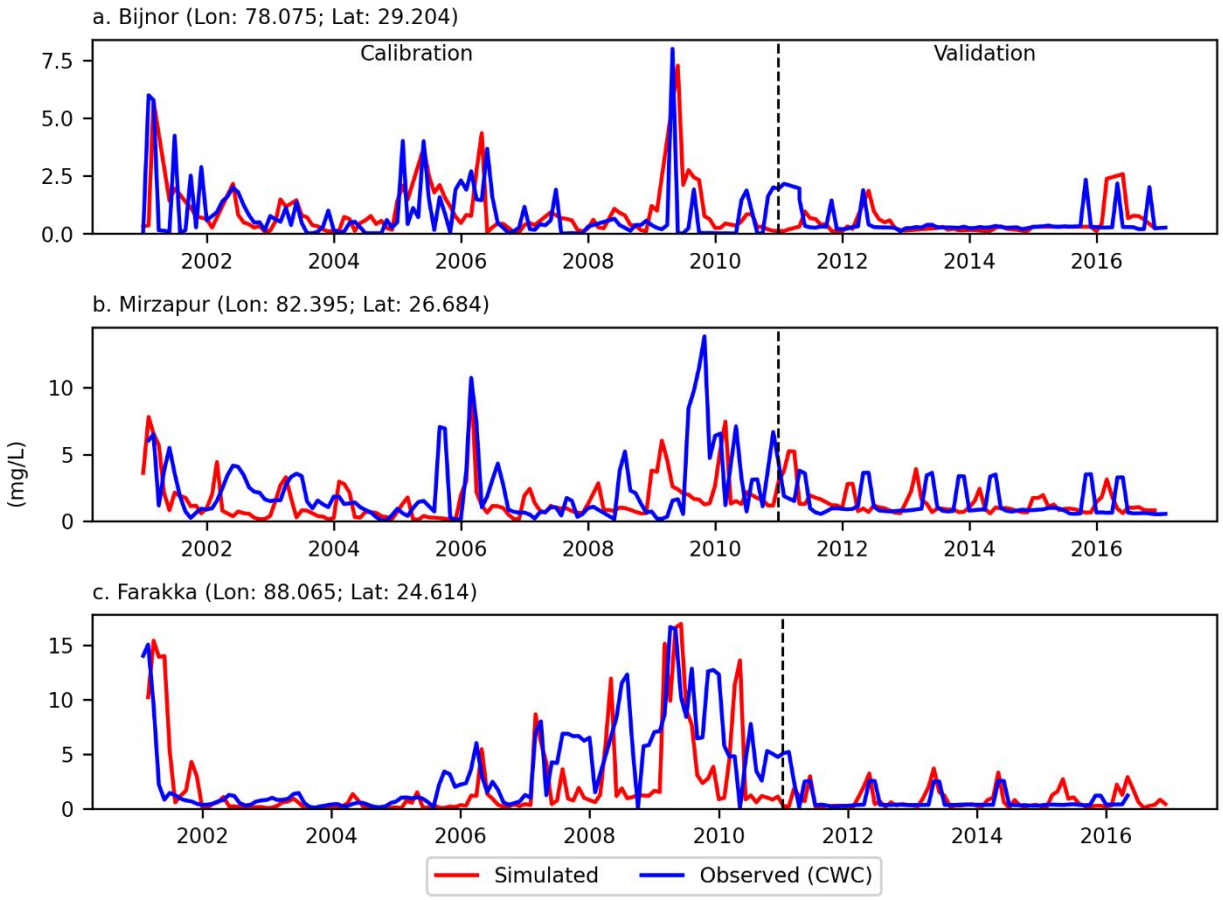

Figure 4.9 (a-c): Calibration and validation results for nutrient concentration at three locations in the Ganga River Basin. (a) Bijnor lies in the upper reach, whereas (b) Mirzapur lies in the middle reach, and (c) Farakka lies in the lower reach of watershed.

For model B, which was calibrated for nutrient concentration, shows fair correlation with an average R^2 of 0.61 and average NSE of 0.56 across all three locations (**Table 4.3**) for the calibration phase. The model performed well in the validation with an average R^2 of 0.53 and average NSE of 0.54 across all three locations. While the upper reach location of Bijnor showed low interannual variation, the middle reach location of Mirzapur and the lower reach location of Farakka showed higher interannual variation for the calibration phase (**Figure 4.9**). The model A (for flux) had a better performance when compared to model B (for concentration).

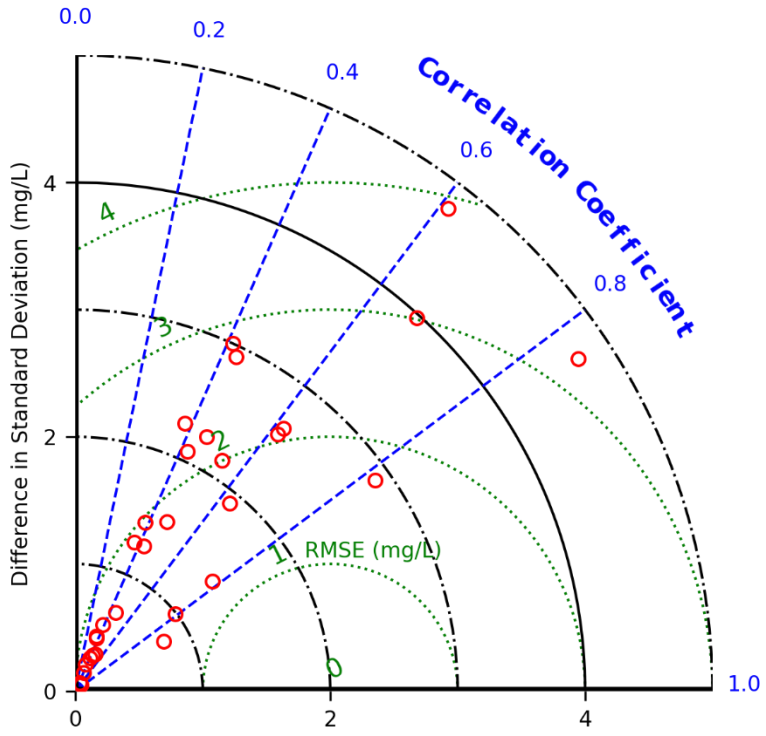

Figure 4.10: Taylor diagram shows the performance of SWAT model in modeling N flux at 32 locations apart from three locations that were used for calibration.

Finally, we compare the observed and simulated N flux to assess the model at locations where the model was not calibrated, using a Taylor diagram (**Figure 4.10**). There were 32 CWC stations apart from the calibration sites with enough data (>40%) for the comparison. The Taylor diagram consists of 32 locations with mean RMSE of 1.9 mg/L with standard deviation of 0.1-4.8 mg/L. The average R across these locations was 0.59. The lower correlation and higher RMSE as well as higher standard deviation can again be attributed to the fact that point sources have not been included in the simulated model. This is compounded by the fact that majority of locations with greater than 30% of data availability for CWC observed data belongs to middle reach section of the Ganga River, which has dominant point source pollution.

4.4.4 Spatial distribution of nutrients

To understand the spatial variation of nutrients, we analyse the N concentration levels and fluxes in SWAT simulated subbasins of the Ganga River basin (**Figure 4.11**) at annual scale. The mean annual concentration, flux, and flux trend were calculated for the time period of 2001-2017 for each SWAT simulated subbasin using simulated N data. For N concentration, we observe high mean annual concentration (>1.6 mg/L) in the middle and lower reach of the river. Apart from the main channel, we observe that there are several

regions of high concentration (>1.0 mg/L) in the northern (Ramganga, Ghaghara, and Gandak subbasins) and western (Chambal subbasin) part of the river basin. For the rest of the river basin, a mean annual concentration of 0-0.4 mg/L was observed. Similar observations were found for the flux patterns with main channel in middle and lower reach having mean annual N flux of greater than 0.8 Mega Tonnes (MT). River channel along Ramganga, Ghaghara, Gandak, Kosi, and Chambal also had higher flux (0.6-0.8 mg/L). We also calculated the trends in annual flux for each SWAT subbasin using non-parametric Mann-Kendall trend test. There are approximately 35 out of 650 subbasins which show significant increasing/decreasing trend. All the significant trends are calculated using $p < 0.05$. Majority of highly decreasing (0.2 – 0.3 Kilo Tonnes (KT)/yr) significant and non-significant trends lie along the main channel of Ganga River whereas some SWAT subbasins in the upper part of river show slightly increasing (0-0.1 KT/yr) trend in N flux. These regions belong to Yamuna and Ramganga subbasins. In addition, northern part of Ghaghara and southern part of Son subbasin show non-significant increasing trend (0.2 – 0.3 KT/yr) in flux. Since the simulated model does not consist of point sources of pollution, we do not observe any significant increasing N fluxes in the middle or lower reach of the river. There are three major factors contributing to decreasing trends in N flux along the main channel and increasing trends along tributaries: Dilution of nutrients in main channel, denitrification of inorganic nitrogen, and tributary retention. As we move downstream of the river, discharge increases along the main channel significantly causing the nutrients to dilute (Bouwman et al., 2005; Schlesinger et al., 2006). As the discharge has increased over the years due to increasing precipitation and snowmelt in the region, decreasing trends along the main channel corroborates with this observation. Second major factor for decreasing trends in most of the SWAT subbasins is due to denitrification by microbial organisms converting nitrites and nitrates into nitrogen, thereby reducing nitrite + nitrate flux over the years (Das et al., 2020; Sharma et al., 2020). Finally, the nutrients are retained by the tributaries in a significantly greater proportions before they flow into the main channel. Tributary subbasins are subject to more farming activities, thereby leading to increase in N and P concentration and flux whereas main channel pollution is majorly due to untreated industrial waste and sewage released directly into the river in addition to contribution of nutrients by the tributaries (Seitzinger et al., 2002).

a. Mean annual N concentration

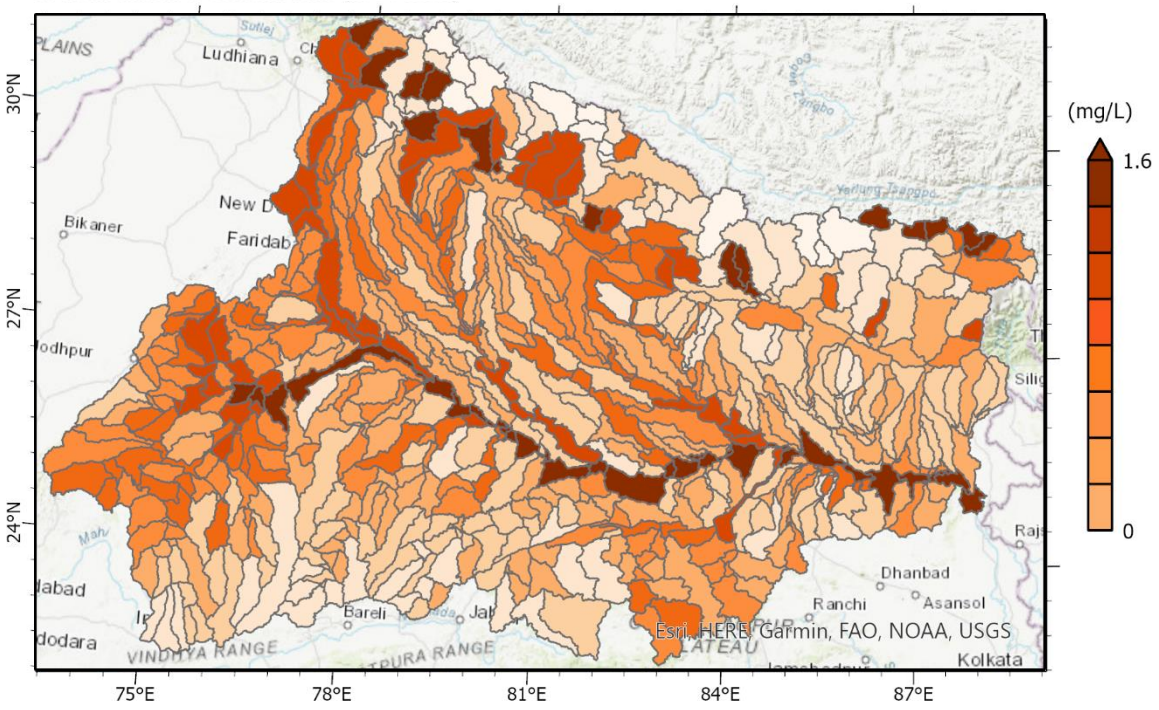

b. Mean annual N flux

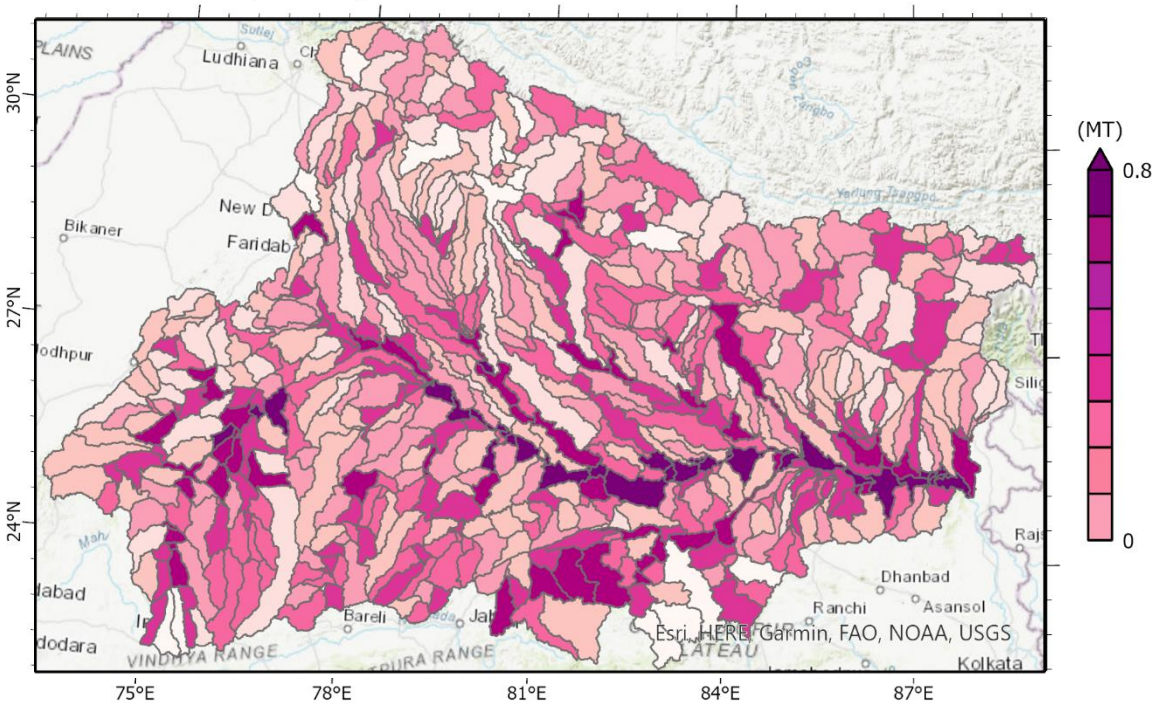

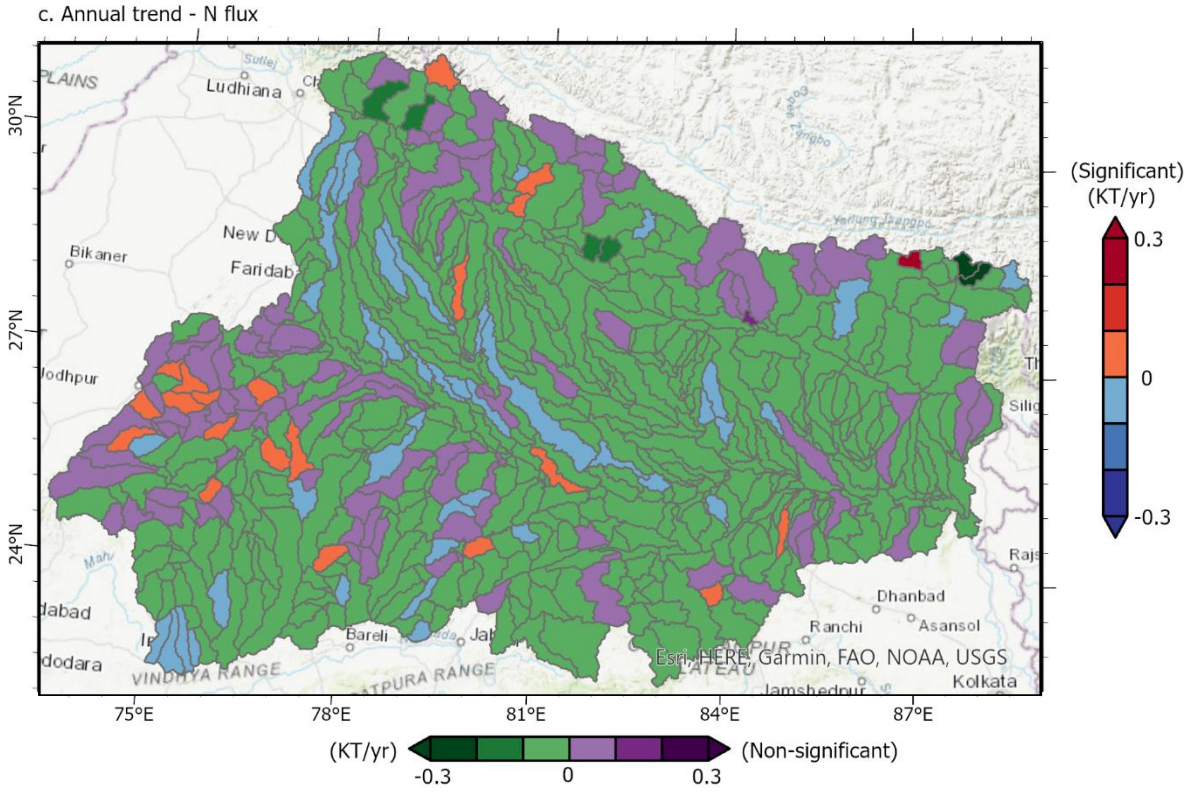

Figure 4.11 (a-c): (a) shows the mean annual nitrite + nitrate concentration over the study period. (b) shows the mean annual flux of nitrite + nitrate for each of the subbasins modelled in the SWAT model for the Ganga River Basin. (c) shows the Sen's slope estimated from Mann-Kendall trend test. The time period used for the annual average is from 2001-2017.

4.4.5 Model assumptions and limitations

In SWAT model building, there were a few assumptions related to the selection of methods to represent hydrologic processes. The 'Penman Monteith' equation was used for calculating evapotranspiration, the 'Muskingum' routing method was used for routing of water from subbasin outlets to downstream point on the river network, and the 'SCS curve number' method was for calculating runoff for HRUs. These assumptions in the study provide an opportunity for improvement in modeling nitrogen transport through future research. Additionally, instream and atmospheric denitrification and fixation processes were not incorporated in the model. The capabilities of the SWAT model that facilitate extensive modeling of N also have certain limitations. The SWAT model requires forcing data, which involves significant pre-processing of the input datasets which is computationally expensive for a large river basin. There are also problems in portraying some reservoir processes as well as point source pollution due to the absence of adequate observation data, required data for input parameters, and lack of technical understanding pertaining to the Ganga River Basin. The SWAT model is a

semi-distributed model which implies all the spatial variability within a HRU is ignored in the model, which limits applications at high spatial resolution. Furthermore, the N dataset is not available continuously over the analysis period and contains a significant number of missing observations. The limitations of this study also include inadequate glacier and snow information as well as weather forcing data at high elevations. Finally, constant land cover was assumed for the period of analysis which might influence the results of the model. Also, the study has statistical limitation in the sense that with lower availability of observations and their field significance along with multi-site calibration, a consistent p-value threshold of less than 0.5 might not produce robust results. Further, the SWAT model was not assessed against a simple harmonic time series model which could provide accurate representation of mean and seasonal variability, given enough number of observations. In addition, double and triple cropping patterns were not incorporated inside the land use information as well as fertilization application for the model. Finally, since both model A and B involved the calibration of streamflow in the first place, model A (for flux) remains biased towards streamflow performance as flux involves streamflow component. The flux model performance was not isolated for the contribution by streamflow and nutrient parameters.

4.5 Conclusions

This study builds a semi-distributed physically based hydrological model (SWAT) to characterize the catchment hydrology and nutrient transport for the Ganga River Basin. Using the flow and nutrient calibrated hydrological models, I compared simulated and observed nutrient flows (N) at 92 locations inside the Ganga River Basin. The SWAT models proved to be a useful hydrological modelling tool especially for an agriculture dominant watershed like the Ganga River Basin. Through the calibration of flow parameters, I obtain an average R^2 of 0.76 during the calibration phase (2001-2010) and an average R^2 of 0.73 during the validation phase (2011-2017) for streamflow across three streamflow calibration sites. The analysis shows that the SWAT model adequately captures the hydrologic characteristics of the Ganga River basin. This SWAT model can be effectively used for water resource and land use management.

The time series and spatial plots of total N show that the central subbasins of the Ganga River basin show five times higher fluxes of N as compared to the other regions whereas the N concentration at middle reach locations such as Kanpur are in the range of 1-15 mg/L, whereas upper reach locations such as Bijnor are in the range of 0-1.5 mg/L. This is due to the fact that anthropogenic activities specifically farming and industrial waste disposal are more extensive in the middle reach of the basin (compared to the upper reaches), and which contribute large amounts of N nutrients, excess of which is drained into the river through run-off.

The study attempts to analyse the impact of farming on river flow by comparing the nutrient changes from the in-situ measured data with the simulated data from the SWAT model. The analysis shows that in the upstream reaches of the river basin, which predominantly remain unexploited, there are lower fluxes of N but for the middle reach and lower reach regions of the river basin, there is a noticeable increase in the nutrient fluxes.

Chapter 5: Conclusions

Overall, through three studies conducted and planned in this dissertation, it can be understood that it is essential to monitor the water resources for agricultural lands in the Indian subcontinent which suffer the most from depleting water resources and more importantly degrading water quality. As a lot of the ground observations for these river basins in India are not publicly available, decision-making has to rely on methods and data (models and satellite sensors) such as those presented in this study. Following are the major findings of this dissertation:

- 74% of the monotonic increasing and decreasing trends in water balance components were correlated to 'Agricultural' land whereas 19% of these trends were associated to 'Urban' land.
- Southern and North-Eastern parts of India experience water deficit due to decreasing monsoonal precipitation combined with increasing ET, which correlates with decrease in TWSA.
- Model simulations for total N revealed that the main channel of the Narmada River basin have 4-8 times higher concentration and fluxes of N as compared to the other regions. The mean monsoonal N concentration at reach locations such as Sandia and Patan are in the range of 2-6 mg/L, whereas upper reach locations such as Mandleshwar are in the range of 6-12 mg/L.
- 35 out of 650 SWAT subbasins for Ganga River Basin showed an increasing trend of N concentration with concentration levels reaching more than three times the allowable limit for water use, especially for the middle reach and lower reach subbasins.
- Model simulation for total N showed that the central subbasins of the Ganga River basin have five times higher N flux as compared to the other regions whereas the N concentration at middle reach locations such as Kanpur are in the higher range (1-15 mg/L), whereas upper reach locations such as Bijnor are in the lower range (0-1.5 mg/L).

It was shown that monsoon season is the driver of annual and seasonal trends in the major water balance components of Indian river basins. Ganga River Basin – the largest watershed in India – showed the highest disruptions in water balance components driven by the monsoon season changes. Through the SWAT modeling for Ganga and Narmada River basins, this dissertation attempts to analyze the impact of farming on river flow by modeling the non-point source pollution using SWAT model. For Narmada River Basin, since this watershed is predominantly polluted by non-point source pollution, the SWAT model built for this watershed can be used for monitoring nitrogen flux and concentrations. Through the trend analysis, it was found that subbasins near the

Narmada watershed boundaries show increasing trends in N concentration primarily caused by the increasing fertilizer applications for the new farmlands in these regions. Point source pollution contribution to nitrogen contamination was significantly less for the Narmada River basin, as non-point source pollution through fertilizer application were identified as the major source.

On the other hand, for Ganga basin, there is a significant point source contribution at numerous locations. This made the modeling process much more complex for the watershed as compared to the Narmada River Basin. The analysis shows that in the upstream reaches of the river basin, which predominantly remain unexploited, there are lower fluxes of N but as we move towards the middle reach and lower reach regions of the river basin, there is a noticeable increase in the nutrient fluxes. As the main channel contains higher concentrations of nitrogen, this water may need to be treated for domestic consumption to ensure safe health. Most of the middle and lower reach locations showed significantly higher concentration of nitrogen in water, which is leading to and will lead to significant eutrophication. The SWAT models will help in monitoring the nitrogen contamination for two Indian river basins, which are an integral part of Indian economy. Water resources planning using these results can help in controlling the agricultural application of fertilizers (specifically in the pre-monsoon/monsoon periods) when a higher rate of flux of nutrients may reach the main channel.

In addition to understanding and finding drivers of the changes in water balance components, this dissertation outlines the importance of monitoring and tracking the resources to manage future water demand and to avoid water management issues. Since, the in-situ observation networks cannot provide enough information about the water quantity and quality inside the entire watershed, models developed in this dissertation provide a consistent way of tracking the water resources in parts of watershed where there is lack of in-situ observations. As these river basins serve as major sources of freshwater for the population in these river basins and are drivers of the economy, it becomes fundamental to examine the seasonal and annual variability of the water budget for these river basins and various contributing factors. Since, the limitations of the SWAT models built for the Narmada and Ganga River basin include the absence of representation of in-stream and atmospheric denitrification and nitrogen fixation process, future studies should incorporate these processes in the hydrological models to provide a more reliable estimate of nitrogen pollution in the river basins. Additionally, the future studies should incorporate double and triple cropping patterns in the model as these watersheds have more than 100% cropping intensity in several parts of the watershed. Inclusion of these limitations and better data inputs can lead to even better model representation of these watersheds and can significantly improve the reliability of forecasts based on these models.

Appendices

Appendix A: Supplementary figures

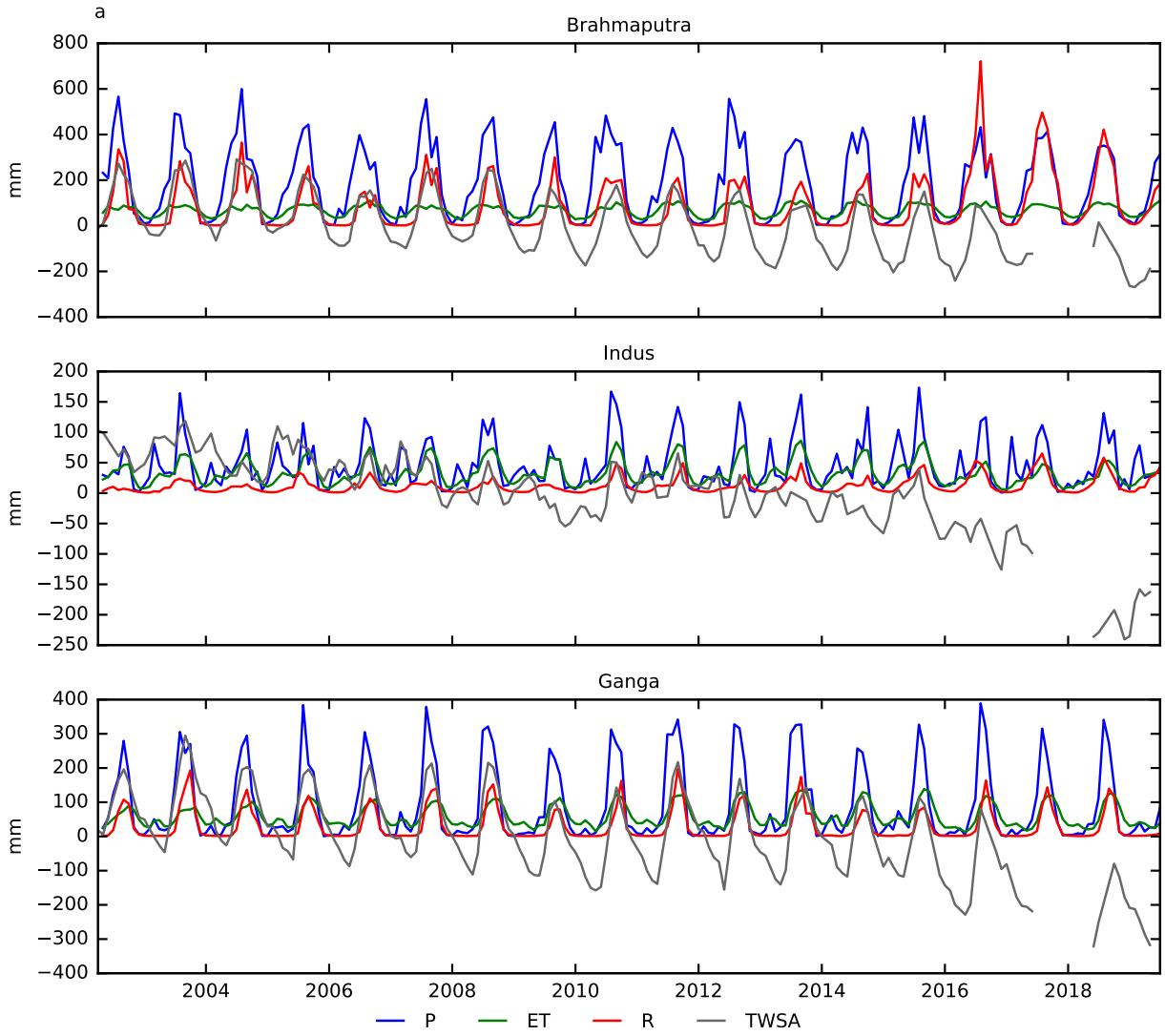

Figure A2.1 (a-b): Time series of individual water balance components. (a) River basins which depict highly decreasing TWSA whereas (b) Rest of the river basins.

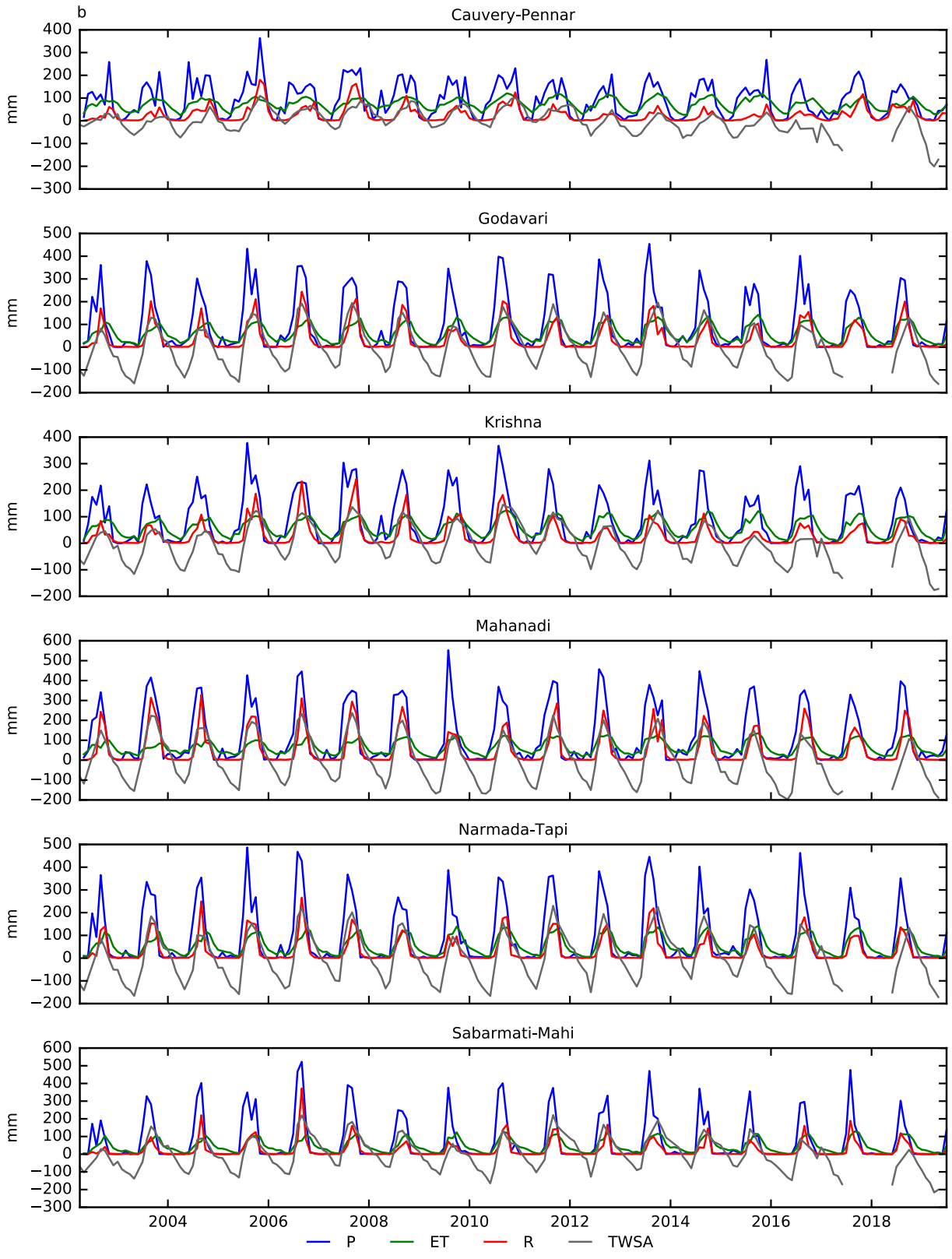
b
Cauvery-Pennar
Godavari
Krishna
Mahanadi
Narmada-Tapi
Sabarmati-Mahi
mm
2004
2006
2008
2010
2012
2014
2016
2018
P
ET
R
TWSA

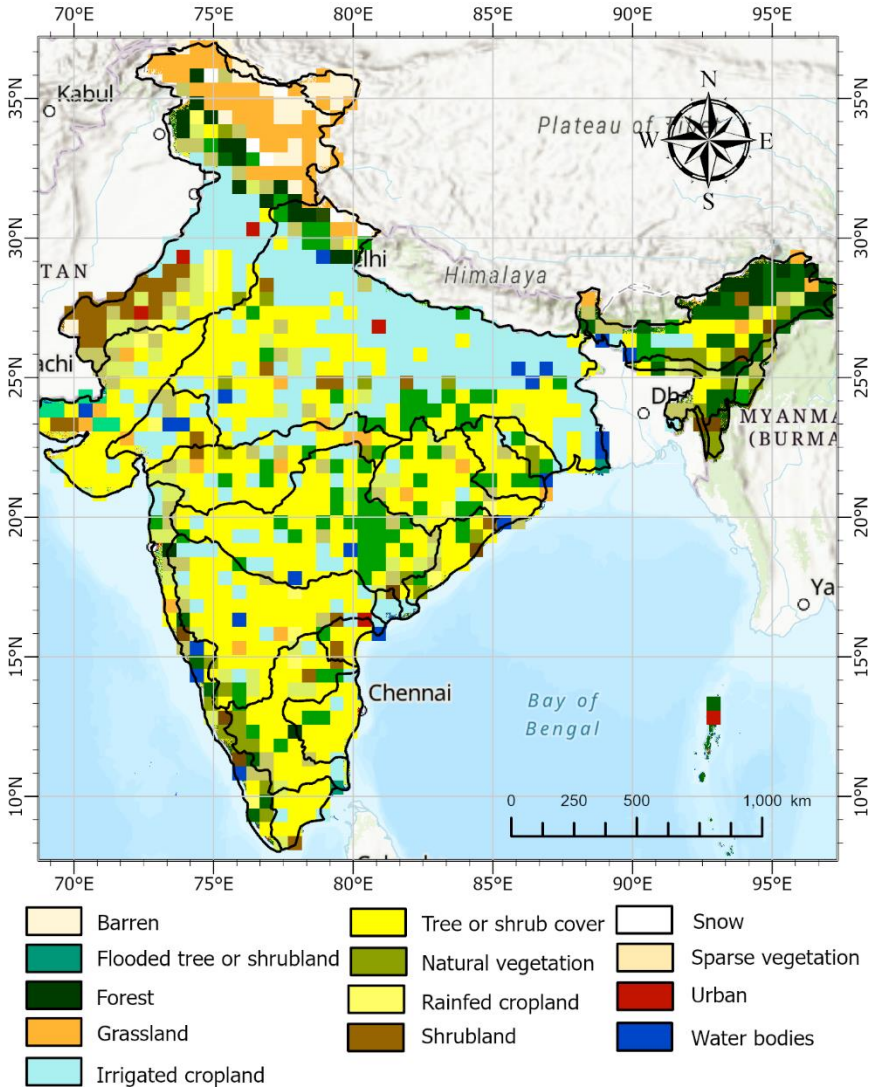

Figure A2.2: Land cover map resampled to 50 km using 'majority' statistics in 2010.

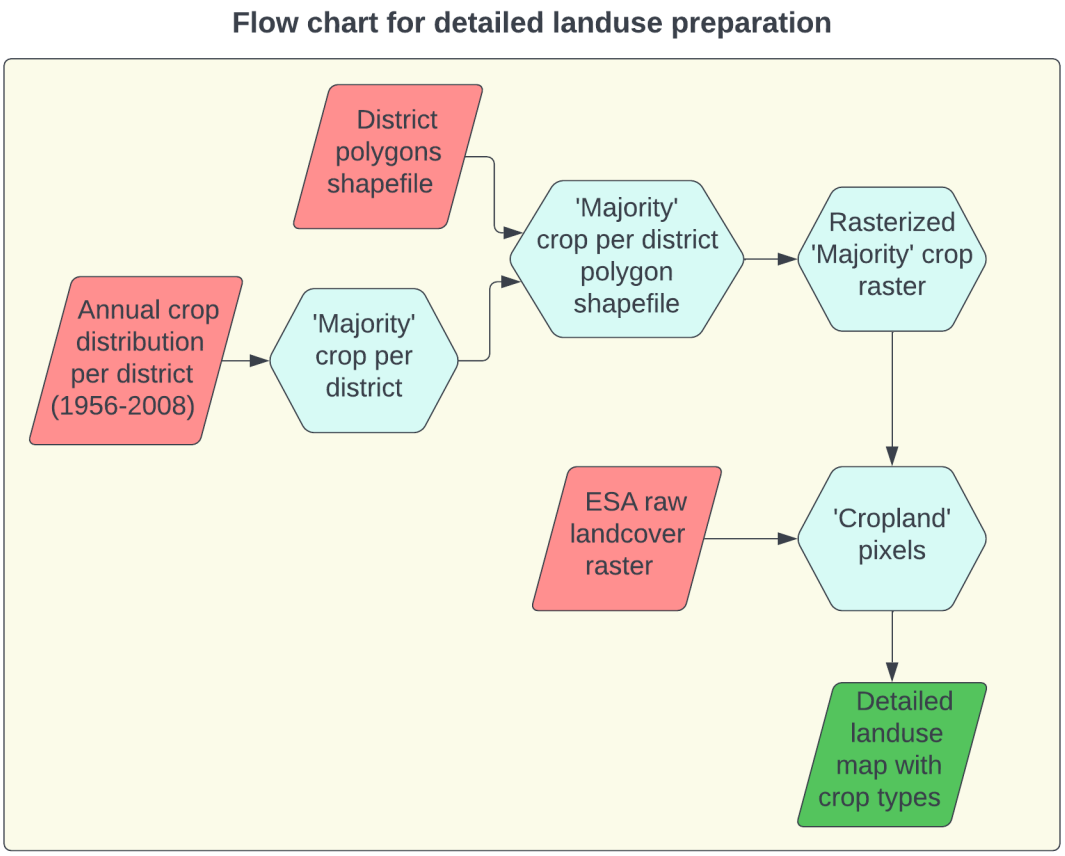

Figure A4.1: Flowchart showing preparation of the new detailed land cover map which contains the crop type for 'Cropland'.

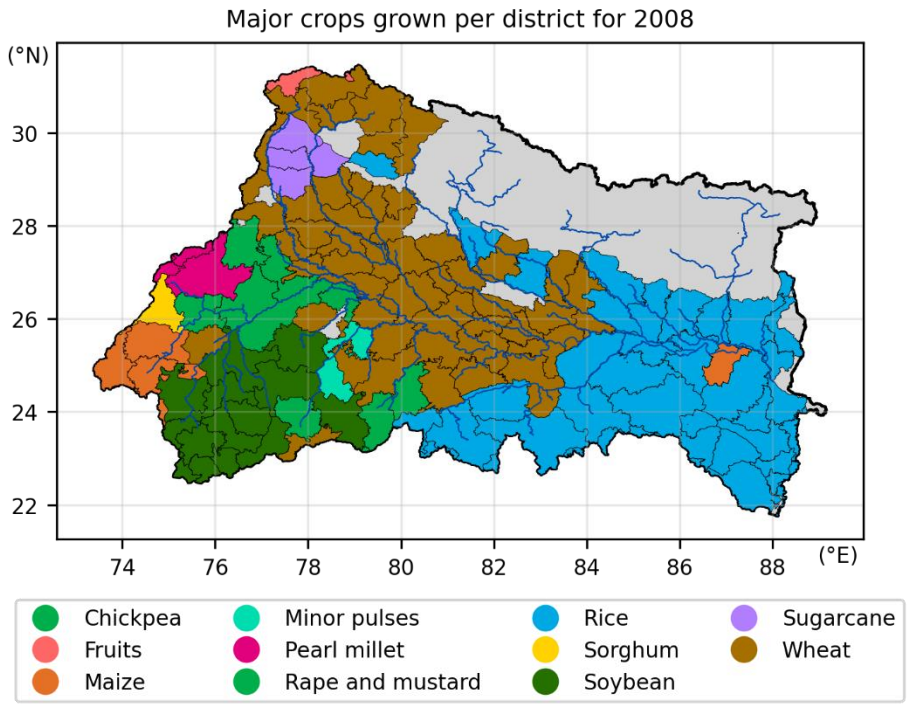

Figure A4.2: Map showing major crops per district for Ganga River Basin for 2008.

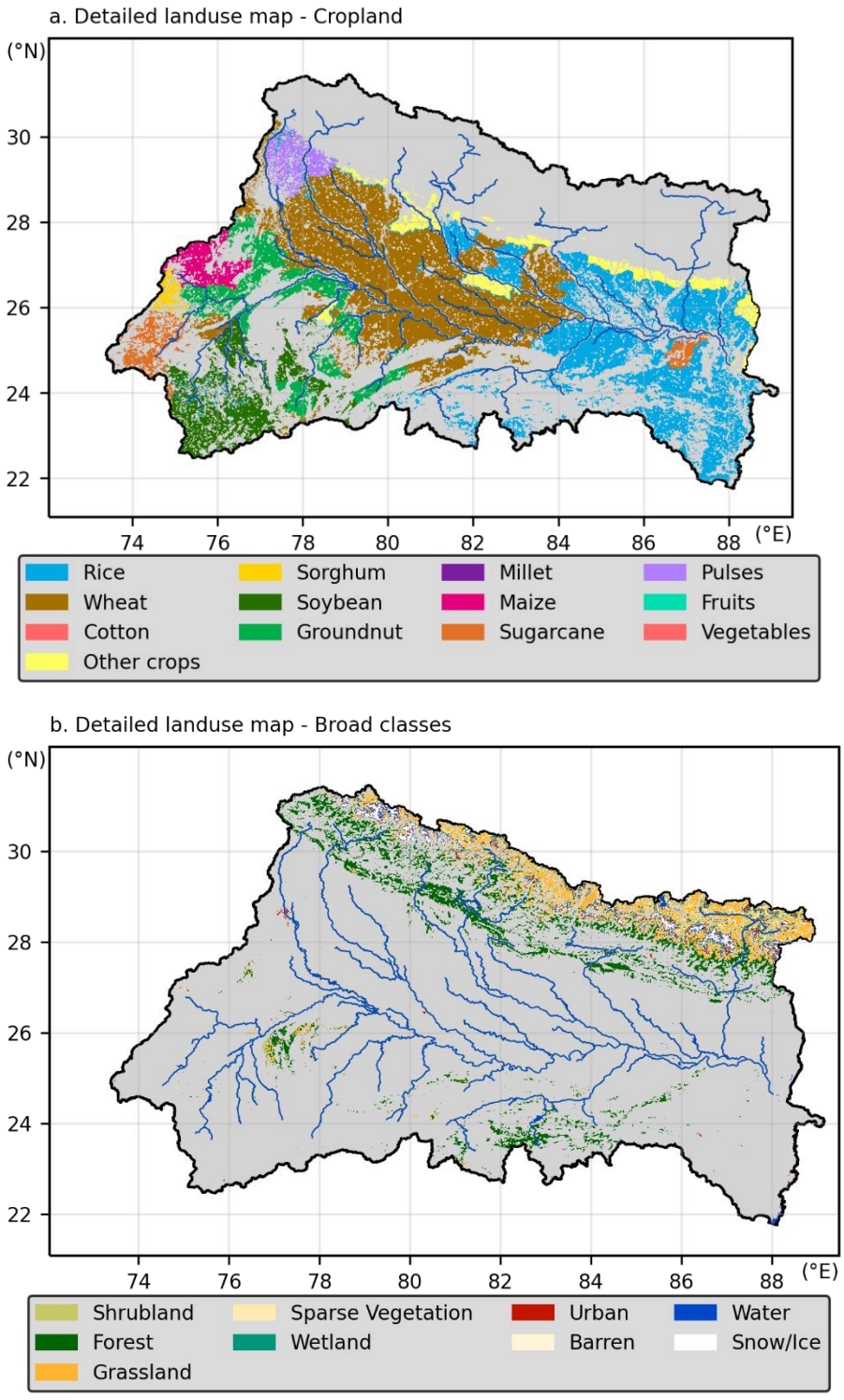

Figure A4.3 (a-b): Detailed land-use map obtained using the method described in Section 3.1 – Detailed land use preparation.

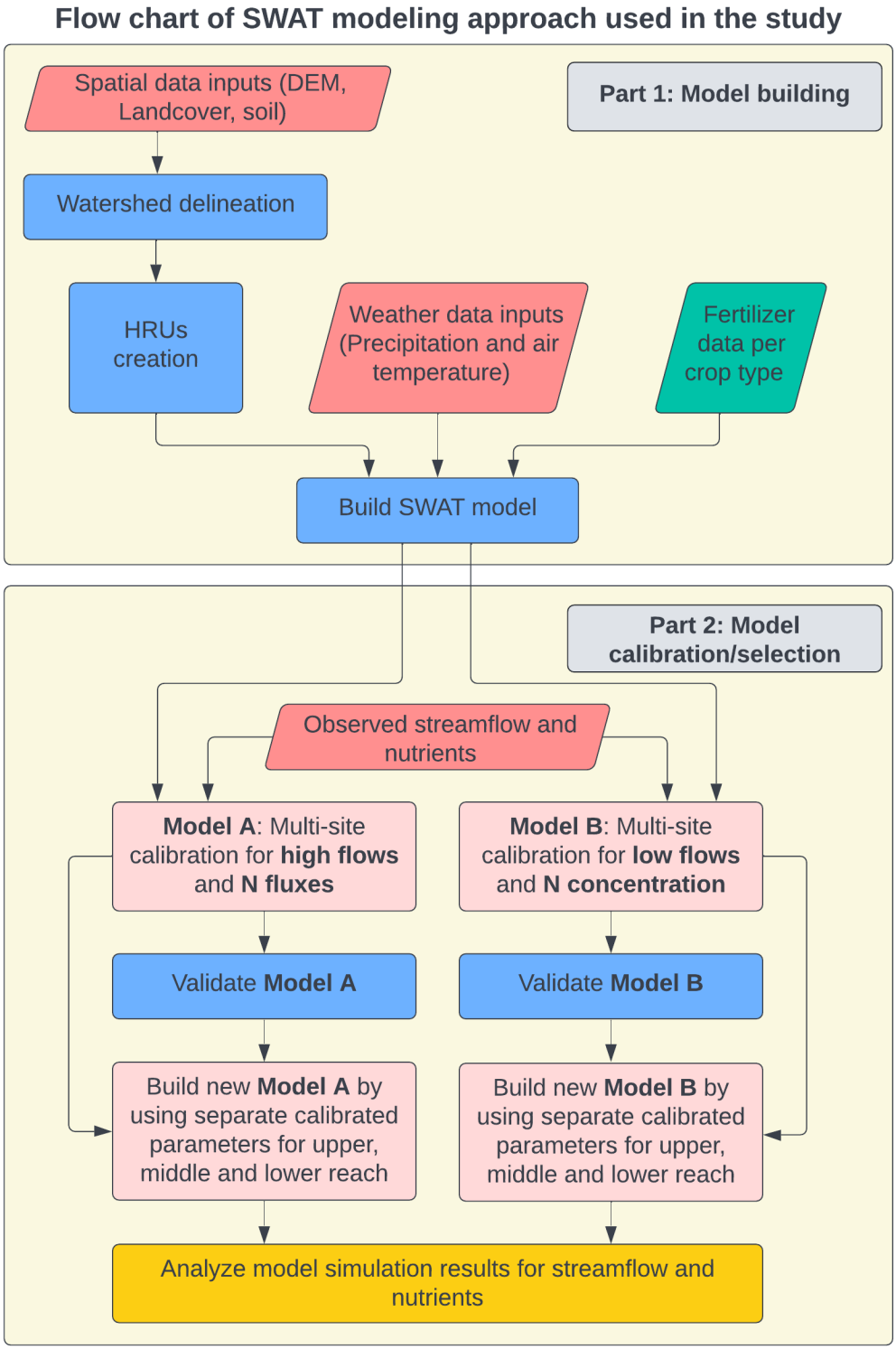

Figure A4.4: Flowchart of SWAT methodology.

Appendix B: Supplementary tables

Table B2.1: Comparison of original resolution (300 m) land cover map with resampled (50 km) land cover map for 2010.

	Agricultural		Forest		Vegetated		Barren		Urban	
	300 m	50 km	300 m	50 km	300 m	50 km	300 m	50 km	300 m	50 km
Brahmaputra	24.95	27.44	59.2	47.36	11.9	21.29	0.85	0.93	0.2	0
Cauvery-Pennar	69.2	76.12	20.55	16.44	7.7	5.13	0.1	0.11	0.55	0
Ganga	78.5	83.75	14.5	10.01	3.45	0.5	0.3	0.33	0.8	1.53
Godavari	68.25	75.06	27.5	22	2.15	0.825	0.1	0.11	0.4	0
Indus	32.45	35.69	16.5	13.2	34.85	32.63	10.8	11.88	0.5	2.68
Krishna	80.2	88.22	9.6	5.48	7.3	1.44	0.2	0.22	0.65	0
Mahanadi	65.2	71.72	29.35	22.43	2.9	0.84	0.2	0.22	0.35	0
Narmada-Tapi	64.9	71.39	26.4	21.12	6.7	3.4	0.1	0.11	0.4	0
Sabarmati-Mahi	78.5	86.35	13.55	8.84	5.05	0.05	0	0	0.9	0

	Water		Snow	
	300 m	50 km	300 m	50 km
Brahmaputra	1.85	2.97	1.2	0
Cauvery-Pennar	1.95	2.2	0	0
Ganga	2.05	3.51	0.5	0.37
Godavari	1.65	1.99	0	0
Indus	0.3	1.18	4.6	2.73
Krishna	2.05	4.64	0	0
Mahanadi	2.05	4.79	0	0
Narmada-Tapi	1.6	3.98	0	0
Sabarmati-Mahi	1.9	4.76	0	0

Table B3.1: Percentage distribution of land-cover type in Narmada River basin estimated by land-cover change analysis using ESA CCI land-cover map from 2000 and 2018.

	Agricultural		Forest		Vegetated		Barren		Urban	
	2000	**2018**	**2000**	**2018**	**2000**	**2018**	**2000**	**2018**	**2000**	**2018**
Narmada-Tapi	62.1	66.7	26.3	25.1	9.9	5.7	0.1	0.1	0.2	0.6

	Water		Snow	
	2000	**2018**	**2000**	**2018**
Narmada-Tapi	1.4	1.8	0	0

References

Abbaspour, K.C., Rouholahnejad, E., Vaghefi, S., Srinivasan, R., Yang, H., Kløve, B., 2015. A continental-scale hydrology and water quality model for Europe: Calibration and uncertainty of a high-resolution large-scale SWAT model. J. Hydrol. 524, 733–752. https://doi.org/10.1016/j.jhydrol.2015.03.027

Aerts, J.C.J.H., Renssen, H., Ward, P.J., De Moel, H., Odada, E., Bouwer, L.M., Goosse, H., 2006. Sensitivity of global river discharges under Holocene and future climate conditions. Geophys. Res. Lett. https://doi.org/10.1029/2006GL027493

AghaKouchak, A., Nasrollahi, N., Habib, E., AghaKouchak, A., Nasrollahi, N., Habib, E., 2009. Accounting for Uncertainties of the TRMM Satellite Estimates. Remote Sens. 1, 606–619. https://doi.org/10.3390/rs1030606

Agricultural Statistics at a Glance, 2019.

Agricultural Statistics at a Glance, 2018.

Aguilar, A., Flores, H., Crespo, G., Marín, M., Campos, I., Calera, A., Aguilar, A.L., Flores, H., Crespo, G., Marín, M.I., Campos, I., Calera, A., 2018. Performance Assessment of MOD16 in Evapotranspiration Evaluation in Northwestern Mexico. Water 10, 901. https://doi.org/10.3390/w10070901

Alcamo, J., Flörke, M., Märker, M., 2007. Future long-term changes in global water resources driven by socio-economic and climatic changes. Hydrol. Sci. J. https://doi.org/10.1623/hysj.52.2.247

Anand, J., Gosain, A.K., Khosa, R., Srinivasan, R., 2018. Regional scale hydrologic modeling for prediction of water balance, analysis of trends in streamflow and variations in streamflow: The case study of the Ganga River basin. J. Hydrol. Reg. Stud. 16, 32–53. https://doi.org/10.1016/j.ejrh.2018.02.007

Arnell, N.W., 2004. Climate change and global water resources: SRES emissions and socio-economic scenarios. Glob. Environ. Chang. https://doi.org/10.1016/j.gloenvcha.2003.10.006

Arnold, J.G., Srinivasan, R., Muttiah, R.S., Williams, J.R., 1998a. Large area hydrologic modeling and assessment part I: Model development. J. Am. Water Resour. Assoc. 34, 73–89. https://doi.org/10.1111/j.1752-1688.1998.tb05961.x

Arnold, J.G., Srinivasan, R., Muttiah, R.S., Williams, J.R., 1998b. LARGE AREA HYDROLOGIC MODELING AND ASSESSMENT PART I: MODEL DEVELOPMENT. J. Am. Water Resour. Assoc. https://doi.org/10.1111/j.1752-1688.1998.tb05961.x

Ashraf, B., Aghakouchak, A., Alizadeh, A., Mousavi Baygi, M., Moftakhari, H.R., Mirchi, A., Anjileli, H., Madani, K., 2017. Quantifying Anthropogenic Stress on Groundwater Resources. Sci. Rep. https://doi.org/10.1038/s41598-017-12877-4

Asoka, A., Gleeson, T., Wada, Y., Mishra, V., 2017. Relative contribution of monsoon precipitation and pumping to changes in groundwater storage in India. Nat. Geosci. 10, 109–117. https://doi.org/10.1038/ngeo2869

Asoka, A., Wada, Y., Fishman, R., Mishra, V., 2018. Strong Linkage Between Precipitation Intensity and Monsoon Season Groundwater Recharge in India. Geophys. Res. Lett. 45, 5536–5544. https://doi.org/10.1029/2018GL078466

Babovic, F., Mijic, A., Madani, K., 2018. Decision making under deep uncertainty for adapting urban drainage systems to change. Urban Water J. 15, 552–560. https://doi.org/10.1080/1573062X.2018.1529803

Bai, P., Liu, X., Yang, T., Liang, K., Liu, C., 2016. Evaluation of streamflow simulation results of land surface models in GLDAS on the tibetan plateau. J. Geophys. Res. 121, 12,180-12,197. https://doi.org/10.1002/2016JD025501

Barnett, T., Malone, R., Pennell, W., Stammer, D., Semtner, B., Washington, W., 2004. The effects of climate change on water resources in the west: Introduction and overview. Clim. Change. https://doi.org/10.1023/B:CLIM.0000013695.21726.b8

Basha, G., Kishore, P., Ratnam, M.V., Jayaraman, A., Kouchak, A.A., Ouarda, T.B.M.J., Velicogna, I., 2017. Historical and Projected Surface Temperature over India during the 20th and 21st century. Sci. Rep. 7, 1–10. https://doi.org/10.1038/s41598-017-02130-3

Berry, P.A.M., Garlick, J.D., Smith, R.G., 2007. Near-global validation of the SRTM DEM using satellite radar altimetry. Remote Sens. Environ. 106, 17–27. https://doi.org/10.1016/j.rse.2006.07.011

Bhanja, S.N., Mukherjee, A., 2019. In situ and satellite-based estimates of usable groundwater storage across India: Implications for drinking water supply and food security. Adv. Water Resour. 126, 15–23. https://doi.org/10.1016/j.advwatres.2019.02.001

Bharti, V., Singh, C., 2015. Evaluation of error in TRMM 3B42V7 precipitation estimates over the Himalayan region. J. Geophys. Res. Atmos. 120, 12458–12473. https://doi.org/10.1002/2015JD023779

Bhuvaneswari, K., Geethalakshmi, V., Lakshmanan, A., Srinivasan, R., Sekhar, N.U., 2013. The Impact of El Niño/Southern oscillation on hydrology and rice productivity in the cauvery basin, India: Application of the soil and water

assessment tool. Weather Clim. Extrem. 2, 39–47. https://doi.org/10.1016/j.wace.2013.10.003

Billah, M.M., Goodall, J.L., Narayan, U., Reager, J.T., Lakshmi, V., Famiglietti, J.S., 2015. A methodology for evaluating evapotranspiration estimates at the watershed-scale using GRACE. J. Hydrol. 523, 574–586. https://doi.org/10.1016/j.jhydrol.2015.01.066

Bouwman, A.F., Van Drecht, G., Knoop, J.M., Beusen, A.H.W., Meinardi, C.R., 2005. Exploring changes in river nitrogen export to the world's oceans. Global Biogeochem. Cycles 19, 1–14. https://doi.org/10.1029/2004GB002314

Bretherton, C.S., Smith, C., Wallace, J.M., 1992. An Intercomparison of Methods for Finding Coupled Patterns in Climate Data. J. Clim. https://doi.org/10.1175/1520-0442(1992)005<0541:aiomff>2.0.co;2

Chang, A.T.C., Chiu, L.S., 1997. Uncertainty in satellite rainfall estimates: Time series comparison. Adv. Sp. Res. 19, 469–472. https://doi.org/10.1016/S0273-1177(97)00056-2

Chen, J., Li, J., Zhang, Z., Ni, S., 2014. Long-term groundwater variations in Northwest India from satellite gravity measurements. Glob. Planet. Change 116, 130–138. https://doi.org/10.1016/j.gloplacha.2014.02.007

Christensen, N., Wood, A., Voisin, N., Lettenmaier, D., Palmer, R., 2004. The effects of climate change on the hydrology and water resources of the Colorado River Basin. Clim. Change. https://doi.org/10.1023/B:CLIM.0000013684.13621.1f

Cleugh, H.A., Leuning, R., Mu, Q., Running, S.W., 2007. Regional evaporation estimates from flux tower and MODIS satellite data. Remote Sens. Environ. https://doi.org/10.1016/j.rse.2006.07.007

Das, S., Ganguly, D., Mukherjee, A., Chakraborty, S., De, T.K., 2020. Exploration of N2 fixation and denitrification processes in the Sundarban mangrove ecosystem, India. Indian J. Geo-Marine Sci. 49, 740–747.

Debnath, P., Mukherjee, A., Das, K., 2018. Characterization of tidally influenced seasonal nutrient flux to the Bay of Bengal and its implications on the coastal ecosystem. Hydrol. Process. 32, 1282–1300. https://doi.org/10.1002/hyp.11507

Do, H.X., Gudmundsson, L., Leonard, M., Westra, S., Seneviratne, S.I., 2017. The Global Streamflow Indices and Metadata Archive (GSIM) – Part 1: The production of daily streamflow archive and metadata. Earth Syst. Sci. Data Discuss. 1–31. https://doi.org/10.5194/essd-2017-103

Du, J., Song, K., 2018. Validation of Global Evapotranspiration Product (MOD16) Using

Flux Tower Data from Panjin Coastal Wetland, Northeast China. Chinese Geogr. Sci. 28, 420–429. https://doi.org/10.1007/s11769-018-0960-8

ESA, 2017a. Land Cover CCI Product User Guide Version 2 Tech. Rep.

ESA, 2017b. Land Cover CCI Product User Guide Version 2. Tech. Rep. Available at: maps.elie.ucl.ac.be/CCI/viewer/download/ESACCI-LC-Ph2-PUGv2_2.0.pdf.

Fang, B., Lakshmi, V., 2014. Soil moisture at watershed scale: Remote sensing techniques. J. Hydrol. https://doi.org/10.1016/j.jhydrol.2013.12.008

Fang, B., Lakshmi, V., Bindlish, R., Jackson, T.J., 2018. Downscaling of SMAP Soil Moisture Using Land Surface Temperature and Vegetation Data. Vadose Zo. J. 17, 170198. https://doi.org/10.2136/vzj2017.11.0198

Fang, B., Lakshmi, V., Bindlish, R., Jackson, T.J., Cosh, M., Basara, J., 2013. Passive Microwave Soil Moisture Downscaling Using Vegetation Index and Skin Surface Temperature. Vadose Zo. J. 12, vzj2013.05.0089. https://doi.org/10.2136/vzj2013.05.0089

Fang, B., Lakshmi, V., Bindlish, R., Jackson, T.J., Liu, P.W., 2020. Evaluation and validation of a high spatial resolution satellite soil moisture product over the Continental United States. J. Hydrol. 588, 125043. https://doi.org/10.1016/j.jhydrol.2020.125043

Fang, B., Lakshmi, V., Jackson, T.J., Bindlish, R., Colliander, A., 2019. Passive/active microwave soil moisture change disaggregation using SMAPVEX12 data. J. Hydrol. 574, 1085–1098. https://doi.org/10.1016/j.jhydrol.2019.04.082

Farr, T.G., Rosen, P.A., Caro, E., Crippen, R., Duren, R., Hensley, S., Kobrick, M., Paller, M., Rodriguez, E., Roth, L., Seal, D., Shaffer, S., Shimada, J., Umland, J., Werner, M., Oskin, M., Burbank, D., Alsdorf, D.E., 2007a. The shuttle radar topography mission. Rev. Geophys. 45. https://doi.org/10.1029/2005RG000183

Farr, T.G., Rosen, P.A., Caro, E., Crippen, R., Duren, R., Hensley, S., Kobrick, M., Paller, M., Rodriguez, E., Roth, L., Seal, D., Shaffer, S., Shimada, J., Umland, J., Werner, M., Oskin, M., Burbank, D., Alsdorf, D.E., 2007b. The shuttle radar topography mission. Rev. Geophys. 45. https://doi.org/10.1029/2005RG000183

Fishman, R.M., Siegfried, T., Raj, P., Modi, V., Lall, U., 2011. Over-extraction from shallow bedrock versus deep alluvial aquifers: Reliability versus sustainability considerations for India's groundwater irrigation. Water Resour. Res. https://doi.org/10.1029/2011WR010617

Gemitzi, A., Lakshmi, V., 2018. Evaluating Renewable Groundwater Stress with GRACE

Data in Greece. Groundwater. https://doi.org/10.1111/gwat.12591

Gosain, A., Rao, S., Basuray, D., 2006. Climate change impact assessment on hydrology of Indian river basins on JSTOR. Curr. Sci. https://doi.org/http://www.jstor.org/stable/24091868

Gupta, H., Chakrapani, G.J., 2005. Temporal and spatial variations in water flow and sediment load in Narmada River Basin, India: Natural and man-made factors. Environ. Geol. 48, 579–589. https://doi.org/10.1007/s00254-005-1314-2

Hashemi, H., Nordin, M., Lakshmi, V., Huffman, G.J., Knight, R., 2017. Bias correction of long-term satellite monthly precipitation product (TRMM 3B43) over the conterminous United States. J. Hydrometeorol. 18, 2491–2509. https://doi.org/10.1175/JHM-D-17-0025.1

He, C., Liu, Z., Wu, J., Pan, X., Fang, Z., Li, J., Bryan, B.A., 2021. Future global urban water scarcity and potential solutions. Nat. Commun. 12, 1–11. https://doi.org/10.1038/s41467-021-25026-3

Hirsch, R.M., Slack, J.R., Smith, R.A., 1982. Techniques of trend analysis for monthly water quality data. Water Resour. Res. 18, 107–121. https://doi.org/10.1029/WR018i001p00107

Hossain, F., Anagnostou, E.N., Bagtzoglou, A.C., 2006. On Latin Hypercube sampling for efficient uncertainty estimation of satellite rainfall observations in flood prediction. Comput. Geosci. 32, 776–792. https://doi.org/10.1016/J.CAGEO.2005.10.006

IIT Consortium, 2015. Agriculture and Agricultural Practices in GRB EMP : Ganga River Basin Environment Management Plan.

Jain, C.K., 2002. A hydro-chemical study of a mountainous watershed: the Ganga, India. Water Res. 36, 1262–1274. https://doi.org/https://doi.org/10.1016/S0043-1354(01)00327-X

Jayakrishnan, R., Srinivasan, R., Santhi, C., Arnold, J.G., 2005. Advances in the application of the SWAT model for water resources management. Hydrol. Process. 19, 749–762. https://doi.org/10.1002/hyp.5624

Jin, L., Whitehead, P.G., Sarkar, S., Sinha, R., Futter, M.N., Butterfield, D., Caesar, J., Crossman, J., 2015. Assessing the impacts of climate change and socio-economic changes on flow and phosphorus flux in the Ganga river system. Environ. Sci. Process. Impacts 17, 1098–1110. https://doi.org/10.1039/c5em00092k

Joshi, D.M., Kumar, A., Agrawal, N., 2009. Studies on physicochemical parameters to

assess the water quality of river ganga for drinking purpose in Haridwar district. Rasayan J. Chem. 2, 195–203.

Kansara, P., Li, W., El-Askary, H., Lakshmi, V., Piechota, T., Struppa, D., Sayed, M.A., 2021. An Assessment of the Filling Process of the Grand Ethiopian Renaissance Dam and Its Impact on the Downstream Countries. Remote Sens. 13, 711. https://doi.org/10.3390/rs13040711

Karaseva, M.O., Prakash, S., Gairola, R.M., 2012. Validation of high-resolution TRMM-3B43 precipitation product using rain gauge measurements over Kyrgyzstan. Theor. Appl. Climatol. 108, 147–157. https://doi.org/10.1007/s00704-011-0509-6

Kim, H., Lakshmi, V., 2019. Global Dynamics of Stored Precipitation Water in the Topsoil Layer From Satellite and Reanalysis Data. Water Resour. Res. 55, 3328–3346. https://doi.org/10.1029/2018WR023166

Kim, H., Lakshmi, V., Kwon, Y., Kumar, S. V., 2021. First attempt of global-scale assimilation of subdaily scale soil moisture estimates from CYGNSS and SMAP into a land surface model. Environ. Res. Lett. 16. https://doi.org/10.1088/1748-9326/ac0ddf

Kim, H., Parinussa, R., Konings, A.G., Wagner, W., Cosh, M.H., Lakshmi, V., Zohaib, M., Choi, M., 2018. Global-scale assessment and combination of SMAP with ASCAT (active) and AMSR2 (passive) soil moisture products. Remote Sens. Environ. 204, 260–275. https://doi.org/10.1016/j.rse.2017.10.026

Kim, H.W., Hwang, K., Mu, Q., Lee, S.O., Choi, M., 2012. Validation of MODIS 16 global terrestrial evapotranspiration products in various climates and land cover types in Asia. KSCE J. Civ. Eng. https://doi.org/10.1007/s12205-012-0006-1

Kingston, D.G., Thompson, J.R., Kite, G., 2011. Uncertainty in climate change projections of discharge for the Mekong River Basin. Hydrol. Earth Syst. Sci. https://doi.org/10.5194/hess-15-1459-2011

Kirtsaeng, S., Mai Sci, C.J., Chanyatham, T., 2011. Comparison and Analysis of Remote Sensing-Based and Ground-Based Precipitation Data over India. Radar rainfall estimation in Southern and Northeastern Thailand View project Comparison and Analysis of Remote Sensing-based and Ground-based Precipitation Data Over India, Chiang Mai J. Sci.

Kite, G., 2001. Modelling the mekong: Hydrological simulation for environmental impact studies. J. Hydrol. https://doi.org/10.1016/S0022-1694(01)00396-1

Kripalani, R.H., Kulkarni, A., Sabade, S.S., Khandekar, M.L., 2003. Indian Monsoon variability in a global warming scenario. Nat. Hazards 29, 189–206.

https://doi.org/10.1023/A:1023695326825

Krishna, M.S., Prasad, M.H.K., Rao, D.B., Viswanadham, R., Sarma, V.V.S.S., Reddy, N.P.C., 2016. Export of dissolved inorganic nutrients to the northern Indian Ocean from the Indian monsoonal rivers during discharge period. Geochim. Cosmochim. Acta 172, 430–443. https://doi.org/10.1016/j.gca.2015.10.013

Krishnamurthy, V., Kirtman, B.P., 2009. Relation between Indian monsoon variability and SST. J. Clim. https://doi.org/10.1175/2009JCLI2520.1

Kummerow, C., Simpson, J., Thiele, O., Barnes, W., Chang, A.T.C., Stocker, E., Adler, R.F., Hou, A., Kakar, R., Wentz, F., Ashcroft, P., Kozu, T., Hong, Y., Okamoto, K., Iguchi, T., Kuroiwa, H., Im, E., Haddad, Z., Huffman, G., Ferrier, B., Olson, W.S., Zipser, E., Smith, E.A., Wilheit, T.T., North, G., Krishnamurti, T., Nakamura, K., Kummerow, C., Simpson, J., Thiele, O., Barnes, W., Chang, A.T.C., Stocker, E., Adler, R.F., Hou, A., Kakar, R., Wentz, F., Ashcroft, P., Kozu, T., Hong, Y., Okamoto, K., Iguchi, T., Kuroiwa, H., Im, E., Haddad, Z., Huffman, G., Ferrier, B., Olson, W.S., Zipser, E., Smith, E.A., Wilheit, T.T., North, G., Krishnamurti, T., Nakamura, K., 2000. The Status of the Tropical Rainfall Measuring Mission (TRMM) after Two Years in Orbit. J. Appl. Meteorol. 39, 1965–1982. https://doi.org/10.1175/1520-0450(2001)040<1965:TSOTTR>2.0.CO;2

Kundzewicz, Z.W., Mata, L.J., Arnell, N.W., Döll, P., Kabat, B., Jimenez, B., Miller, K. a, Oki, T., Sen, Z., Shiklomanov, I., 2007. Freshwater resources and their management, in: Climate Change 2007: Impacts, Adaptation and Vulnerability. Contribution of Working Group II to the Fourth Assessment Report of the Intergovernmental Panel on Climate Change. https://doi.org/10.1017/CBO9781107415324.004

Lakshmi, V., Fayne, J., Bolten, J., 2018. A comparative study of available water in the major river basins of the world. J. Hydrol. https://doi.org/10.1016/j.jhydrol.2018.10.038

Lakshmi, V., Wood, E.F., 1998. Diurnal cycles of evaporation using a two-layer hydrological model. J. Hydrol. 204, 37–51. https://doi.org/10.1016/S0022-1694(97)00108-X

Lakshmi, V., Wood, E.F., Choudhury, B.J., 1997. A soil-canopy-atmosphere model for use in satellite microwave remote sensing. J. Geophys. Res. Atmos. 102, 6911–6927. https://doi.org/10.1029/96JD03763

Le, H., Sutton, J., Bui, D., Bolten, J., Lakshmi, V., Le, H.M., Sutton, J.R.P., Bui, D. Du, Bolten, J.D., Lakshmi, V., 2018. Comparison and Bias Correction of TMPA Precipitation Products over the Lower Part of Red–Thai Binh River Basin of Vietnam. Remote Sens. 10, 1582. https://doi.org/10.3390/rs10101582

Le, M.H., Lakshmi, V., Bolten, J., Bui, D. Du, 2020. Adequacy of Satellite-derived Precipitation Estimate for Hydrological Modeling in Vietnam Basins. J. Hydrol. 586, 124820. https://doi.org/10.1016/j.jhydrol.2020.124820

Lettenmaier, D.P., 1988. MULTIVARIATE NONPARAMETRIC TESTS FOR TREND IN WATER QUALITY1. JAWRA J. Am. Water Resour. Assoc. 24, 505–512. https://doi.org/10.1111/J.1752-1688.1988.TB00900.X

Li, D., Zhao, T., Shi, J., Bindlish, R., Jackson, T.J., Peng, B., An, M., Han, B., 2015. First Evaluation of Aquarius Soil Moisture Products Using *In Situ* Observations and GLDAS Model Simulations. IEEE J. Sel. Top. Appl. Earth Obs. Remote Sens. 8, 5511–5525. https://doi.org/10.1109/JSTARS.2015.2452955

Li, X., Zhang, Q., Ye, X., Li, X., Zhang, Q., Ye, X., 2013. Dry/Wet Conditions Monitoring Based on TRMM Rainfall Data and Its Reliability Validation over Poyang Lake Basin, China. Water 5, 1848–1864. https://doi.org/10.3390/w5041848

Liu, X., Yu, L., Sia, Y., Zhang, C., Lu, H., Yu, C., Gong, P., 2018. Identifying patterns and hotspots of global land cover transitions using the ESA CCI land cover dataset. Remote Sens. Lett. 9, 972–981. https://doi.org/10.1080/2150704X.2018.1500070

Lohmann, D., Mitchell, K.E., Houser, P.R., Wood, E.F., Schaake, J.C., Robock, A., Cosgrove, B.A., Sheffield, J., Duan, Q., Luo, L., Higgins, R.W., Pinker, R.T., Tarpley, J.D., 2004. Streamflow and water balance intercomparisons of four land surface models in the North American Land Data Assimilation System project. J. Geophys. Res. Atmos. 109, 1–22. https://doi.org/10.1029/2003jd003517

Lorenz, C., Kunstmann, H., Devaraju, B., Tourian, M.J., Sneeuw, N., Riegger, J., Lorenz, C., Kunstmann, H., Devaraju, B., Tourian, M.J., Sneeuw, N., Riegger, J., 2014. Large-Scale Runoff from Landmasses: A Global Assessment of the Closure of the Hydrological and Atmospheric Water Balances*. J. Hydrometeorol. 15, 2111–2139. https://doi.org/10.1175/JHM-D-13-0157.1

MacDonald, A., Bonsor, H., Taylor, R., Shamsudduha, M., Burgess, W.G., Ahmed, K.M., Mukherjee, A., Zahid, A., Lapworth, D., Gopal, K., Rao, M.S., Moench, M., Bricker, S., Yadav, S.K., Satyal, Y., Smith, L., Dixit, A., Bell, R., van Steenbergen, F., Basharat, M., Gohar, M.S., Tucker, J., Calow, R., Maurice, L., 2015. Groundwater resources in the Indo-Gangetic Basin: resilience to climate change and abstraction. Open Report, OR/15/047. https://doi.org/10.13140/RG.2.1.3822.1524

MacDonald, A.M., Bonsor, H.C., Ahmed, K.M., Burgess, W.G., Basharat, M., Calow, R.C., Dixit, A., Foster, S.S.D., Gopal, K., Lapworth, D.J., Lark, R.M., Moench, M., Mukherjee, A., Rao, M.S., Shamsudduha, M., Smith, L., Taylor, R.G., Tucker, J., Van Steenbergen, F., Yadav, S.K., 2016. Groundwater quality and depletion in the Indo-

Gangetic Basin mapped from in situ observations. Nat. Geosci. https://doi.org/10.1038/ngeo2791

Madhusoodhanan, C.G., Sreeja, K.G., Eldho, T.I., 2016. Climate change impact assessments on the water resources of India under extensive human interventions. Ambio 45, 725–741. https://doi.org/10.1007/s13280-016-0784-7

Mall, R.K., Gupta, A., Singh, R., Singh, R.S., Rathore, L.S., 2006. Jun06-Water-Cc-Cgc-India-Cursci 90.

Matta, G., 2015. Effect of water quality on phytoplankton ecology of Upper Ganga Canal . Int. J. Sci. Eng. Res. 6, 762–768.

Mishra, V., Lilhare, R., 2016a. Hydrologic sensitivity of Indian sub-continental river basins to climate change. Glob. Planet. Change 139, 78–96. https://doi.org/10.1016/J.GLOPLACHA.2016.01.003

Mishra, V., Lilhare, R., 2016b. Hydrologic sensitivity of Indian sub-continental river basins to climate change. Glob. Planet. Change 139, 78–96. https://doi.org/10.1016/j.gloplacha.2016.01.003

Mishra, V., Lilhare, R., 2016c. Hydrologic sensitivity of Indian sub-continental river basins to climate change. Glob. Planet. Change 139, 78–96. https://doi.org/10.1016/j.gloplacha.2016.01.003

Misra, A.K., 2014. Climate change and challenges of water and food security. Int. J. Sustain. Built Environ. https://doi.org/10.1016/j.ijsbe.2014.04.006

Mohammed, I.N., Bolten, J.D., Srinivasan, R., Lakshmi, V., 2018. Satellite observations and modeling to understand the Lower Mekong River Basin streamflow variability. J. Hydrol. https://doi.org/10.1016/j.jhydrol.2018.07.030

Mondal, A., Lakshmi, V., 2021. Estimation of total water storage changes in India. https://doi.org/10.1080/17538947.2021.1914759. https://doi.org/10.1080/17538947.2021.1914759

Mondal, A., Lakshmi, V., Hashemi, H., 2018a. Intercomparison of trend analysis of Multisatellite Monthly Precipitation Products and Gauge Measurements for River Basins of India. J. Hydrol. https://doi.org/10.1016/j.jhydrol.2018.08.083

Mondal, A., Lakshmi, V., Hashemi, H., 2018b. Intercomparison of trend analysis of Multisatellite Monthly Precipitation Products and Gauge Measurements for River Basins of India. J. Hydrol. 565, 779–790. https://doi.org/10.1016/J.JHYDROL.2018.08.083

Moriasi, D.N., Gitau, M.W., Pai, N., Daggupati, P., 2015. Hydrologic and water quality

models: Performance measures and evaluation criteria. Trans. ASABE 58, 1763–1785. https://doi.org/10.13031/trans.58.10715

Morrissey, M.L., Greene, J.S., 1998. Uncertainty analysis of satellite rainfall algorithms over the tropical Pacific. J. Geophys. Res. Atmos. 103, 19569–19576. https://doi.org/10.1029/98JD00309

Mu, Q., Zhao, M., Running, S.W., 2011. Improvements to a MODIS global terrestrial evapotranspiration algorithm. Remote Sens. Environ. https://doi.org/10.1016/j.rse.2011.02.019

Mukhopadhyay, S.K., Biswas, H., De, T.K., Jana, T.K., 2006. Fluxes of nutrients from the tropical River Hooghly at the land-ocean boundary of Sundarbans, NE Coast of Bay of Bengal, India. J. Mar. Syst. 62, 9–21. https://doi.org/10.1016/j.jmarsys.2006.03.004

Nazemi, A., Madani, K., 2018. Urban water security: Emerging discussion and remaining challenges. Sustain. Cities Soc. https://doi.org/10.1016/j.scs.2017.09.011

Neitsch, S.L., Arnold, J.G., Kiniry, J.R., Williams, J.R., 2011. COLLEGE OF AGRICULTURE AND LIFE SCIENCES Soil and Water Assessment Tool Theoretical Documentation Version 2009.

Oki, T., Kanae, S., 2006. Global hydrological cycles and world water resources. Science (80-.). https://doi.org/10.1126/science.1128845

Pandey, B.K., Khare, D., Kawasaki, A., Mishra, P.K., 2019. Climate Change Impact Assessment on Blue and Green Water by Coupling of Representative CMIP5 Climate Models with Physical Based Hydrological Model. Water Resour. Manag. 33, 141–158. https://doi.org/10.1007/s11269-018-2093-3

Pathak, D., Whitehead, P.G., Futter, M.N., Sinha, R., 2018. Water quality assessment and catchment-scale nutrient flux modeling in the Ramganga River Basin in north India: An application of INCA model. Sci. Total Environ. 631–632, 201–215. https://doi.org/10.1016/j.scitotenv.2018.03.022

Piao, S., Ciais, P., Huang, Y., Shen, Z., Peng, S., Li, J., Zhou, L., Liu, H., Ma, Y., Ding, Y., Friedlingstein, P., Liu, C., Tan, K., Yu, Y., Zhang, T., Fang, J., 2010. The impacts of climate change on water resources and agriculture in China. Nature. https://doi.org/10.1038/nature09364

Prakash, S., Gairola, R.M., 2014. Validation of TRMM-3B42 precipitation product over the tropical Indian Ocean using rain gauge data from the RAMA buoy array. Theor. Appl. Climatol. 115, 451–460. https://doi.org/10.1007/s00704-013-0903-3

Prasetia, R., As-syakur, A.R., Osawa, T., 2013. Validation of TRMM Precipitation Radar satellite data over Indonesian region. Theor. Appl. Climatol. 112, 575–587. https://doi.org/10.1007/s00704-012-0756-1

Ragab, R., Prudhomme, C., 2002. Climate change and water resources management in arid and semi-arid regions: Prospective and challenges for the 21st century. Biosyst. Eng. https://doi.org/10.1006/bioe.2001.0013

Rajeevan, M., Bhate, J., Kale, J., Lal, B., 2006. High resolution daily gridded rainfall data for the Indian region: Analysis of break and active monsoon spells. Curr. Sci.

Rickards, N., Thomas, T., Kaelin, A., Houghton-Carr, H., Jain, S.K., Mishra, P.K., Nema, M.K., Dixon, H., Rahman, M.M., Horan, R., Jenkins, A., Rees, G., 2020. Understanding future water challenges in a highly regulated indian river basin-modelling the impact of climate change on the hydrology of the upper Narmada. Water (Switzerland) 12. https://doi.org/10.3390/w12061762

Rijsberman, F.R., 2006. Water scarcity: Fact or fiction? Agric. Water Manag. 80, 5–22. https://doi.org/10.1016/J.AGWAT.2005.07.001

Rodell, M., Famiglietti, J.S., Wiese, D.N., Reager, J.T., Beaudoing, H.K., Landerer, F.W., Lo, M.-H., 2018. Emerging trends in global freshwater availability. Nature 557, 651–659. https://doi.org/10.1038/s41586-018-0123-1

Rodell, M., Houser, P.R., Jambor, U., Gottschalck, J., Mitchell, K., Meng, C.-J., Arsenault, K., Cosgrove, B., Radakovich, J., Bosilovich, M., Entin*, J.K., Walker, J.P., Lohmann, D., Toll, D., 2004. The Global Land Data Assimilation System. Bull. Am. Meteorol. Soc. https://doi.org/10.1175/BAMS-85-3-381

Rodell, M., Velicogna, I., Famiglietti, J.S., 2009a. Satellite-based estimates of groundwater depletion in India. Nature. https://doi.org/10.1038/nature08238

Rodell, M., Velicogna, I., Famiglietti, J.S., 2009b. Satellite-based estimates of groundwater depletion in India. Nature 460, 999–1002. https://doi.org/10.1038/nature08238

Rodríguez, E., Morris, C.S., Belz, J.E., Chapin, E.C., Martin, J.M., Daffer, W., Hensley, S., 2005. An Assessment of the SRTM Topographic Products. https://doi.org/https://doi.org/10.14358/PERS.72.3.249

Ross, R.S., Krishnamurti, T.N., Pattnaik, S., Pai, D.S., 2018. Decadal surface temperature trends in India based on a new high-resolution data set. Sci. Rep. 8, 2–11. https://doi.org/10.1038/s41598-018-25347-2

Rozante, J.R., Moreira, D.S., de Goncalves, L.G.G., Vila, D.A., Rozante, J.R., Moreira,

D.S., Goncalves, L.G.G. de, Vila, D.A., 2010. Combining TRMM and Surface Observations of Precipitation: Technique and Validation over South America. Weather Forecast. 25, 885–894. https://doi.org/10.1175/2010WAF2222325.1

Saha, S., Moorthi, S., Pan, H.L., Wu, X., Wang, Jiande, Nadiga, S., Tripp, P., Kistler, R., Woollen, J., Behringer, D., Liu, H., Stokes, D., Grumbine, R., Gayno, G., Wang, Jun, Hou, Y.T., Chuang, H.Y., Juang, H.M.H., Sela, J., Iredell, M., Treadon, R., Kleist, D., Van Delst, P., Keyser, D., Derber, J., Ek, M., Meng, J., Wei, H., Yang, R., Lord, S., Van Den Dool, H., Kumar, A., Wang, W., Long, C., Chelliah, M., Xue, Y., Huang, B., Schemm, J.K., Ebisuzaki, W., Lin, R., Xie, P., Chen, M., Zhou, S., Higgins, W., Zou, C.Z., Liu, Q., Chen, Y., Han, Y., Cucurull, L., Reynolds, R.W., Rutledge, G., Goldberg, M., 2010. The NCEP climate forecast system reanalysis. Bull. Am. Meteorol. Soc. 91, 1015–1057. https://doi.org/10.1175/2010BAMS3001.1

Saraswat, C., Kumar, P., Dasgupta, R., Avtar, R., Bhalani, P., 2019. Sustainability assessment of the groundwater quality in the Western India to achieve urban water security. Appl. Water Sci. 9, 1–17. https://doi.org/10.1007/s13201-019-0956-2

Sarkar, S.K., Saha, M., Takada, H., Bhattacharya, A., Mishra, P., Bhattacharya, B., 2007. Water quality management in the lower stretch of the river Ganges, east coast of India: an approach through environmental education. J. Clean. Prod. 15, 1559–1567. https://doi.org/https://doi.org/10.1016/j.jclepro.2006.07.030

Schlesinger, W.H., Reckhow, K.H., Bernhardt, E.S., 2006. Global change: The nitrogen cycle and rivers. Water Resour. Res. 42, 5–6. https://doi.org/10.1029/2005WR004300

Schmidt, R., Schwintzer, P., Flechtner, F., Reigber, C., Güntner, A., Döll, P., Ramillien, G., Cazenave, A., Petrovic, S., Jochmann, H., Wünsch, J., 2006. GRACE observations of changes in continental water storage. Glob. Planet. Change 50, 112–126. https://doi.org/10.1016/J.GLOPLACHA.2004.11.018

Seitzinger, S.P., Styles, R. V., Boyer, E.W., Alexander, R.B., Billen, G., Howarth, R.W., Mayer, B., Van Breemen, N., 2002. Nitrogen retention in rivers: Model development and application to watersheds in the northeastern U.S.A. Biogeochemistry 57–58, 199–237. https://doi.org/10.1023/A:1015745629794

Sen, I.S., Boral, S., Ranjan, S., Tandon, S.K., 2018. Small but Important: The Role of Small Floodplain Tributaries to River Nutrient Budgets. ACS Earth Sp. Chem. 2, 64–71. https://doi.org/10.1021/acsearthspacechem.7b00112

Seo, K.W., Waliser, D.E., Tian, B., Famiglietti, J.S., Syed, T.H., 2009. Evaluation of global land-to-ocean fresh water discharge and evapotranspiration using space-based observations. J. Hydrol. 373, 508–515. https://doi.org/10.1016/j.jhydrol.2009.05.014

Shah, H.L., Mishra, V., Shah, H.L., Mishra, V., 2016. Hydrologic Changes in Indian Subcontinental River Basins (1901–2012). J. Hydrometeorol. 17, 2667–2687. https://doi.org/10.1175/JHM-D-15-0231.1

Shah, T., 2009. Climate change and groundwater: India's opportunities for mitigation and adaptation. Environ. Res. Lett. https://doi.org/10.1088/1748-9326/4/3/035005

Sharma, P., Meher, P.K., Kumar, A., Gautam, Y.P., Mishra, K.P., 2014. Changes in water quality index of Ganges river at different locations in Allahabad. Sustain. Water Qual. Ecol. 3–4, 67–76. https://doi.org/https://doi.org/10.1016/j.swaqe.2014.10.002

Sharma, S., Dixit, S., Jain, P., Shah, K.W., Vishwakarma, R., 2008. Statistical evaluation of hydrobiological parameters of Narmada River water at Hoshangabad City, India. Environ. Monit. Assess. 143, 195–202. https://doi.org/10.1007/s10661-007-9968-8

Sharma, S., Khan, S.A., Kumar, A., Jha, P.K., Jindal, T., 2020. Eutrophication Risk Assessment by Estimation of Denitrification Rate in Yamuna River Sediments. Trans. Indian Natl. Acad. Eng. 5, 51–60. https://doi.org/10.1007/s41403-020-00089-8

Shukla, A., Ojha, C., Singh, R., Pal, L., Fu, D., Shukla, A.K., Ojha, C.S.P., Singh, R.P., Pal, L., Fu, D., 2019. Evaluation of TRMM Precipitation Dataset over Himalayan Catchment: The Upper Ganga Basin, India. Water 11, 613. https://doi.org/10.3390/w11030613

Shukla, T., Sen, I.S., Boral, S., Sharma, S., 2021. A time-series record during COVID-19 lockdown shows the high resilience of dissolved heavy metals in the Ganga river. Environ. Sci. Technol. Lett. https://doi.org/10.1021/acs.estlett.0c00982

Simpson, J., Kummerow, C., Tao, W.-K., Adler, R.F., 1996. On the Tropical Rainfall Measuring Mission (TRMM). Meteorol. Atmos. Phys. 60, 19–36. https://doi.org/10.1007/BF01029783

Smith, R.A., Schwarz, G.E., Alexander, R.B., 1997. Regional interpretation of water-quality monitoring data. Water Resour. Res. 33, 2781–2798. https://doi.org/10.1029/97WR02171

Soni, A., Syed, T.H., 2015. Diagnosing Land Water Storage Variations in Major Indian River Basins using GRACE observations. Glob. Planet. Change 133, 263–271. https://doi.org/10.1016/j.gloplacha.2015.09.007

Srivastava, A.K., Rajeevan, M., Kshirsagar, S.R., 2009. Development of a high resolution daily gridded temperature data set (1969-2005) for the Indian region. Atmos. Sci. Lett. 10, 249–254. https://doi.org/10.1002/asl.232

Swenson, S., Wahr, J., 2009. Monitoring the water balance of Lake Victoria, East Africa, from space. J. Hydrol. 370, 163–176. https://doi.org/10.1016/J.JHYDROL.2009.03.008

Swenson, S., Wahr, J., 2006. Post-processing removal of correlated errors in GRACE data. Geophys. Res. Lett. 33, L08402. https://doi.org/10.1029/2005GL025285

Swenson, S., Wahr, J., Milly, P.C.D., 2003. Estimated accuracies of regional water storage variations inferred from the Gravity Recovery and Climate Experiment (GRACE). Water Resour. Res. 39. https://doi.org/10.1029/2002WR001808

Syed, T.H., Famiglietti, J.S., Rodell, M., Chen, J., Wilson, C.R., 2008. Analysis of terrestrial water storage changes from GRACE and GLDAS. Water Resour. Res. 44. https://doi.org/10.1029/2006WR005779

Tang, R., Shao, K., Li, Z.-L., Wu, H., Tang, B.-H., Zhou, G., Zhang, L., 2015. Multiscale Validation of the 8-day MOD16 Evapotranspiration Product Using Flux Data Collected in China. IEEE J. Sel. Top. Appl. Earth Obs. Remote Sens. 8, 1478–1486. https://doi.org/10.1109/JSTARS.2015.2420105

Tapley, B.D., Bettadpur, S., Ries, J.C., Thompson, P.F., Watkins, M.M., 2004. GRACE Measurements of Mass Variability in the Earth System. Science (80-.). 305, 503–505. https://doi.org/10.1126/science.1099192

Tare, V., Yadav, A.V.S., Bose, P., 2003. Analysis of photosynthetic activity in the most polluted stretch of river Ganga. Water Res. 37, 67–77. https://doi.org/10.1016/S0043-1354(01)00385-2

Taylor, R.G., Scanlon, B., Döll, P., Rodell, M., Van Beek, R., Wada, Y., Longuevergne, L., Leblanc, M., Famiglietti, J.S., Edmunds, M., Konikow, L., Green, T.R., Chen, J., Taniguchi, M., Bierkens, M.F.P., Macdonald, A., Fan, Y., Maxwell, R.M., Yechieli, Y., Gurdak, J.J., Allen, D.M., Shamsudduha, M., Hiscock, K., Yeh, P.J.F., Holman, I., Treidel, H., 2013a. Ground water and climate change. Nat. Clim. Chang. https://doi.org/10.1038/nclimate1744

Taylor, R.G., Todd, M.C., Kongola, L., Maurice, L., Nahozya, E., Sanga, H., Macdonald, A.M., 2013b. Evidence of the dependence of groundwater resources on extreme rainfall in East Africa. Nat. Clim. Chang. https://doi.org/10.1038/nclimate1731

The World Bank, n.d. Helping India Manage its Complex Water Resources [WWW Document]. URL https://www.worldbank.org/en/news/feature/2019/03/22/helping-india-manage-its-complex-water-resources

Tiwari, A., Dwivedi, A., Mayank, P., 2016. Time Scale Changes in the Water Quality of the Ganga River, India and Estimation of Suitability for Exotic and Hardy Fishes. J. Waste Water Treat. Anal. 7. https://doi.org/10.4172/2157-7587.1000254

van Beek, L.P.H., Wada, Y., Bierkens, M.F.P., 2011a. Global monthly water stress: 1. Water balance and water availability. Water Resour. Res. 47. https://doi.org/10.1029/2010WR009791

van Beek, L.P.H., Wada, Y., Bierkens, M.F.P., 2011b. Global monthly water stress: 1. Water balance and water availability. Water Resour. Res. 47. https://doi.org/10.1029/2010WR009791

van Vliet, M.T.H., Jones, E.R., Flörke, M., Franssen, W.H.P., Hanasaki, N., Wada, Y., Yearsley, J.R., 2021. Global water scarcity including surface water quality and expansions of clean water technologies. Environ. Res. Lett. 16. https://doi.org/10.1088/1748-9326/abbfc3

Vörösmarty, C.J., Green, P., Salisbury, J., Lammers, R.B., 2000. Global water resources: Vulnerability from climate change and population growth. Science (80-.). https://doi.org/10.1126/science.289.5477.284

Voss, K.A., Famiglietti, J.S., Lo, M., de Linage, C., Rodell, M., Swenson, S.C., 2013. Groundwater depletion in the Middle East from GRACE with implications for transboundary water management in the Tigris-Euphrates-Western Iran region. Water Resour. Res. 49, 904–914. https://doi.org/10.1002/wrcr.20078

Wada, Y., Van Beek, L.P.H., Bierkens, M.F.P., 2012. Nonsustainable groundwater sustaining irrigation: A global assessment. Water Resour. Res. https://doi.org/10.1029/2011WR010562

Wada, Y., Van Beek, L.P.H., Van Kempen, C.M., Reckman, J.W.T.M., Vasak, S., Bierkens, M.F.P., 2010. Global depletion of groundwater resources. Geophys. Res. Lett. https://doi.org/10.1029/2010GL044571

Wahr, J., Swenson, S., Velicogna, I., 2006. Accuracy of GRACE mass estimates. Geophys. Res. Lett. 33, L06401. https://doi.org/10.1029/2005GL025305

Wallace, J.M., Smith, C., Bretherton, C.S., 1992. Singular Value Decomposition of Wintertime Sea Surface Temperature and 500-mb Height Anomalies. J. Clim. https://doi.org/10.1175/1520-0442(1992)005<0561:svdows>2.0.co;2

Whitehead, P.G., Sarkar, S., Jin, L., Futter, M.N., Caesar, J., Barbour, E., Butterfield, D., Sinha, R., Nicholls, R., Hutton, C., Leckie, H.D., 2015. Dynamic modeling of the Ganga river system: Impacts of future climate and socio-economic change on flows and nitrogen fluxes in India and Bangladesh. Environ. Sci. Process. Impacts 17, 1082–1097. https://doi.org/10.1039/c4em00616j

Whitehead, P.G., Wilson, E.J., Butterfield, D., 1998. A semi-distributed Integrated Nitrogen model for multiple source assessment in Catchments (INCA): Part I -

Model structure and process equations. Sci. Total Environ. 210–211, 547–558. https://doi.org/10.1016/S0048-9697(98)00037-0

World Bank, 2010. Deep Wells and Prudence: Towards Pragmatic Action for Addressing Groundwater Overexploitation in India. Int. Bank Reconstr. Dev. World Bank. https://doi.org/9504

Xu, R., Tian, F., Yang, L., Hu, H., Lu, H., Hou, A., n.d. Ground validation of GPM IMERG and TRMM 3B42V7 rainfall products over southern Tibetan Plateau based on a high-density rain gauge network. https://doi.org/10.1002/2016JD025418

Zaitchik, B.F., Rodell, M., Olivera, F., 2010. Evaluation of the Global Land Data Assimilation System using global river discharge data and a source-to-sink routing scheme. Water Resour. Res. 46, 1–17. https://doi.org/10.1029/2009WR007811

Zawadzki, J., Kędzior, M., 2014. Statistical analysis of soil moisture content changes in Central Europe using GLDAS database over three past decades. Open Geosci. 6, 344–353. https://doi.org/10.2478/s13533-012-0176-x